University of Alberta

DYNAMIC SIMULATION AND OPTIMAL TRAJECTORY PLANNING FOR AN OILSAND PRIMARY SEPARATION VESSEL

by

Wesley A.M. Gilbert

A thesis submitted to the Faculty of Graduate Studies and Research in partial fulfillment of the requirements for the degree of **Master of Science**.

in

Process Control

Department of Chemical and Materials Engineering

Edmonton, Alberta
Fall 2004

Your file Votre référence
ISBN: 0-612-95753-5
Our file Notre référence
ISBN: 0-612-95753-5

This thesis is dedicated to my parents, Dr. Allan Gilbert and Mrs. Sharon Gilbert, as well as to my girlfriend Lena Athanasopoulos for their support and patience.

Acknowledgements

I would like to thank both my supervisors Dr. Michael Lipsett and Dr. Fraser Forbes, for their continuing guidance and encouragement throughout the course of this thesis.

I would also like to thank Dr. Jacob Masliyah for his advice and guidance throughout this project. As well, I would like to thank Jonathon Spence, Samson Ng, and Robert Siy, as well as the remainder of the Syncrude Research Extraction team, for their advice during the course of this project.

Finally I would like to thank NSERC and the University of Alberta for the funding that made this thesis project possible.

Contents

List of Tables

List of Figures

List of Symbols

Nomenclature

$\mathbf{x}$	vector of dynamic variables
$\mathbf{z}$	vector of algebraic variables
$\mathbf{u}$	vector of input variables
$\mathbf{f}$	vector of dynamic equations
$\mathbf{g}$	vector of equalities
$\mathbf{h}$	vector of inequalities
$\mathbf{p}$	vector of time independent parameters
t	independent variable (time)
$\varsigma^+(x)$	increasing sigmoid function
$\varsigma^-(x)$	decreasing sigmoid function
n_p	number of particles
n_b	number of bitumen particles
n_s	number of solid particles
n_{sp}	number of species ($n_{sp} = n_s + n_b + 1$)
V_{mix}	Effective Tumbler and Mixing Tank Volume
V_f	Froth Volume
V_m	Middlings Volume
V_t	Tailings Volume
V_{vessel}	Vessel Volume
A	Vessel Area
Q_{fd}	Feed Flow Rate
Q_f	Froth Flow Rate
Q_m	Middlings Flow Rate (input)
Q_t	Tailings Flow Rate (input)
Q_{fl}	Flood Water Flow Rate (input)
α_i^j	volume fraction of species i in layer j
v_i^f	particle i settling velocity, froth/middlings interface
v_i^t	particle i settling velocity, middlings/tailings interface
v_I	Froth/Middlings Interfacial velocity
ρ_i	Species i Density
ρ_m	Density of Middlings
ρ_t	Density of Tailings

d_i	Species i Diameter
λ_i	species i Middlings Withdrawal Factor [28]
σ_i^f	species i Froth/Middlings Settling Factor
σ_i^t	species i Middlings/Tailings Settling Factor
θ_i	Concha/Swanson shape factor
β_i	Concha/Swanson shape factor
γ_1	fines hindering factor
γ_2	fines hindering factor

Accronyms

CHWE	Clark's Hot Water Extraction
DRU	Diluent Recovery Unit
PSV	Primary Separation Vessel
EXP2000	Extraction Pilot 2000 L
DCS	Distributed Control System
DAE	Differential-Algebraic Equations
CST	Continuous Stirred Tank
ODE	Ordinary Differential Equations
MPEC	Mathematical Program With Equilibrium Constraints
BDF	Backwards Differentiation Formulae
IRK	Implicit Runge Kutta
NLP	Non-linear Programming
DP	Dynamic Programming
IDP	Iterative Dynamic Programming
CVP	Control Vector Parametrization
SOCS	Sparse Optimal Control Software
IST	Input Switching Time
RIOT	Restricted Input Optimal Trajectory
SQP	Sequential Quadratic Programming

1 Introduction

This section provides a brief overview of the Syncrude oilsands process, followed by a definition of the problem that will be considered in this thesis.

Oilsands are a non-conventional source of crude oil, whereby shallow deposits of bitumen-laden sands are usually mined, then processed to produce synthetic crude oil. The oil separation process entails efficiently liberating and then aerating bitumen droplets from the sand, using water and process chemicals. The process is based on the Clark Hot Water Extraction (CHWE) process, which operates at around 75°C, and uses caustic to increase separation performance [33]. Although there is a shift to more energy efficient processing using lower temperatures, the method behind the extraction process remains essentially the same. This chapter begins by describing the oilsand production and upgrading process, with emphasis on the extraction of bitumen from the oilsand. The chapter continues with a discussion of the EXP2000 Syncrude extraction pilot plant, and concludes with an overview of the thesis, scope and objectives.

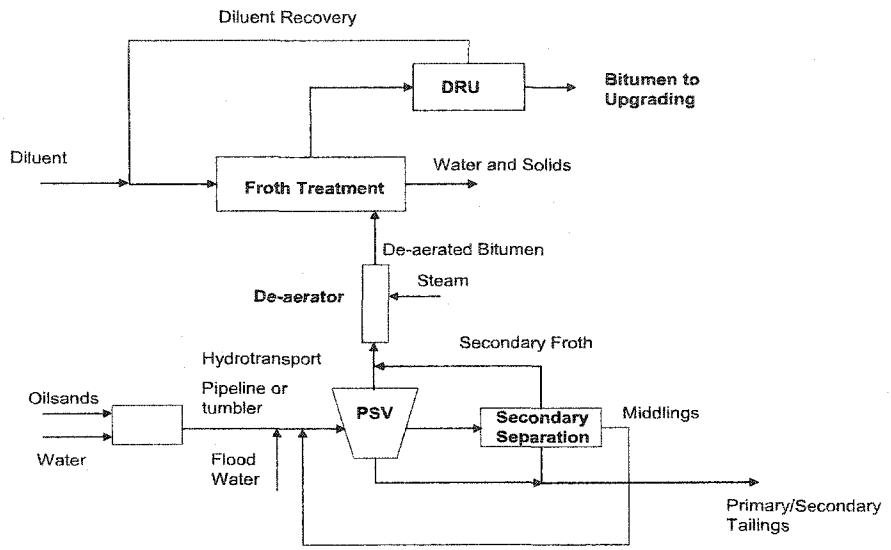

Figure 1.1: Oilsands Extraction Process Schematic [33]

1.1 Syncrude Oilsands Process

Oilsand requires a number of processing steps before the finished synthetic crude oil product can be sold and sent off to other refining facilities. The section begins by introducing the methods behind oilsands processing, with emphasis on the process units of relevance to this work.

1.1.1 Overall Process

A simplified schematic for oilsand processing is shown in Figure 1.1. The process shown here is a generalized schematic, where minor differences are employed throughout industry. Initially the bitumen-rich sand must be found and mined. Current practices for mining oilsands is fragmentation and loading by shovels, and haulage by truck for crushing and slurry preparation. Orebodies are heterogeneous, and so oilsands composition is quite a variable mixture of bitumen, clay fines, sand and water. Oilsand grade, a term used to describe the concentration of bitumen, is also highly dependent on where in the orebody the oilsands originate. The truck and shovel method employed results in continual changes in grade being fed to the process.

Previous mining methods used parallel process trains with considerable blending of dry

ore. A conditioning step was added to liberate the bitumen from the oilsand, which was delivered using conveyers. The oilsand was fed into tumblers, along with water, steam and additional chemical agents. The rotation of the tumbler helped to break up the ore and aerate the liberated bitumen, which was then fed to screens to remove any oversized material. The slurry stream was then sent by pipeline for separation.

A second and more efficient method uses a hydrotransport pipeline to transport the ore from the mine. The extent of stock piling is reduced, where only a small surge pile develops. Ore ageing is found to have detrimental effects on oilsands processing, and so smaller stock piles are desired [26].

Oilsand is first passed through a crusher and fed using conveyers to a mixing box which combines the oilsand with water, air, surfactant and caustic (or other process additives). Hydrotransport has the added benefit of performing the conditioning step while the slurry is pumped. The turbulent flow within the pipeline aids in lump digestion, bitumen liberation and air attachment. Once the material arrives at the plant, it is fed directly to separation.

The liberation step separates bitumen from the sand and aeration creates a density difference between aerated bitumen and water. The difference in density amongst the three main species is then exploited using gravity separation. Bitumen and sand are separated from process water and fine solids using a number of gravity separation vessels. The oilsand is fed into the middle of the first and largest vessel, the primary separation vessel (PSV), which performs the majority of the separation. A bitumen rich stream (froth) floats off the top of the vessel; solids drop to the bottom (tailings); and a mixture containing mostly water resides in the middle of the vessel (middlings). The middlings and in some processes the tailings streams are combined and fed to additional separation units, referred to as secondary separation, which are vessels or mechanical flotation cells. In general, the bitumen rich streams from both primary and secondary separation are combined and sent downstream.

The mixture of sand and water, with fine solids, produced by the separation processes is then pumped to a settling pond, where the water and sand separate, again using gravity separation. The clarified water from the top of the pond is recycled back to the process. Fines concentrate at the bottom of the pond, and are treated for eventual final deposition

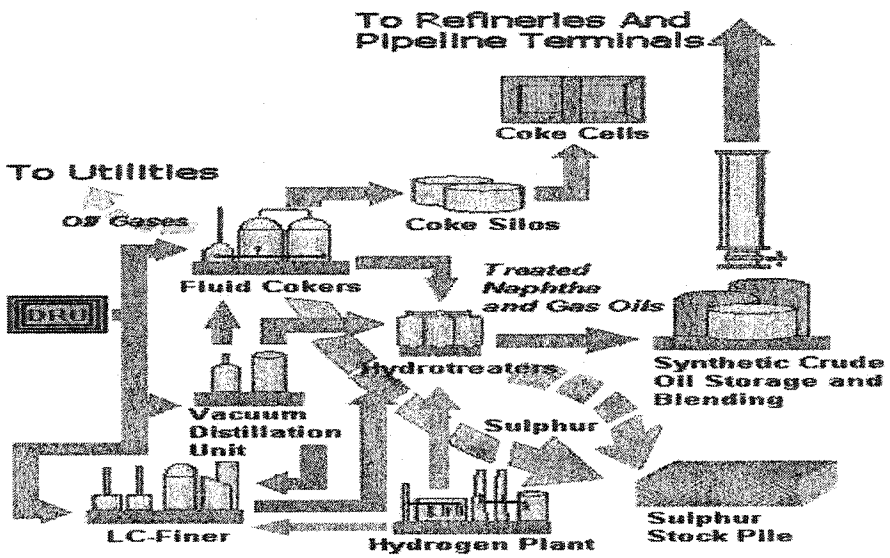

Figure 1.2: Upgrading schematic [26]

and reclamation.

At Syncrude, the bitumen rich streams are combined and diluted using naphtha, to ease in pumping the highly viscous bitumen to downstream processes. The diluted bitumen is then fed to a series of inclined plate settlers and centrifuges to remove any remaining water and fine solids. The bitumen/naphtha mixture is then sent to the diluent recovery unit to remove the naphtha. Any remaining impurities in the naphtha are removed, and the naphtha recycled. The bitumen is then sent to upgrading.

Figure 1.2 shows the upgrading processes. The LC-Finer processes a mixture of bitumen from the diluent recovery unit, by hydrocracking it and sending it to the hydrotreaters.

The vacuum distillation unit takes off some of the high quality sweet oil, and then breaks the hydrocarbon mixture up, feeding the quality hydrocarbons to the hydrotreaters. Heavier hydrocarbons are sent to Fluid Cokers. In the fluid cokers, bitumen is cracked into synthetic crude oils, fuel gas and coke. The synthetic crude oils are sent to the hydrotreaters and the off-gases are sent for further processing. The coke is burnt as fuel and any leftover coke is stockpiled.

The off-gases produced during fluid coking are stripped of hydrogen sulphide in the amine plant. The resulting sweet gas is sent to storage and blending, and is eventually put into the pipeline. Natural gas and steam are combined and fed to a reformer, which

produces hydrogen and carbon dioxide. The carbon dioxide is removed and the hydrogen sent to the hydrotreaters.

The hydrotreaters convert the feed into higher value products, using heat, pressure and hydrogen. Any impurities are stripped using naphtha, and the now sweet gas is sent to tankage and sent by pipeline for refining, primarily into transportation fuels.

All sulphur produced in upgrading is stored in solid blocks near the mine, until sold as a co-product.

1.1.2 Extraction

Primary separation is the first step in processing the mined oilsands. Slurry feed to the vessel generally has a density of about $1450 \mathrm{kg/m^3}$ with an average composition of 7% aerated bitumen, 43% water and 50% solids by weight. The vessel is cylindrical in shape with the exception of the conical section near the bottom. A PSV has an approximate residence time of 45 minutes. Many factors affect the separability of the bitumen from the oilsands, including [33]:

- ore grade
- percent fines
- particle size distribution (of bitumen droplets)
- clay mineralogy and surface activity
- bitumen chemistry
- surfactant concentration (natural and synthetic)
- temperature
- conditioning time (with respect to completeness of bitumen liberation and aeration)
- process water chemistry (pH, bicarbonates, monovalent & divalent ions)
- connate water chemistry

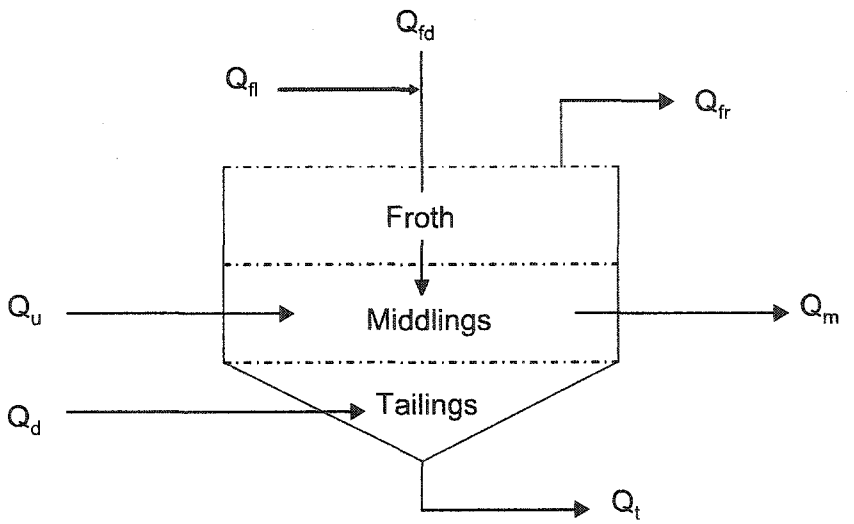

Figure 1.3: PSV schematic

- bulk fluid characteristics (viscosity, density)
- hydrodynamics within the PSV

In this work, emphasis is placed on the first three factors: ore grade, percent fines and particle size distribution. There are a number of theories as to how ore grade and percent fines effect the particle size distribution of the bitumen particles [33]. In general, lower grade and a high concentration of fines result in lower recovery.

Figure 1.3 shows a simple schematic of the PSV, with three layers of well mixed components. The layers are referred to as the froth (top), middlings and tailings (bottom) layers. The bitumen rich froth layer generally contains a froth quality ratio of approximately 60% bitumen, 10% solids and 30% water by weight, but these are highly dependent on the ore feed and process performance. In this layer it is desirable to keep the concentration of water as close to 30% as possible. A water concentration of 35% is considered the maximum, as higher water content increases the load on downstream separation processes. The froth is removed from the vessel into a weir, from which the froth is sent downstream for further processing.

Middlings are withdrawn from the vessel for further processing to recover those bitumen particles that did not report to the froth layer. For poor ores, the rate of the middlings

withdrawal must be increased to account for the increase in fines. This is a control on viscosity, where more flood water is added and a greater load is placed on secondary flotation. It is desirable to have as high a density as possible within the middlings layer to facilitate separation; however, with higher densities comes higher viscosities. Increases in viscosity of the layer can result in actual gelling of the vessel, when thixotropic clays create such a high viscosity that buoyant forces are insufficient to overcome viscous forces. As a result operation is carried out at lower densities.

The middlings withdrawal stream is further processed in secondary separation vessels. The froth recovered from these cells contains roughly 24% bitumen, 59% water and 17% solids by weight. The froth streams are combined with that from primary separation and are sent for further processing downstream. The high concentrations of solids and water in the secondary recovery froth increase the load on the downstream inclined plate settlers and centrifuges. Therefore, it is desirable to maximize the amount of bitumen recovered through primary separation.

A high concentration of solids, mixed with water and small amounts of bitumen, are removed from the bottom of the conical section of the PSV to be pumped into tailings ponds. In the tailings ponds, the solids are allowed to settle out and the clarified water is recycled. The high concentration of solids within the tailings withdrawal pipeline introduces another operational constraint. The velocity of the slurry in the tailings pipeline must be chosen such that it is greater than the minimum deposition velocity, which is the minimum flow rate that prevents sand from settling out in the pipeline. Settling of sands within the pipeline will eventually lead to a blockage, resulting in a process upset.

1.1.3 EXP2000 Pilot Plant

The EXP2000 pilot, located at the Syncrude Research Centre, is a scaled down version of the oilsand extraction processes. Pilot plant studies provide alternative means of performing otherwise costly experiments on the large scale process. A schematic of the Syncrude extraction pilot is shown in Figure 1.4. This thesis focuses on the development of optimal control strategies for the PSV of the EXP2000. For the remainder of this work, references to the PSV pertain to the pilot plant separation circuit shown in Figure 1.4. This,

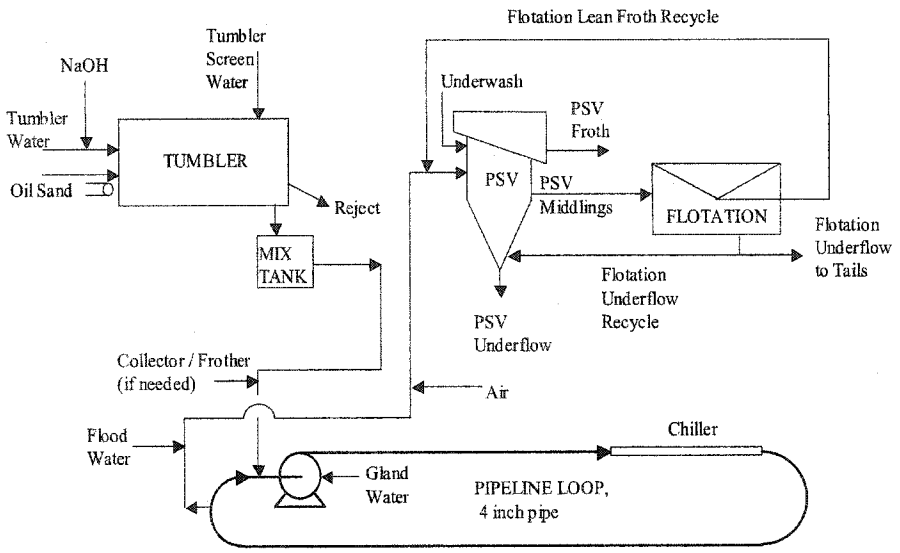

Figure 1.4: EXP2000 Process Schematic [25]

however, in no way limits the application of the results of this work.

1.2 Problem Definition and Motivation

The liberation and separation of bitumen from the solids can be argued to be the most important step in oilsands processing. Currently the control strategy employed does not use any sort of automated control structure, with control action being taken by the operators to ensure stable operation. By using information about important process parameters before or during process upsets, the operator can be assisted to make the appropriate control interventions.

The implementation of an optimal control strategy could increase the amount of bitumen that is recovered in primary separation, and overall recovery of the process. Furthermore it is desirable to maximize primary froth recovery, as the streams from secondary recovery contain greater amounts of solids and water. Maximizing PSV froth recovery will reduce the load placed on the downstream separation processes, as the high quality froth from primary separation requires less processing and energy to remove remaining solids and water. This will be of great importance for low grade ores where the presence of fines greatly hinders the amount of bitumen reporting to the froth, increasing the load to

secondary separation.

The PSV is described as being in constant flux, never reaching steady state operation [33]. For this reason dynamic modelling is expected to provide a more realistic representation than steady-state modelling.

Optimization of a dynamic model (*i.e.* a model involving differential or integral equations) using standard dynamic optimization techniques produces trajectories that are highly erratic. For many industrial processes, these input trajectories cannot be implemented using existing control structures, and so they go unused. Implementing these trajectories for processes where operator intervention alone is the method of process control may be undesirable or impossible. This work will investigate methods for developing input trajectories which are easily implemented.

1.3 Scope and Objectives

This work begins by developing a model for a gravity separation process, using the framework presented by Masliyah *et al.*[32], and the constitutive relationships used by Forbes [28]. Optimal trajectories are then found for changes in the feed ore grade. Due to the plug flow nature of the feed, step changes in ore grade are considered. The step changes are chosen to resemble those that are found to frequently occur in practice.

Simulations are conducted to verify that the model behaves as expected in practice; however, further model validation is required and is outside the scope of this work'. The model is then used to develop optimal input trajectories using dynamic optimization.

The open-loop control practices currently used to control the PSV require that the input trajectories generated using dynamic optimization techniques be easily implemented. For this reason a new optimization approach is proposed, where the trajectories generated are limited to paths, that operations personnel can easily implement either manually or within existing automation systems. In this thesis, trajectories are limited to combinations of step and ramp functions, which are easily programmed into existing distributed control systems (DCS).

Input restriction will also provide a means of comparing existing control structures with higher performance controllers. Sufficient differences between the restricted and

unrestricted problems may provide insight into how much may be gained, by changing control practices.

The method is first applied to a few benchmark problems, examined frequently throughout literature, and then applied to the PSV model. The development of these restricted input trajectories are the first step to providing optimal operating guidelines for operations personnel.

The comparison of the restricted and unrestricted input trajectories are also used to analyze the benefits of adopting some sort of closed loop operation. Whether a sophisticated controller structure should be adopted depends on the relative gains for each of the input trajectories. The method is applied in numerical experiments of both common and problematic grade transitions.

2

PSV Modelling and Simulation

This section looks at the development of the dynamic model for the PSV. The model is then prepared for simulation, and fit to experimental data from Syncrude pilot plant transient experiments.

The modelling of the PSV follows that of the model developed by Masliyah *et al.* [32], which was the basis of the work by Forbes [28]. The model proposed here uses the same physical modelling practices as those used by Masliyah; however, the simplicity of Forbes model is desirable for this work. Dynamic models for use in dynamic optimizations should contain the smallest number of equations, while still accurately describing the process phenomena.

In this model the PSV is broken up into three different, distinguishable levels: froth, middlings and tailings. Each layer is modelled as if it comprises of a continuous medium, with interactions between the froth/middlings and middlings/tailings. Particles are modelled using steady-state settling relationships (Stokes law), in combination with hindered settling models for suspensions of particles. The model consists of material balances and constitutive relationships, which can be written as a system of

differential/algebraic equations (DAE). Such DAE systems require specialized methods for simulation. The model equations contain hybrid dynamics (continuous/discrete behaviour), requiring further special handling.

This chapter presents the PSV model, followed by the approach and relevant material that is pertinent for accurate simulation. The chapter concludes by conducting simulations of the process, and provides a verification of the model.

2.1 Process Model

Before discussion of the mathematical modelling, the following assumptions are stated. Each layer is well mixed, where the froth/middlings interface is dynamically modelled, and the middlings/tailings interface is assumed to be stationary as is generally found in practice. Throughout the entire vessel one-dimensional flow is assumed. Particle flow across the middlings/tailings interface is limited to the downward direction, assuming that once a particle moves to the tailings it is trapped in this layer until removed by the underflow. At the froth/middlings interface particles are allowed to flow from the middlings to the froth, and vice versa, to account for the dynamic interface. Hindered settling correlations are used within the middlings layer to describe the movement of particles.

The use of steady-state settling equations is a large assumption; however, this is the only current means of describing particle movement. This model does not include the effects of caustic addition, temperature, and vessel geometry which are not expected to effect the results appreciably, as temperature and chemical concerns mainly affect the PSD of the feed.

Three species are present within the vessel: aerated bitumen, solids (including fines) and water. The particle size distributions for the aerated bitumen and solids are represented using three particle sizes. Aerated bitumen and coarse solid particles are assumed to be spherical; whereas, the fine solids are comprised of clay platelets. The aerated bitumen droplets and solids entering the vessel are assumed to have constant density and dimension. The density of the water is assumed to be constant. The viscosity of the the middlings layer is assumed to be that of water, for the purposes of the settling models.

The material balance of a species can be found by using this general form of a mass

balance.

$$(Accum.of Material) = (Material In) - (Material Out) + (Material Generated) \tag{2.1}$$

In this case there is no material generation, as there are no chemical reactions occurring in this system.

The inputs (manipulated variables), to the process model include the middlings, tailings and flood water flow rates. Outputs variables include the bitumen, water and solid mass compositions in the froth, middlings and tailings outlet streams. The measurement of these outputs online is currently not possible, and these must be inferred.

Downward movement of a species is taken as the positive direction. Additional equations are added to account for the non-plug flow behaviour of the EXP2000 extraction circuit. The froth layer is considered first. All equations presented below were taken from the model developed by Masliyah *et al.* [32], unless otherwise stated.

2.1.1 Froth Layer

The volume of the froth can be described using the following differential equation.

$$\frac{dV_f}{dt} = v_I A \tag{2.2}$$

The volume of the froth, V_f, depends solely on the velocity of the interface, assuming that the top of the froth is fixed. The mass balance for particle j in the froth layer is described by:

$$\frac{d\left(\rho_j \alpha_j^f V_f\right)}{dt} = \rho_j \left(S_j - Q_f \alpha_j^f\right) \tag{2.3}$$

$$S_j = \begin{cases} -\alpha_j^m (v_j^m - v_I)A, & v_j^m - v_I < 0 \\ -\alpha_j^f (v_j^m - v_I)A, & v_j^m - v_I \geq 0 \end{cases} \tag{2.4}$$

There are only two flows within the froth layer, that leaving the top of the vessel and that entering from the middlings layer. The flux from the middlings to the froth is described by S_j where two different expressions in equation 2.4 describe the flow. If the interfacial velocity is found to be greater than the particle velocities, then flux occurs from the froth to the middlings, and *vice versa*.

Applying the chain rule to equation 2.3 and using equation 2.2 while assuming constant density, the material balance can be converted into the following volume balance equation.

$$\frac{d\alpha_j^f}{dt} = \frac{1}{V_f}\left(S_j - Q_f \alpha_i^j\right) \tag{2.5}$$

$$S_j = \begin{cases} -\alpha_j^m v_j^m A + v_I A\left(\alpha_j^m - \alpha_j^f\right), & v_j^m - v_I < 0 \\ -\alpha_j^f v_j^m A, & v_j^m - v_I \geq 0 \end{cases} \tag{2.6}$$

Where the j^{th} particle stands for either bitumen or solid particles.

The equation for the carrier fluid volumetric fraction is developed in the same fashion as above. Here the following algebraic relationship is used to describe the motion.

$$\alpha_w^f = 1 - \sum \alpha_j^f \tag{2.7}$$

where the set $\{j\}$, again represents all the particles present within the vessel. The introduction of the dynamic interface results in a model that contains discrete events and in its present form is described as a hybrid system. Hybrid systems exhibit both continuous and discrete behaviour. Here the continuous time nature of the differential equations is combined with that of discrete changes in the flux across the froth/middlings interface (*i.e.* S_j). During numerical solution of these equations it becomes necessary to find exact instances where discrete changes occur, to remove errors incurred by overstepping. Methods for dealing with these types of equations will be discussed in section 2.2.2.

2.1.2 Middlings Layer

The equation for the volume of the middlings is characterized in the same manner as above, in the opposite direction. An increase in the froth layer has an equal decrease in the middlings layer. Like the froth volume, the middlings volume depends solely on the movement of the froth/middlings interface.

$$\frac{dV_m}{dt} = -v_I A \tag{2.8}$$

The volume balances for the middlings are found in the same manner as above with additional terms included for the feed, middlings withdrawal and tailings layer interactions.

$$\frac{d\alpha_j^m}{dt} = \frac{1}{V_m}\left(Q_{fd}\alpha_j^{fd} - \lambda_j Q_m \alpha_j^m - \alpha_j^m v_j^T A + S_j\right) \tag{2.9}$$

$$S_j = \begin{cases} v_j^m \alpha_j^m A, & v_j^m - v_I \leq 0 \\ v_j^m \alpha_j^f A + v_I A(\alpha_j^m - \alpha_j^f), & v_j^m - v_I > 0 \end{cases}$$

In the above equation there are terms describing both motion into and out of the layer. Feed is injected into the middlings layer, and a term for the removal of material from the middlings is included as well (Q_m). The remaining two terms are the fluxes to the froth and tailings layers. Middlings correction factors λ_j in both the Masliyah and Forbes models account for differences between concentrations found in the layer and those found in the middlings withdrawal stream.

The presence of the middlings correction factors λ_j for the bitumen and solids particles requires an additional equation to ensure volume continuity in the middlings outlet stream.

$$\alpha_w^m \lambda_w + \sum \alpha_b^m \lambda_b + \sum \alpha_s^m \lambda_s^m = 1 \tag{2.10}$$

Development of the dynamic water balance proceeds in the same manner as for the particles; however, the following algebraic relationship will be used.

$$\alpha_w^f = 1 - \sum \alpha_j^m \tag{2.11}$$

Again we see a set of hybrid dynamical equations that must be addressed before simulation can proceed.

2.1.3 Tailings Layer

The equations for the tailings layer are greatly simplified compared to those of the froth and middlings layer due to the static interface. The boundary of this layer is assumed to be fixed, therefore no dynamic relationship is required for the volume of this layer. The particle balance for this layer is shown in equation 2.12.

$$\frac{d\alpha_j^t}{dt} = \frac{1}{V_t}\left(\alpha_j^M v_j^t A - Q_t \alpha_j^t\right) \tag{2.12}$$

The algebraic water balance is:

$$\alpha_w^t = 1 - \sum \alpha_j^t \tag{2.13}$$

The above equations both contain the dynamic material balance and volume balance equations used in each layer. Figure 1.4 shows there is mixing of the feed prior to the PSV. The assumption that the feed is plug flow does not hold for the EXP2000 and so feed equations must also be added to the model.

2.1.4 Feed Equations

Simple first order filters were applied to the feed. The tumbler is found to exhibit plug flow; however, the mixing tank behaves as a continuous stirred tank (CST). The following equations were added for the feed.

$$\frac{d\alpha_j^{fd}}{dt} = \frac{Q_{fd}}{V_{mix}}(\alpha_j^{ore} - \alpha_j^f d) \tag{2.14}$$

The parameter V_{mix} may be taken from literature; however, here an effective volume for both the tumbler and mixer is estimated using the parameter identification procedure described in Appendix A.

2.1.5 Constitutive Relationships

Settling models are used to discuss the movement of particles across their respective interfaces. In the above dynamic equations settling velocities of the particles were converted to volumetric fluxes using equation 2.15.

$$u_j^i = \alpha_j^m(v_j^i + v_w^i) \tag{2.15}$$

where i represents the interface and j the species. The above equation shows that the flux is a function of both the relative velocities of the species, as well as the bulk flow. Fluxes moving from the middlings to the tailings are constrained to be positive, or zero, to satisfy the assumption that once a particle moves to the tailings layer it remains there until removed from the vessel. The opposite is true for particle movement to the froth, where fluxes are constrained to be negative values.

The relative velocities of the particles are determined using the hindered settling model of Forbes [28], which includes various models that take into account particle shapes and interactions. The relative settling equation (2.16), developed by Swanson [45] [46], includes factors for different shaped particles within the suspension.

$$v_j^{unhindered} = \frac{\sigma_j(4/3gd_i^2(\rho_j - \rho_m))}{\theta_j(2d^{3/2}(g\rho_j\rho_m/3)^{1/2} + \sqrt{48}\beta_j v)} \tag{2.16}$$

The parameters θ and β are correction factors in the settling relationship defined by Swanson, which correct for the non-spherical shapes of particles.

Concha's correlation (equation 2.17) for hindered settling in a suspension was used to account for the interaction between the different species [19].

$$\frac{v_j^{corrected}}{v_j^{unhindered}} = \frac{\left(1 - 1.45\sum \alpha^{particles}\right)^{1.83}}{1 + 0.75^{1/3}} \tag{2.17}$$

An additional relationship is added to the Concha correlation to account for the increased hindering effects of the fines (equation 2.18) [28].

$$\alpha_{apparent}^{particles} = \left(1 + \gamma_1\left(\frac{\alpha_{fines}^m}{\sum \alpha_{particles}^m}\right)^2 + \gamma_2\left(\frac{\alpha_{coarsefines}^m}{\sum \alpha_{particles}^m}\right)^2\right)\alpha_{actual}^{particles} \tag{2.18}$$

Equation 2.18 must satisfy $0 \leq \alpha_{apparent}^{particles} \leq 1$. Methods for enforcing these constraints during simulation are considered in the following section.

Densities of a layer are calculated using the following linear combination of the particle mass fractions:

$$\rho_i = \sum_j^{n_{sp}} x_j^i \rho_j \tag{2.19}$$

where i represents the layer and j the species.

Water velocities through the interfaces are defined using overall material balances on both the middlings and tailings layers.

$$v_w^m = \frac{1}{\alpha_w^m A}\left(Q_{fd} - Q_m - Q_t + \sum_j^{n_p} \alpha_j^m v_j^f\right) \tag{2.20}$$

$$v_w^t = \frac{1}{\alpha_w^m A}\left(Q_t - \sum_j^{n_p} \alpha_j^m v_j^t\right) \tag{2.21}$$

An overall volume balance is also used to determine the volumetric flow coming off the top of the PSV.

$$Q_{fd} - Q_f - Q_m - Q_t = 0 \tag{2.22}$$

By using three overall material balances, the following is inherently stated for each of the three layers:

$$\sum_{j}^{n_p} \frac{d}{dt}\alpha_j + \frac{d}{dt}\alpha_w = 0 \tag{2.23}$$

Consequently evaluation of the dynamic water balances combined with the material balances on the particles produces a set of equations that is no longer linearly independent. The algebraic relationships are used to remove the linear dependence.

The movement of the interface is modelled as a one-dimensional shockwave, as outlined in Wallis [50].

$$\text{Wave Velocity} = \frac{\text{Flux Received} - \text{Flux Removed}}{\text{Volume Fraction Difference}}$$

Mathematically stated the Wallis shockwave equation for a first order of approximation gives:

$$v_I = \frac{\sum_{j=1}^{n_b} \alpha_{b_j}^m v_{b_j}^m - \sum_{j=1}^{n_b} \alpha_{b_j}^f v_{b_j}^f}{\sum_{j=1}^{n_b} \alpha_{b_j}^m - \sum_{j=1}^{n_b} \alpha_{b_j}^f} \tag{2.24}$$

Before the above equations can be simulated, the discrete nature of the froth and middlings differential equations, *i.e.* the hybrid dynamics, must be addressed. Also the presence of sign changing restrictions on the fluxes, as well as that in equation 2.18 must be considered. The model is a set of DAEs which presents challenges for simulation.

2.2 Process Simulation

Before proceeding with the simulation of the model presented in the previous section, it is necessary to recast the equations into a form that can be numerically integrated. The set of equations contains both differential and algebraic equations that must be integrated using only certain types of numerical integration routines. Furthermore, the presence of both continuous and discrete behaviour, and the sign change restrictions on some of the variables each requires further consideration.

2.2.1 Sign Change Restriction

Equation 2.18 and the bounds on the fluxes between layers require that a variable be either positive or negative, but not both. Two methods of managing these sign change restrictions were examined at the cost of adding discontinuities to the model equations. Absolute value relationships like those used in Forbes [28] can be used to achieve the desired result. Equations 2.25 and 2.26 show the absolute value method of constraining the settling velocities to be above and below zero, respectively.

$$v_j^m = \frac{v_j - |v_j|}{2} \tag{2.25}$$

$$v_j^t = \frac{v_j + |v_j|}{2} \tag{2.26}$$

Enforcement of the constraints can also be done through the use of max/min functions. The ease of programming these functions makes this the method of choice; however, neither method was found to affect accuracy, as the two methods make an equivalent discontinuity in the equations.

2.2.2 Discrete Event Handling

Before it is possible to perform the simulation, it is necessary to determine how the discrete events found in the middlings and froth equations will be handled. The combination of continuous equations with discrete events, *i.e.* at certain points in time the set of equations changes. Models that contain a mixture of both continuous and discrete behaviour are termed hybrid systems. Many models can be modelled in this fashion and within the last decade many researchers have begun to focus in this area.

Two of the possible methods include using a hybrid system simulator to perform the simulation, or using some sort of approximation to the true system using either smoothing or discontinuous functions.

Hybrid system simulators use existing numerical integration routines, combined with root solvers to determine where a discrete change in states occurs. The solution method works by integrating the ordinary differential equation (ODE) or DAE system, while monitoring for discrete events [47]. If the occurrence of a discrete event is found, the

integrator backs up until the root is found. Once found the necessary changes to the model are made and the states are reset as necessary. The process of locating when a discrete event occurs can greatly add to the simulation time. There is also the risk that the simulator may fail in finding the correct root, if the governing dynamics of the equations are fast, or the equations are stiff.

Hybrid systems do not have a rich optimization history, and this is the underlying reason why this method was not adopted for the purposes of this thesis. The use of mathematical programs with equilibrium constraints (MPECs) are beginning to receive some attention in the area of chemical engineering, as a possible means of hybrid system optimization [42].

A Sigmoidal function may be used to approximate discontinuities, without losing differentiability of the equation. The addition of the sigmoidal function also removes the necessity of finding the exact instance where a discrete event may occur in the analogous hybrid system. This reduces the simulation time, as well as allows integration using existing algorithms. Sigmoidal functions are an approximation, and certain systems may not be accurately modelled using this manner. For the case of the PSV, the use of a sigmoidal function for the transition between different events is considered to be appropriate, as the system being described here has slow dynamics. The sigmoidal function takes the following forms; 2.27 and 2.28, and were taken from Yin *et al.* [53].

$$\varsigma^{+}(x) = \frac{1}{1 + a(e^{(x-x_o)})^n} \tag{2.27}$$

$$\varsigma^{-}(x) = 1 - \frac{1}{1 + a(e^{(x-x_o)})^n} \tag{2.28}$$

where n and a are tuning parameters which can be used to change the shape of sigmoid function. Equation 2.27 is an increasing sigmoid, whereas equation 2.28 is a decreasing sigmoid. Figure 2.1(a) and 2.1(b) shows these sigmoidal functions for different values of n and a.

For some types of problems it may be possible to use max/min functions to exploit discrete events of a certain form. These functions add discontinuity to the problem, but they are much simpler to implement than sigmoidal functions. For the dynamic equations listed above, only discontinuity in the derivatives occurs, as both expressions are equivalent during a discrete change in the model equations. The equivalence during a discrete event

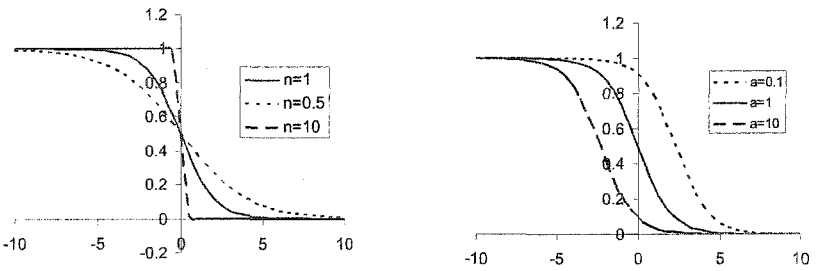

(a) Response of Sigmoidal Function to Changes in n

(b) Response of Sigmoidal Function to Changes in a

Figure 2.1: Dependence of Sigmoid Curve on Design Parameters

makes the use of max/min functions possible. The addition of discontinuous functions (max/min) can result in inaccuracies in the solution, as they incur errors due to overshooting the discrete changes, which a hybrid simulator would locate. To minimize the error, high simulation tolerances can be used, at the expense of smaller step sizes and longer solution times.

Either max/min functions or sigmoid functions can be used in the PSV model equations. Max/min functions are adopted for their ease of use. As well, the solution times for numerical integration are small and the use of high tolerances is not a problem for a well-behaved dynamical model.

2.2.3 Systems of Differential/Algebraic Equations

With the set of equations presented above, it is not possible to formulate the problem as a set of ordinary differential equations (ODE). This set of ODEs and algebraic equations results in what is referred to as a set of differential/algebraic equations (DAE). The section begins by discussing the types of DAEs, followed by their numerical solution.

DAEs are difficult to solve, as the presence of equality constraints may relate different states together, reducing the degrees of freedom. Numerical integration of DAEs requires that consistent initial guesses to the problem be found prior to solution. For some cases the number of initial conditions is less than that of a similar ODE problem, as a result of the relationships between variables. The problems become harder to solve as the relationships

between variables become more complicated. The presence of the algebraic relationships may cause variables to move in directions different than those predicted using conventional numerical methods. Not all sets of DAEs suffer from this problem, and some problems can easily be solved using common numerical methods.

The index of the DAE is a measure to predict how difficult solution will be [13]. This index is defined as the number of differentiations that are necessary to reduce the DAE to an ODE. For high index DAEs, taking the derivatives of the algebraic equations may be an error prone task, and not necessarily the best way of solving the problem. Research is continuing to efficiently integrate DAE problems. Methods for dealing with higher index DAE systems become dependent on the structure of the equations that need to be solved. There are different methods being proposed for handling higher index DAEs, such as the method of dummy derivatives, sequential regularization methods, and index reduction using automatic differentiation ([40] [2] [16]). The need for one of these alternative solution methods is dependent on the set of DAEs.

The method of index reduction is the most common method used to reduce high index DAE problems to a set of equations that can be solved using conventional numerical techniques. Beginning with an explicit DAE:

$$\begin{aligned} \dot{\mathbf{x}} &= \mathbf{f}(\mathbf{x}, \mathbf{z}, t) \\ \mathbf{0} &= \mathbf{g}(\mathbf{x}, \mathbf{z}, t) \end{aligned} \tag{2.29}$$

and differentiating $\mathbf{g}$ with respect to the dependent variable t gives:

$$\begin{aligned} \dot{\mathbf{x}} &= \mathbf{f}(\mathbf{x}, \mathbf{z}, t) \\ \dot{\mathbf{z}} &= \mathbf{g}_{\mathbf{x}}(\mathbf{x}, \mathbf{y}, t)\dot{\mathbf{x}} + \mathbf{g}_{\mathbf{y}}(\mathbf{x}, \mathbf{y}, t)\dot{\mathbf{y}} + \mathbf{g}_{t}(\mathbf{x}, \mathbf{y}, t) \end{aligned} \tag{2.30}$$

where $\mathbf{g}_i$ is the Jacobian of the vector of equations $\mathbf{g}$ with respect to the vector of variables i.

If the Jacobian $\mathbf{g}_\mathbf{z}$ is non-singular, meaning the set of equations is now a set of ODEs, then the original DAE system is index one; however, if the $\mathbf{g}_\mathbf{z}$ is singular, then the equations are rearranged and put back into 2.29 and differentiation continues. Index reduction is generally a method of last resort.

Hessenberg forms are the most common class of DAEs. The Hessenberg index-1 form is shown in equation 2.31.

$$\begin{aligned} \dot{\mathbf{x}} &= \mathbf{f}(t, \mathbf{x}, \mathbf{z}) \\ \mathbf{0} &= \mathbf{g}(t, \mathbf{x}, \mathbf{z}) \\ det(\mathbf{g_z}) &\neq \mathbf{0} \end{aligned} \tag{2.31}$$

For this case the above form is described as a semi-explicit DAE system of index 1. The above problem is the simplest of the different types of DAEs as they are very closely related to implicit ODEs. In most cases it is possible to first solve for the algebraic variables, and then substitute into the ODE subsystem. This results in a general ODE system to be solved. This method is not recommended for numerical simulation [1], as the process can be complicated and erroneous.

Further forms include the Hessenberg Index-2 and -3, shown in equations 2.32 and 2.33.

$$\begin{aligned} \dot{\mathbf{x}} &= \mathbf{f}(\mathbf{x}, \mathbf{z}, t) \\ \mathbf{0} &= \mathbf{g}(\mathbf{x}, t) \end{aligned} \tag{2.32}$$

$$\begin{aligned} \dot{\mathbf{x}} &= \mathbf{f}(\mathbf{x}, \mathbf{y}, \mathbf{z}, t) \\ \dot{\mathbf{y}} &= \mathbf{g}(\mathbf{x}, \mathbf{y}, t) \\ \mathbf{0} &= \mathbf{h}(\mathbf{y}, t) \end{aligned} \tag{2.33}$$

These problems become harder to solve, as these forms contain hidden constraints on the states, as well as have the effect of reducing the expected number of initial conditions necessary. Due to the increased complexity of higher index DAE's it may become necessary to use those techniques referenced earlier, or an index reduction technique.

For index-1 and Hessenberg index-2 DAEs the methods found effective include backwards differentiation formulae (BDF) [29], and implicit Runge-Kutta. The BDF are the favoured method due to their ease of implementation. The general method can be stated as follows.

$$\sum_{i=0}^{k} \alpha_i y_{n-i} = h\beta_o f(t_n, y_n) \tag{2.34}$$

where k represents the number of past values that are to be used. A table of coefficients for the different orders can be found in any numerical methods text.

The PSV model presented above (Eq. 2.2:2.24) is of type Hessenberg Index-1 form. It should be noted that the Jacobian for the algebraic constraints with respect to the algebraic variables was found to be invertible.

For the solution of DAEs, a consistent initial guess is required before the numerical solution can proceed. The following section deals with this problem.

2.2.4 The Consistent Initial Guess Problem

For semi-explicit index-1 DAE's, it is not the numerical integration which is the major computational effort, as a fifth-order BDF formula is generally used for this problem. Major computational effort must be used to determine the consistent initial conditions, which can be done by solving the set of equations. To simplify the problem, steady-state conditions are imposed and all derivative terms are set to zero. The resultant model takes the following form.

$$\mathbf{0} = \mathbf{F}(\mathbf{x})$$

Applying this method to the PSV model equations, we have a set of nonlinear equations (*i.e.* $\mathbf{F}(\mathbf{x})$), with the presence of discontinuities due to the max/min functions.

The presence of these discontinuous elements added to the difficulty of solving these equations, and solution of the original set of equations was difficult. To simplify the problem, operating regimes were chosen away from those areas prone to discontinuities.

To solve this problem the Newton-Raphson method was employed:

$$\nabla\mathbf{F}(\mathbf{x}_i)\mathbf{x}_{i+1} = -\mathbf{F}(\mathbf{x}_i) + \nabla\mathbf{F}(\mathbf{x}_i)\mathbf{x}_i \tag{2.35}$$

where $\nabla\mathbf{F}(\mathbf{x}_i)$ is the Jacobian of $\mathbf{F}(\mathbf{x})$ at iteration i. The problem can be solved using a variety of methods including Gauss elimination or other decomposition techniques [17].

Once a consistent initial guess is found, numerical solution of the equations can be conducted using those methods presented in the previous section.

2.3 Simulation Verification

The model presented above contains physical and empirical parameters which must be identified. Identification of these parameters can be done either through literature or using plant data. Experimental parameter identification involves two steps: 1) develop a set of experiments and 2) evaluate the parameters such that they optimize a desired objective, with repetition if necessary.

Appendix A discusses the second step of the parameter identification problem, where the parameters are determined to minimize the square of the residuals. Parameter identification of the PSV model equations with transient EXP2000 data was found to be poor. The experimental procedure was found to have insufficient excitation for identification purposes, as a single pulse function was used. Most compositions showed no response to the step in feed ore. The errors associated with the composition and recovery measurements made many compositions appear constant. Measurements made using the EXP2000 have approximately a 5% relative error. These errors are a result of a number of contributing factors; however, analysis errors associated with the samples are the major contributor. Trends were found to occur only in the middlings and tailings layers. For parameter identification to be successful, more definite changes in the outputs will be necessary to adequately fit the model.

The use of recycle streams from secondary flotation units, not included in the model, are expected to have effects on the results. The presence of the recycle stream affects the particle size distributions, but those are not considered in this work.

The parameters identified using the method of Appendix A will be used, for lack of better values. In current literature, the parameter estimates were derived for the Syncrude PSV, and deemed not useful for the EXP2000. For this work, bringing the outputs close to that in the actual EXP2000 is sufficient, where additional work is needed to validate the model.

The model is simulated using steps in commonly found feed ores. The ore recipes are tabulated in Appendix C in Tables C.1:C.3, where particle size distributions were determined using the method in Forbes [28].

To verify that the model behaved properly the PSV model was then simulated starting

Parameter	Magnitude	units	Comments
λ_b	0.3273		Bitumen Middlings Withdrawal Factor [28]
λ_s	1.257		Solid Middlings Withdrawal Factor [28]
σ_b^f	0.4925		Bitumen Froth/Middlings Settling Factor
σ_b^t	0.3006		Bitumen Middlings/Tailings Settling Factor
σ_s^f	0.0		Solids Froth/Middlings Settling Factor
σ_s^t	0.0, 0.0, 1.0		Solids Middlings/Tailings Settling Factor
ρ_b	0.8, 0.75, 0.7	g/cm^3	Density of Aerated Bitumen
d_b	0.028, 0.058, 0.07	mm	Diameter of Bitumen Bubbles
d_s	7.8, 13.11, 125.0	μm	Diameter of Solid Particles
Qm	0.3685	dm^3/s	Middlings Withdrawal Rate
Qt	0.4227	dm^3/s	Tailings Withdrawal Rate
Q_{fl}	205	g/s	Flood Flow Rate
V_{mix}	415.0	dm^3	Effective Tumbler and Mixing Tank Volume

Table 2.1: Simulation Parameters

with a high grade ore and stepping down in ore grade every 50 minutes. Flood, underflow and middlings withdrawal were kept at their respective levels as listed in Table 2.1. The compositions of the froth, middlings and tailings are shown in Figure 2.2. The froth and middlings trajectories were as expected, where the trajectories of all species followed a first order system, with expected decreases in bitumen and increases in solid concentrations observed. The bitumen tailings trajectories were found to follow a unique path, where during a medium feed ore the equations were dominated by density effects, and for low grade ores the large amount of poorly aerated bitumen droplets resulted in an increased composition. High grade ores were found to have comparable bitumen concentrations in the tailings with low grade ore; a consequence of the higher concentration of bitumen in the feed.

2.4 Summary

A model for the PSV for oilsand processing was developed from a steady-state formulation. The use of dynamic equations (*i.e.* material balances), combined with steady-state relationships to describe the movement of particles is currently the only method used. The independence of the model on temperature, caustic and other chemical additions may affect the separation; however, temperature and chemical effects likely have more effect on

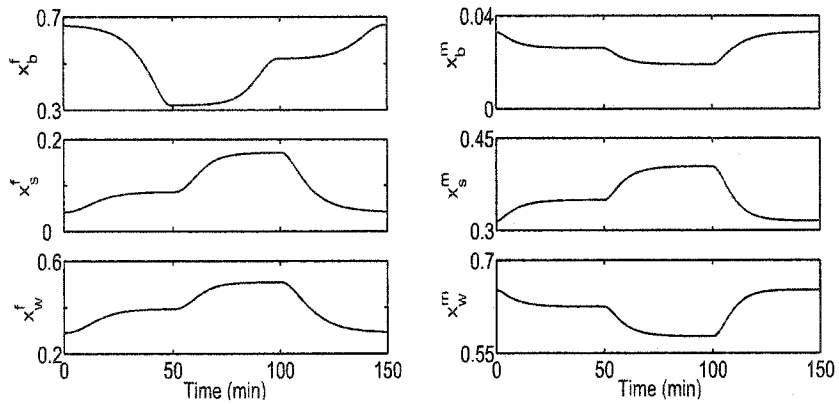

(a) Froth Layer Compositions

(b) Middlings Layer Compositions

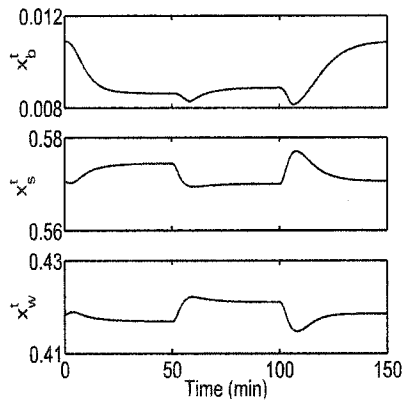

(c) Tailings Layer Compositions

Figure 2.2: Simulation of PSV Model with Steps in Feed Grade

the particle size distributions formed during the conditioning process, than during gravity separation. Overall the model captures many of the important occurring phenomena in the vessel, and remains simple enough for dynamic optimization practices.

3

Optimal Trajectory Planning

This chapter introduces the different methods used for dynamic optimization and begins by providing a discussion of the trajectory optimization problem, as well as providing an overview of the three main areas by which these problems are solved: 1) Calculus of Variations, 2) embedded simulation and 3) discretization methods.

The input trajectories produced using available methods may be highly complex; consequently, implementing these trajectories in process industries, which operate using open-loop control practices, is usually not possible. In this work a restricted form approach to trajectory optimization problems is introduced, where input trajectories are limited to sets of step and ramp functions. Input trajectories of this form are easily implemented using existing Distributed Control Systems (DCS), and can provide immediate results.

Both restricted and unrestricted trajectory optimizations are then applied to three benchmark examples drawn from the dynamic optimization literature, and the effectiveness of the methods is compared.

3.1 Optimal Trajectory Problem

Developing optimal operating policies is of great interest to the process industries. To develop optimal operating policies it is necessary to have a dynamic model of the process. The optimal trajectory problem for a set of DAE can be stated as follows:

$$
\begin{aligned}
&\min_{\mathbf{u}(t)} \quad \Phi\left[\mathbf{x}(t), \mathbf{z}(t), \mathbf{u}(t), t\right] \\
&s.t. \\
&\qquad \mathbf{f}(\dot{\mathbf{x}}(t), \mathbf{x}(t), \mathbf{z}(t), \mathbf{u}(t), t) = \mathbf{0} \\
&\qquad \mathbf{g}(\mathbf{x}(t), \mathbf{z}(t), \mathbf{u}(t), t) = \mathbf{0} \\
&\qquad \mathbf{h}(\mathbf{x}(t), \mathbf{z}(t), \mathbf{u}(t), t) \leq \mathbf{0} \\
&\qquad \mathbf{x}(t)^L \leq \mathbf{x}(t) \leq \mathbf{x}(t)^U \\
&\qquad \mathbf{z}(t)^L \leq \mathbf{z}(t) \leq \mathbf{z}(t)^U \\
&\qquad \mathbf{u}(t)^L \leq \mathbf{u}(t) \leq \mathbf{u}(t)^U
\end{aligned}
\tag{3.1}
$$

Where L and U represent lower and upper bounds on the differential/algebraic states and control variables. Here Φ represents the desired objective to be minimized. The modelled differential equations are contained in $\mathbf{f}$, which can arise from material and energy balances. The equality constraints, $\mathbf{g}$, contain any process constraints or constitutive relationships, such as those describing the motion of particles in a suspension as in Chapter 2. The inequalities, $\mathbf{h}$ are process constraints. The lower and upper bounds on the variables can also be included in $\mathbf{h}$; however, by convention, the bounds are written explicitly in the problem formulation.

Certain inequalities can cause index increases during the optimization process, and care should be taken to minimize the number. In this case, where active inequalities do increase the index, points where the inequalities become active or inactive must be found to improve accuracy. Work by Feehery and Barton [27] discusses the use of dummy derivatives to reduce equality constrained high index DAE problems to index-one form. As well Feehery and Barton propose a method for the dynamic optimization of systems of equations with inequalities which increase the index [27].

Using a method comparable to that of constrained NLPs, the following augmented

objective function (Lagrangian) is used.

$$J = \Phi(\mathbf{x}(t), \mathbf{z}(t), \mathbf{u}(t), t) - \int_{t_I}^{t^F} H dt \tag{3.2}$$

Where the function Φ is the objective function in equation 3.1, and H is referred to as the Hamiltonian, which is defined as:

$$H = \boldsymbol{\lambda}(t)^T \mathbf{f} + \boldsymbol{\mu}(t)^T \mathbf{g} + \boldsymbol{\delta}(t)^T \mathbf{h} \tag{3.3}$$

where $\boldsymbol{\lambda}(t)$, $\boldsymbol{\mu}(t)$ and $\boldsymbol{\delta}(t)$ are the Lagrange multipliers and are functions of time.

Solution of the above continuous time optimization problem can be accomplished *via* optimality conditions. This is known as the Calculus of Variations. Differentiation of the Lagrangian can prove to be a difficult task, and the presence of equality and inequality constraints usually makes using Calculus of Variations intractable.

For these reasons most trajectory optimization problems cannot be solved in this form. Methods have been developed that use an approximation to the above problem. There are two main methods, those which employ an embedded simulation within the optimization, and those which transform the infinite dimensional problem into a finite one and use collocation methods to approximate solutions of the dynamic variables.

3.2 Embedded Simulation

This section explores those dynamic optimization methods that use embedded simulation. The optimizer and simulator operate separately where information is passed between the two when necessary. Dynamic programming, iterative dynamic programming and control vector parametrization are the three main dynamic optimization methods of this type. For all three of these methods, repetitive numerical solution of the equations is required, resulting in the majority of the computational expense.

3.2.1 Dynamic Programming

In Dynamic Programming the overall optimization problem is broken down into similar subproblems. The subproblems are then solved and combined to represent the overall solution. For optimal control these subproblems are derived by breaking the desired time

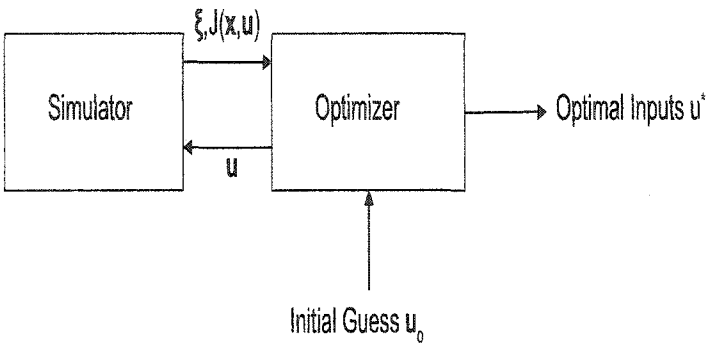

Figure 3.1: Dynamic Programming Flow Sheet

interval up into sections. The optimal inputs for each of the subproblems are then combined to yield the overall optimal operating policy. The method must also link the state values at the subproblem boundaries, termed defect constraints. A visual representation is provided in Figure 3.1 The method begins by supplying an initial guess for the inputs, which is given to the optimizer. The optimizer calls on the simulator to solve the model equations for each of the subproblems, and evaluates the defects ξ between the states, which are equality constraints in the optimization problem. The exchange between the optimizer and simulator occurs until the optimal set of inputs, $\mathbf{u}^*$ is found, that satisfy the defect equality constraints.

Dynamic Programming cannot directly handle problems with path constraints, which limits the number of problems that can be solved using this method. This issue led to the development of many other dynamic optimization techniques, one of the more recent methods is Iterative Dynamic Programming.

3.2.2 Iterative Dynamic Programming

Iterative Dynamic Programming (IDP) developed by Luus [37], builds on the original method of Dynamic Programming. IDP follows an identical structure to that shown in Figure 3.1, where modifications are made only in the logic performed within the optimizer.

The desired time interval is broken down into m sub-intervals as done for Dynamic Programming. At the beginning and end of the intervals, termed grid points, each state is allowed to take on N values within a range x_i. The same is done for the controls, where

P values for each input are chosen at each grid point within a range u_i. Clipping is used to enforce path constraints on the controls if necessary. The optimization then begins by using the initial guess to determine the center points for the states and controls. The N and P points for each of the states and controls, as well as their respective ranges, are then chosen at each grid point.

Beginning with the last interval $[M\ M+1]$ each state grid point is simulated using each of the inputs values in u, and the objective is then evaluated for each. The best control policy is then chosen which gives the best objective value.

Stepping backwards to the interval $[M-1\ M]$, again each of the states are evaluated using all the controls. Once the optimal policy for this interval is determined it is unlikely that the states calculated through simulation at M^{th} grid point will exactly match with those chosen. So the state closest to that found using the simulation is chosen and the optimal policy from this state is used to continue the simulation to the final time.

The procedure continues for the remaining time intervals in the backwards direction until the first time interval is reached, ending the first iteration. Successive iterations are done in the same fashion, with the optimal states and inputs at the previous intervals used as the center points and a reduction in the size of the regions for u and x to remove the discontinuity in the states between intervals to a desired tolerance.

The method presented above is able to handle path constraints, but does not scale well with problem size. Large scale industrial problems generally have large numbers of states and inputs associated with them, greatly increasing the computational load, resulting in large solution times, and reducing the range of applicability of the method.

3.2.3 Control Vector Parametrization

Control Vector Parametrization (CVP) is another embedded simulation technique which can be used to solve dynamic optimization problems. The method is different from both Dynamic and Iterative Dynamic Programming. This method has been used to solve various dynamic optimization problems in the literature [51][38]. The method works by

parameterizing the control trajectory

$$u_i(t) = \sum_{j=1}^{k} a_{i,j}\phi_{i,j}(t - t_{i,j}) \tag{3.4}$$

where here i represents the i^{th} control variable, $\phi_{i,j}$ the j^{th} function and $a_{i,j}$,$t_{i,j}$ are the amplitude and switching times of the function, respectively. The parameters $\mathbf{p}$ is the vector set $[\mathbf{a}, \mathbf{t}]$, where $\mathbf{a}$ is the vector containing all of the weights (a_i) and $\mathbf{t}$ is the set of all switching times.

The overall method of CVP is similar to that depicted above for Dynamic Programming, but the control vector $\mathbf{u}$ is replaced by the parameter vector $\mathbf{p}$. The simulation is carried out by converting the vector of parameters into an input trajectory. Along with the model equations, simulation of the adjoint equations (sensitivity) equations with respect to the control parameters may be done to decrease solution times. Termination occurs when the optimal set of parameters $\mathbf{p}^*$ is found by the optimizer. Here the variable ξ relates to path constraint violations, and again is set to zero as equality constraints in the optimization problem.

A few general points are made about control vector parametrization: 1) one function is used during an interval; 2) the method handles singular sets of equations, as the model equations are used for simulation only and 3) evaluation of the adjoint equations can be difficult.

3.3 Discretization Techniques

Discretization techniques are those methods where the continuous time problem is reduced to a finite dimensional optimization problem, by discretizing the time horizon using a set of points. The methods differ only in the approach to the discretization and handling of the approximations to the dynamic states. The two methods discussed here are Direct Transcription and Orthogonal Collocation on Finite Elements.

3.3.1 Orthogonal Collocation on Finite Elements

Orthogonal Collocation on Finite Elements, proposed by Cuthrell and Biegler [21], approximates the continuous time problem by using discrete points in time, termed mesh

or grid points. The resulting finite optimization problem still contains differential states, which must be removed before the dynamic optimization can proceed. This method takes the differential/algebraic states and control variables and approximates their solution using orthogonal polynomial approximations. In their work, Cuthrell and Biegler, used Lagrange interpolating polynomials, which take the following form:

$$\mathbf{x}_{N+1}(t) = \sum_{k=0}^{N} \left[\boldsymbol{x}_k \left(\prod_{j=0,i}^{N} \frac{t - t_N}{t_j - t_N} \right) \right] \tag{3.5}$$

$$\mathbf{z}_N(t) = \sum_{k=1}^{N} \left[\boldsymbol{z}_k \left(\prod_{j=1,k}^{N} \frac{t - t_N}{t_j - t_N} \right) \right] \tag{3.6}$$

$$\mathbf{u}_N(t) = \sum_{k=1}^{N} \left[\boldsymbol{u}_k \left(\prod_{j=1,k}^{N} \frac{t - t_N}{t_j - t_N} \right) \right] \tag{3.7}$$

Where $k+1$ and k represent the orders of the state and control variable Lagrange polynomials, where the roots of these polynomials t_j lie on the mesh points. The Lagrange polynomials have the property that at the mesh points the polynomial reduces to $x_i^{N+1} = x_i$. To simplify the upcoming substitutions, the product term in each of equations 3.5 through 3.7 is replaced by $\xi(t)$, $\tau(t)$ and $\varphi(t)$ for the state, algebraic and control variables, respectively.

Substitution of the Lagrange polynomials into the optimal trajectory problem gives the following optimization problem.

$$\begin{aligned}
&\min_{\mathbf{u}(t)} \quad \Phi\left[\boldsymbol{x}_k, \boldsymbol{z}_k, \boldsymbol{u}_k, t_k\right] \\
&s.t. \\
&\quad \mathbf{f}\left(\sum_{k=0}^{N} \boldsymbol{x}_k \dot{\boldsymbol{\xi}}(t), \boldsymbol{x}_k, \boldsymbol{z}_k, \boldsymbol{u}_k, t_k \right) = \mathbf{0} \\
&\quad \mathbf{g}(\boldsymbol{x}_k, \boldsymbol{z}_k, \boldsymbol{u}_k, t_k) = \mathbf{0} \\
&\quad \mathbf{h}(\boldsymbol{x}_k, \boldsymbol{z}_k, \boldsymbol{u}_k, t_k) \leq \mathbf{0} \\
&\quad \mathbf{x}_k^L \leq \mathbf{x}_k \leq \mathbf{x}_k^U \\
&\quad \mathbf{z}_k^L \leq \mathbf{z}_k \leq \mathbf{z}_k^U \\
&\quad \mathbf{u}_k^L \leq \mathbf{u}_k \leq \mathbf{u}_k^U \\
&\quad \mathrm{k} = 1,\ldots,\mathrm{M}+1
\end{aligned} \tag{3.8}$$

Using the orthogonality of the Lagrange polynomials it is possible to remove the time dependent terms from the problem as $\xi(t_k) = \tau(t_k) = \varphi(t_k) = 1$ at the k^{th} grid point. The problem then reduces to finding the roots of the approximating Lagrange polynomials, or equivalently the values of the states and control variables at the grid points k. The term $\dot{\xi}(t)$ requires the differentiation of a Lagrange polynomial [49].

The above formulation as stated is referred to as the "Global Collocation Method". The method behaves poorly for systems of equations where there are sections of fast and slow dynamics. For high-order polynomial terms, the fast dynamics may be captured adequately; however, the overshoot caused by these higher order polynomials introduces error, and does not approximate the regions of slow dynamics well. The opposite is true for low order polynomials where large approximation errors will accumulate in nodes where the dynamics are fast. For this reason the method is further extended on finite elements.

The problem as stated above is broken up into smaller intervals, where in each interval the Global Collocation method is used. Equality constraints are added to ensure continuity of the states and control variables between finite elements. The solution is therefore composed of a set of polynomial approximations to the solution. The reader is referred to [21] for an complete discussion of the method.

Discretization of the method above depends on the order of the approximating polynomials used. This inflexibility in the number of grid points makes input restriction difficult, and is not used.

3.3.2 Direct Transcription

The Direct Transcription method, as discussed in Betts [10], takes the desired time interval $[t^I t^F]$ and breaks it up into M different intervals, or $M + 1$ points in time (not necessarily equi-spaced). The equations for the optimal trajectory problem are then solved at each of the desired time points (mesh points). The optimal trajectory problem can then be stated

as:

$$
\begin{aligned}
&\min_{\mathbf{u}_k} \quad \Phi\left[\mathbf{x}_k, \mathbf{z}_k, \mathbf{u}_k, t_k\right] \\
&s.t. \\
&\quad \mathbf{f}(\dot{\mathbf{x}}_k, \mathbf{x}_k, \mathbf{z}_k, \mathbf{u}_k, t_k) = \mathbf{0} \\
&\quad \mathbf{g}(\mathbf{x}_k, \mathbf{z}_k, \mathbf{u}_k, t_k) = \mathbf{0} \\
&\quad \mathbf{h}(\mathbf{x}_k, \mathbf{z}_k, \mathbf{u}_k, t_k) \leq \mathbf{0} \\
&\quad \mathbf{x}_k^L \leq \mathbf{x}_k \leq \mathbf{x}_k^U \\
&\quad \mathbf{z}_k^L \leq \mathbf{z}_k \leq \mathbf{z}_k^U \\
&\quad \mathbf{u}_k^L \leq \mathbf{u}_k \leq \mathbf{u}_k^U \\
&\quad \text{k = 1,...,M+1}
\end{aligned}
\tag{3.9}
$$

The system of equations shown in the above formulation still contains derivative and/or integral terms, and cannot be solved in the present form. It is possible to use numerical techniques to evaluate integral terms, and collocation methods to replace the differential variables, where the methods used depend on the equations to be solved and the desired accuracy. The problem is then in a format which can be solved using appropriate optimization solvers. The method can be described by the following steps.

1. Break up time interval $[t_I t_F]$ into M intervals or, $M + 1$ discrete points, which will be referred to as a mesh or grid.

2. Discretize the differential variables and integral equations on the grid.

3. Reformulate and solve using the appropriate optimization technique.

4. Repeat steps 1-3 refining the grid points to obtain an acceptable accuracy.

Mesh refinement is done to improve the accuracy by either using an increased number of grid points, or moving existing grid points to an area where more points are required to effectively capture the dynamics. Increasing the number of grid points increases the size of the optimization problem, thereby increasing the solution time. Improved accuracy may also be obtained by increasing the order of the numerical method used to discretize the

differential variables. Increases in the order corresponds to increases in the computational load (*i.e.* larger number of function evaluations) and again the improved accuracy results in larger solution times.

For problems with discontinuities in the decision variables, or state space changes due to different constraints at different periods of time, the problem can be broken up into individual stages or phases. Additional equality constraints may be necessary to ensure continuity in the certain state or control variables; however this is dependent on the problem.

The optimization problems which result from discretization methods are highly sparse, and this sparsity can be exploited. Calculation of the Jacobian or the Hessian for sparse systems of equations can be done so in a more efficient manner by grouping variables into indexed sets [44].

3.4 Restricted Form

Optimization of transient operations (*e.g.* batch processing, grade transitions, etc.), is crucial to the success of many manufacturers. There is considerable literature on solving these dynamic optimization problems as open-loop control problems. The resulting optimal transition policies are often very irregular and as a result, difficult to implement; and so most operating plants are forced to treat transients in a sub-optimal fashion. A key difficulty with the existing approaches to solving the grade transition problem is that optimal policies are not restricted to take on forms that are readily implementable within the plant. Any general approach to the problem of determining optimal grade transitions must consider the restrictions placed on the allowable form of the input trajectories by the functionality of the plant automation system or operating procedures.

Optimization of industrial operations is characterized by a few to a few hundred degrees of freedom, constraints on the inputs and outputs, and restrictions on the forms that the optimal transition policy can take. Most often, the trajectories to be optimized are the setpoints for the process controllers. These setpoint trajectories must be implemented via a plant automation system, or manually by an operator. Plant automation systems (*e.g.* distributed control systems) easily allow the input of simple steps and ramp changes to the

setpoints. Thus, restricting the inputs to steps and ramp functions gives input policies that are easily implemented on existing control systems.

In this section the method of input restriction is proposed which builds on the ideas of Dabros *et al.*[22] wherein optimal input trajectories were restricted to take on the form of a small number of steps. The previous work of Dabros *et al.* treated the dynamic optimization problem by discretizing in time and treating the resulting problem as a quasi-steady state, algebraic optimization problem using conventional nonlinear programming solvers. Results are similar to those generated using CVP by Wang *et al.*and Mangesh and Gudi desired [51] [38]; however, here the limitations of CVP to a single function during a time interval are improved upon.

Two cases are considered for input restriction: firstly, the generalized problem where the set of inputs is allowed to be any number of any set of functions (*i.e.* linear, polynomial, exponential); and secondly, the reduced and simplified case, where the input trajectories are limited to sets of steps and ramps.

Mathematical programs with equilibrium constraints (MPECs) are necessary for the generalized problem. MPECs are just beginning to gain attention in the area of chemical engineering, with the development of new solvers [42]. The presence of equilibrium constraints, or complementarity conditions, such as:

$$x_1 x_2 = 0$$

enforces that either x_1 and/or x_2 be zero. Equilibrium constraints, for input restriction, are included to enforce that only one input trajectory function is chosen during a time interval.

Beginning with the dynamic optimization problem (3.1), additional constraints are added to constrain the inputs to a set of functions $\boldsymbol{u}(t_j) \in U$, where U is a set of n input functions,

occurring at m different intervals in time. The following dynamic optimization results:

$$
\begin{aligned}
&\min_{\alpha,t_j} \quad \Phi\left[\mathbf{x}(t),\mathbf{z}(t),\mathbf{u}(t),t\right] \\
&s.t. \\
&\quad \mathbf{f}(\dot{\mathbf{x}}(t),\mathbf{x}(t),\mathbf{z}(t),\mathbf{u}(t),t)=0 \\
&\quad \mathbf{g}(\mathbf{x}(t),\mathbf{z}(t),\mathbf{u}(t),t)=0 \\
&\quad \mathbf{h}(\mathbf{x}(t),\mathbf{z}(t),\mathbf{u}(t),t)\leq 0 \\
&\quad \mathbf{x}(t)^L \leq \mathbf{x}(t) \leq \mathbf{x}(t)^U \\
&\quad \mathbf{z}(t)^L \leq \mathbf{z}(t) \leq \mathbf{z}(t)^U \\
&\quad \mathbf{u}(t)^L \leq \mathbf{u}(t) \leq \mathbf{u}(t)^U \\
&\quad t_j^L \leq t_j \leq t_j^U \\
&\quad \mathbf{u}(t_j)=\sum_{i=1}^{n}\alpha_{ij}u_{ij} \\
&\quad \alpha_{ij}\alpha_{kj}=0 \\
&i=1,..,n \quad j=0,..,m \quad k=0,..,i-1,i+1,..n \\
&t_0<t_1<...<t_m
\end{aligned}
\tag{3.10}
$$

where the complementarity conditions in 3.10 are the equilibrium constraints in the MPEC problem.

Solving programs with equilibrium constraints is an iterative process, where the equilibrium constraints are relaxed using inequalities. The complementarity condition takes the form:

$$-\epsilon < x_1 x_2 < \epsilon$$

where ϵ is a tuning parameter. MPECs are solved by allowing ϵ to first be large, followed by decreases in ϵ until the equilibrium constraint is enforced to within a sufficient tolerance.

For most cases the above formulation is too complicated and a simplified method is developed. For the case where open loop control strategies are used, it may be only possible to implement simple inputs such as steps and ramps. By limiting the input function space to steps and ramps, the complexity of the problem is greatly reduced due to the removal of the need for the complementarity conditions in the dynamic optimization problem. Limitation

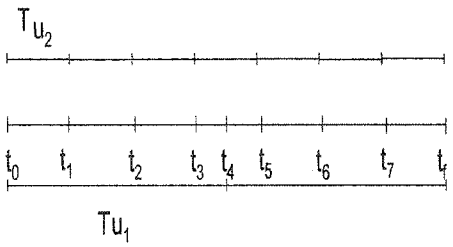

Figure 3.2: Time Grid Development-2 Inputs

of the input trajectories to these simple input functions results in a formulation that can be easily solved using existing optimization solvers, and follows that provided by Betts [10]. In this approach changes in **x**, **z**, **u**, **f**, **g** and **h** are allowed at discrete points in time, termed input switching times (IST). The IST are decided using the prescribed switching intervals, defined as the input interval T_{u_i}. Each input has associated with it a set of IST $\mathbb{T}_i$, where more than one input can use the same IST. Figure 3.2 shows a simple grid of IST for a two input system, with input intervals of T_{u_1} and T_{u_2}. Here the sets of IST are

$$\mathbb{T}_1 = \{t_0, t_4, t_f\}$$
$$\mathbb{T}_2 = \{t_0, t_1, t_2, t_3, t_5, t_6, t_7, t_f\}$$

where $\mathbb{T}_1$ and $\mathbb{T}_2$ are the sets of input switching times for $u_1(t)$ and $u_2(t)$, respectively. At any given IST, the switching set of inputs, (*i.e.* those with the current IST within their set of IST), are allowed to implement another step or ramp function. Any input not in the switching set remains unchanged in its present interval. States are assumed to be continuous across all IST, with continuity enforced using equality constraints. Discretizing Problem (3.1) using the IST grid, and applying the necessary constraints, the following

continuous version of the restricted input optimal trajectory (RIOT) problem results;

$$
\begin{aligned}
&\min_{\mathbf{a}_o^k, \mathbf{a}_1} \quad \Phi\left[\mathbf{x}^k(t), \mathbf{z}^k(t), \mathbf{u}^k(t), t^k\right] \\
&s.t. \\
&\quad \mathbf{f}(\dot{\mathbf{x}}^k(t), \mathbf{x}^k(t), \mathbf{z}^k(t), \mathbf{u}^k(t), t^k) = \mathbf{0} \\
&\quad \mathbf{g}(\mathbf{x}^k(t), \mathbf{z}^k(t), \mathbf{u}^k(t), t^k) = \mathbf{0} \\
&\quad \mathbf{h}(\mathbf{x}^k(t), \mathbf{z}^k(t), \mathbf{u}^k(t), t^k) \leq \mathbf{0} \\
&\quad u_j^k = a_{o_j}^k + a_{1_j}^k t \quad t_k \in \mathbb{T}_j \\
&\quad u_j^k = u_j^{k-1} \quad t_k \notin \mathbb{T}_j \\
&\quad \mathbf{x}_F^{k-1} = \mathbf{x}_I^k \quad k = 1, .., h \\
&\quad \mathbf{z}_F^{k-1} = \mathbf{z}_I^k \quad k = 1, .., h \\
&\quad \mathbf{x}(t)^L \leq \mathbf{x}^k(t) \leq \mathbf{x}(t)^U \\
&\quad \mathbf{z}(t)^L \leq \mathbf{z}^k(t) \leq \mathbf{z}(t)^U \\
&\quad \mathbf{u}(t)^L \leq \mathbf{u}^k(t) \leq \mathbf{u}(t)^U \\
&\quad j = 1..p
\end{aligned}
\tag{3.11}
$$

where $\mathbf{a}_o$ and $\mathbf{a}_1$ are vectors of time independent parameters for the step and ramp formalization, and are the decision variables of interest in this problem. Here the objective function, differential, equality and inequality constraints remain unchanged. Following these equations the input restriction and continuity equations are included. Other possible constraints that may be included are smoothness of the input trajectory, as well as rate limits on inputs.

The above form of the RIOT problem allows both step and ramp functions; however, reformulating the problem to include either function is trivial, where step functions alone can be achieved simply by setting $\mathbf{a}_1 = \mathbf{0}$. Ramp functions only require $\mathbf{a}_0 = \mathbf{0}$, with the addition of continuity constraints between IST.

As stated, problem (3.11) cannot generally be solved using dynamic programming techniques, and discretization must be used to reduce the problem to an algebraic optimization problem. Discretizing time into q mesh points in each input interval, the

RIOT problem reduces to the following form

$$
\begin{aligned}
&\min_{\mathbf{a}_o^k, \mathbf{a}_1} \quad \Phi\left[\mathbf{x}_i^k, \mathbf{z}_i^k, \mathbf{u}_i^k, t_i^k\right] \\
&s.t. \\
&\quad \mathbf{f}(\dot{\mathbf{x}}_i^k, \mathbf{x}_i^k, \mathbf{z}_i^k, \mathbf{u}_i^k, t_i^k) = \mathbf{0} \\
&\quad \mathbf{g}(\mathbf{x}_i^k, \mathbf{z}_i^k, \mathbf{u}_i^k, t_i^k) = \mathbf{0} \\
&\quad \mathbf{h}(\mathbf{x}_i^k, \mathbf{z}_i^k, \mathbf{u}_i^k, t_i^k) \leq \mathbf{0} \\
&\quad u_j^k = a_{o_j}^k + a_{1_j}^k t, \quad t_k \in \mathbb{T}_j, \quad \forall i \\
&\quad u_j^k = u_j^{k-1}, \quad t_k \ni \mathbb{T}_j, \quad \forall i \\
&\quad \mathbf{x}^L \leq \mathbf{x}_i^k \leq \mathbf{x}^U \\
&\quad \mathbf{z}^L \leq \mathbf{z}_i^k \leq \mathbf{z}^U \\
&\quad \mathbf{u}^L \leq \mathbf{u}_i^k \leq \mathbf{u}^U \\
&\quad \Delta t^L \leq \Delta t^k \leq \Delta t^U \\
&\quad \mathbf{x}^{k-1} = \mathbf{x}^k \\
&\quad \mathbf{z}^{k-1} = \mathbf{z}^k \\
&\quad i = 1, .., q \quad j = 1..p \quad k = 1, .., h
\end{aligned}
\tag{3.12}
$$

where $q \geqslant 2$, a requirement that must be met to satisfy the presence of IST bounds and to ensure input restrictions. In this form the RIOT problem still may contain functions of derivatives and integrals in the state variables. The method of direct transcription [10] is well suited for solving RIOT problems, where differential/integrals terms are directly transcribed using common numerical methods. After transcription, algebraic optimization techniques can then be used to solve problem (3.12).

The RIOT problem is solved using the following steps:

1. Formulate problem as a dynamic optimization problem of the form given in (3.1).
2. Determine the IST grid using the predefined values of the input intervals for all inputs.
3. Restrict inputs using equality constraints, treating those inputs which are switching and not switching appropriately.

4. Introduce continuity constraints at the IST for all states, the problem is now in the form of Problem (3.11).

5. Discretize the continuous problem into a grid of mesh points, and use Direct Transcription to remove any derivative and integral terms.

6. Solve using appropriate algebraic optimization techniques.

7. If error tolerances are not met, refine mesh and/or increase order of numerical approximation, then go back to step 6.

Mesh refinement can be accomplished by using some sort of refinement rules, such as those given in Betts and Huffman [11], which are adopted in this work.

3.5 Case Studies

The method presented above will be illustrated using three commonly studied problems: 1) the single integrator system 2) the consecutive reaction problem; and 3) the parallel reaction problem.

The problems were solved using Boeing's® Sparse Optimal Control Software (SOCS), using sequential quadratic programming, and exploiting problem sparsity to efficiently solve optimal control problems. All problems were solved to meet SOCS minimum allowable objective and ODE tolerances, using the trapezoidal rule or a higher order method. Mesh refinement and numerical methods were allowed to change freely as mesh refinement continued. Optimizations were done using a dual AMD 2400+ with 1 Gb RAM.

3.5.1 Single Integrator Problem

The single integrator problem examined by Goh and Teo [30], Guay *et al.* [31] and Luus [36] was solved using unrestricted and restricted forms. An analytical solution for the single integrator has been solved via linear least squares optimal control theory [14].

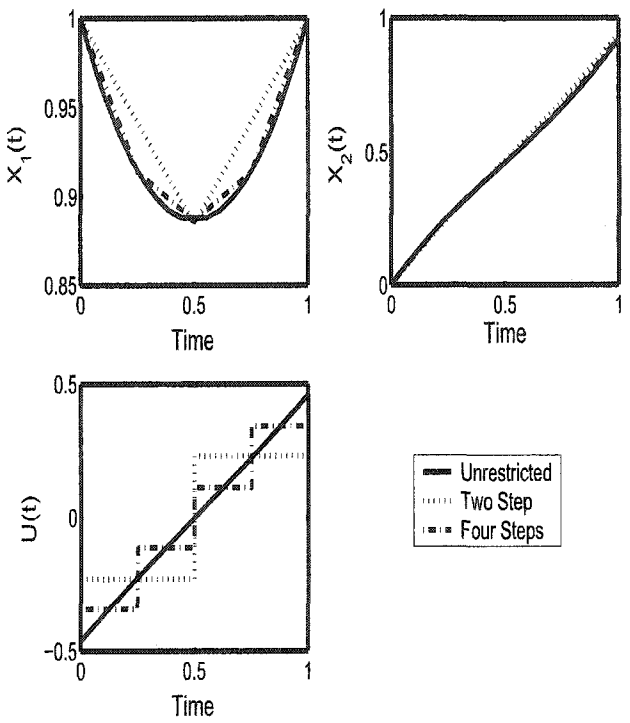

Figure 3.3: Optimal Trajectories for the Single Integrator Problem

The single integrator problem can be stated as:

$$\min_{u(t)} \quad x_2(t_f), \quad t_f = 1$$

s.t.

$$\begin{aligned} \dot{x_1}(t) &= u(t) \\ \dot{x_2}(t) &= x_1^2(t) + u^2(t) \\ x_1(0) &= 1 \\ x_2(0) &= 0 \\ x_1(1) &= 1 \end{aligned} \tag{3.13}$$

Restricting the inputs of the integrator system to be step functions, and using Direct Transcription, the RIOT optimization problem can be reformulated to give

$$
\begin{aligned}
&\min_{\beta} \quad x_2(t_f), \quad t_f = 1 \\
&\text{s.t.} \\
&\quad \dot{x_1^k}(t) = u^k(t) \\
&\quad \dot{x_2^k}(t) = (x_1^k)^2(t) + (u^k)^2(t) \\
&\quad u^k(t) = \beta_k \\
&\quad x_{1_I}^{k+1} = x_{1_F}^k \\
&\quad x_{2_I}^{k+1} = x_{2_F}^k \\
&\quad x_1(0) = 1 \\
&\quad x_2(0) = 0 \\
&\quad x_1(1) = 1 \\
&\quad k = 1, .., n
\end{aligned}
\tag{3.14}
$$

Figure 3.3 shows the optimal trajectories of both the restricted and unrestricted problems. For the unrestricted problem, the optimal value of the objective function, $x_2^*(t_f)$, was found to agree to within 6 significant figures of the analytical solution to the problem, and was deemed sufficient for the purposes of this work. Table 3.1 shows the optimal objectives for the restricted and unrestricted problems. All RIOT problem solutions were found to have

Case	$x_2^*(t_f)$
Unrestricted	0.924234
1-Step	1.000000
2-Step	0.942308
4-Step	0.928705
8-Step	0.925349
16-Step	0.924513

Table 3.1: Optimal Objective for Single Integrator Reaction Problem: Restricted and Unrestricted

objectives function values greater than the unrestricted form. For the case where only one step function is allowed the degrees of freedom become zero and the solution reduces to $u(t) = 0$. For this case the problem can be solved analytically.

3.5.2 Consecutive Reaction Problem

The consecutive reaction problem, first examined by Ray [43], McAuley and Dadebo [23], and Guay et al. [31] follows the following reaction

$$\mathrm{A} \underset{k_1}{\longrightarrow} \mathrm{B} \underset{k_2}{\longrightarrow} \mathrm{C}$$

It is desired to maximize the recovery of the middle product by manipulation of the reactor temperature. The problem can be stated mathematically as

$$\begin{aligned}
&\max_{u(t)} \quad x_2(t_f), \quad t_f = 1 \\
&\text{s.t.} \\
&\quad \dot{C_A}(t) = -u(t)C_A^2(t) \\
&\quad \dot{C_B}(t) = -0.03875u^2(t)C_B(t) + u(t)C_B^2(t) \\
&\quad C_A(0) = 1 \\
&\quad C_B(0) = 0 \\
&\quad 0.9092 \leq u(t) \leq 7.4831
\end{aligned} \tag{3.15}$$

where the input $u(t)$ is defined as $u \equiv 4000e^{-2500/T}$. Restricting the input $u(t)$ to take on n steps, the problem then becomes the following

$$\begin{aligned}
&\max_{\beta} \quad x_2(t_f), \quad t_f = 1 \\
&\text{s.t.} \\
&\quad \dot{C_a}^k(t) = -u(t)^k(C_a^k)^2(t) \\
&\quad \dot{C_b}^k(t) = -0.03875(u^k)^2(t)C_b^k(t) + u^k(t)(C_a^k)^2(t) \\
&\quad u^k(t) = \beta_k \\
&\quad C_{A_I}^{k+1} = C_{A_F}^k \\
&\quad C_{B_I}^{k+1} = C_{B_F}^k \\
&\quad C_A(0) = 1 \\
&\quad C_B(0) = 0 \\
&\quad 0.9092 \leq u^k(t) \leq 7.4831 \\
&\quad k = 1, .., n
\end{aligned} \tag{3.16}$$

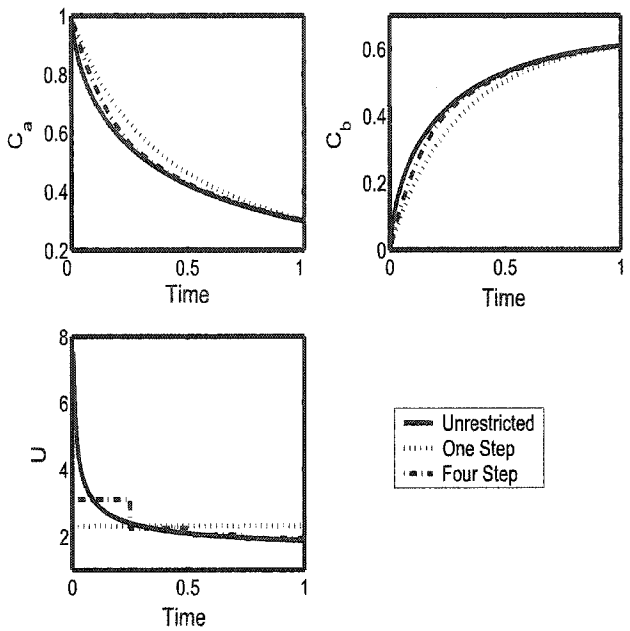

Figure 3.4: Optimal Trajectories for the Consecutive Reaction Problem

where I and F refer to the beginning and end of the current input interval. The optimal trajectories for both the restricted and unrestricted problems are shown in Figure 3.4. The optimal conversion $C_b^*(t_f)$ for the unrestricted trajectory problem was found to be 0.610803, in good agreement with those published in the literature. The restricted and unrestricted optimal objective function values are shown in Table 3.2. All RIOT

Case	$x_2^*(t_f)$
Unrestricted	0.610803
1-Step	0.605947
2-Step	0.607827
4-Step	0.609101
8-Step	0.609893
16-Step	0.610354

Table 3.2: Optimal Objective for Consecutive Reaction Problem: Restricted and Unrestricted

formalizations had optimal solutions less than the unrestricted problem, however the loss in performance associated with this problem was quite small. Even for a one-step input restriction, a loss of less than one percent occurs. This consecutive reaction problem is

therefore insensitive to input restriction.

3.5.3 Parallel Reaction Problem

The parallel reaction problem presented here has been examined thoroughly in the literature by Beigler [12], Ray [43] and others [34] [35] [23]. Here two reactions are taking place within a tubular reactor, which are stated as

$$\begin{aligned} &\mathrm{A} \xrightarrow[k_1]{} \mathrm{B} \\ &\mathrm{A} \xrightarrow[k_2]{} \mathrm{C} \end{aligned}$$

Defining the dimensionless concentrations of species A and B in the reactor as $x_1 \equiv C_A/C_{A_o}$ and C_B/C_{A_o} where C_{A_o} is defined as the initial concentration of A, the following maximization problem results

$$\begin{aligned} &\max_{u(t)} \quad x_2(t_f), \quad t_f = 1 \\ &\text{s.t.} \\ &\qquad \dot{x_1}(t) = -u(t)x_1(t) - \frac{1}{2}u^2(t)x_1(t) \\ &\qquad \dot{x_2}(t) = u(t)x_1(t) \\ &\qquad x_1(0) = 1 \\ &\qquad x_2(0) = 0 \\ &\qquad 0 \leq u(t) \leq 5 \end{aligned} \tag{3.17}$$

where $u(t) \equiv k_1 L/v$, L is the reactor length, and v is the spacial velocity. Dividing the problem into n_p input intervals, and recasting in continuous RIOT form

$$
\begin{aligned}
&\max_{\beta} \quad x_2(t_f), \quad t_f = 1 \\
&\text{s.t.} \\
&\quad \dot{x_1}^k(t) = -u(t)^k x_1^k(t) - \frac{1}{2}(u^k(t))^2 x_1^k(t) \\
&\quad \dot{x_2}^k(t) = u(t)^k x_1^k(t) \\
&\quad u^k(t) = \beta_k \\
&\quad x_{1_I}^{k+1} = x_{1_F}^k \\
&\quad x_{2_I}^{k+1} = x_{2_F}^k \\
&\quad x_1(0) = 1 \\
&\quad x_2(0) = 0 \\
&\quad 0 \leq u^k(t) \leq 5 \\
&\quad k = 1, .., n_p
\end{aligned}
\tag{3.18}
$$

Both problems (3.17) and (3.18) were then discretized and Direct Transcription was used to convert to a NLP. The optimal value of $x_2^*(t_f) = 0.573545$, corresponding well with those presented in literature. The optimal trajectories for the unrestricted, 1–step and 4–step restricted cases are shown in Figure 3.5. Table 3.3 shows the optimal values of the objective for the unrestricted and restricted input problems.

Case	$x_2^*(t_f)$
Unrestricted	0.573545
1-Step	0.535112
2-Step	0.556178
4-Step	0.566406
8-Step	0.571294
16-Step	0.573233

Table 3.3: Optimal Objective for Parallel Reaction Problem: Restricted and Unrestricted

All restricted solutions were less then their unrestricted counterpart. Here the difference between the restricted and unrestricted solutions have a greater sensitivity to the number

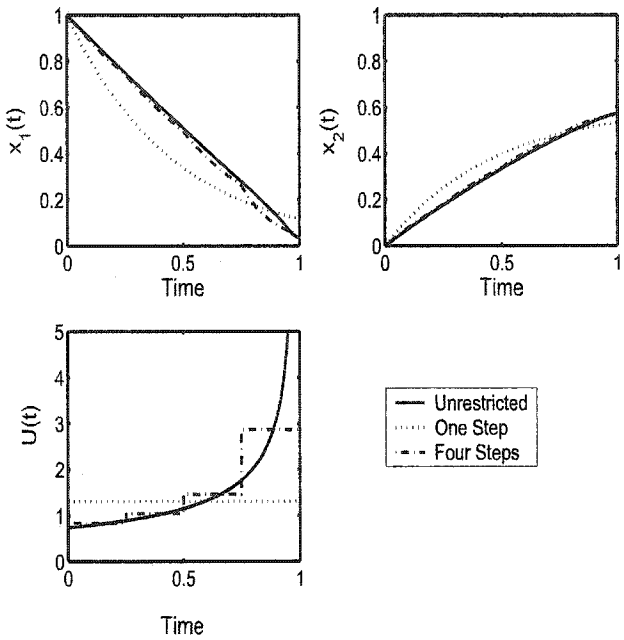

Figure 3.5: Optimal Trajectories for the Parallel Reaction Problem

of steps allowed, with approximately a 6% difference in the one step restricted and unrestricted solutions.

3.5.4 Results and Discussion

As stated above, all RIOT problem solutions to the integrator, consecutive, and parallel reaction problems were found to have objectives that were larger for the integrator problem and smaller for the reaction problems than their unrestricted counterparts. Comparison of the objectives for both the unrestricted and restricted inputs are given in Figure 3.6 for all three case studies. It appears that, as the number of steps are increased, the RIOT formulation approaches the optimal value of the unrestricted case asymptotically. The RIOT problems with two allowable steps show approximately 1–3% difference when compared to the unrestricted solutions, with the loss becoming negligible for both the 8 and 16 step cases.

Restriction of the inputs was found to affect the computational efficiency of the problem. Figure 3.7 shows the effects of input restriction on the computation time. All problems are found to have an approximately linearly increasing relationship between the computational

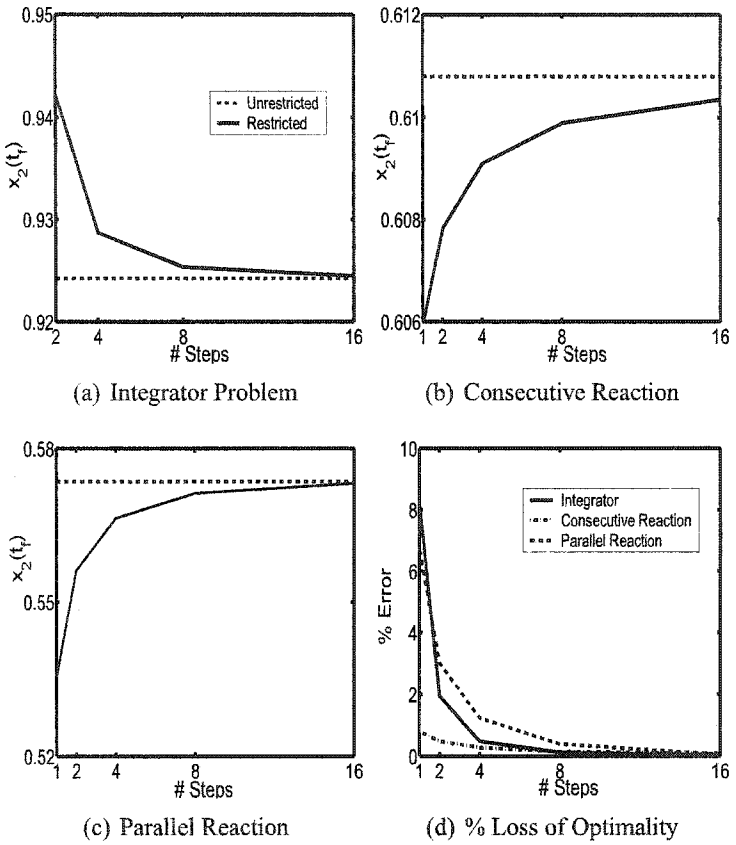

(a) Integrator Problem (b) Consecutive Reaction

(c) Parallel Reaction (d) % Loss of Optimality

Figure 3.6: Unrestricted and Restricted Input: Objective and Error Comparison

time and the number of steps. Interestingly for highly restricted systems (low number of steps), the computational costs were below that of the unrestricted problem. This suggests that it may be possible to reduce optimization costs by reformulation of a problem in RIOT form. For highly restrictive problems the degrees of freedom are lowered and the number of additional constraints added to the system are minimal, which is expected to give rise to shorter solution times. As the number of allowable steps is increased, the problem gains more degrees of freedom and an increasing number of equality constraints, which leads to large solution times. For the parallel reaction problem, even the 16–step restricted input computational costs were below that of the unrestricted case. The number of mesh refinement iterations necessary was found to increase with increasing number of steps, and for both problems the number of mesh refinements became larger than that necessary for

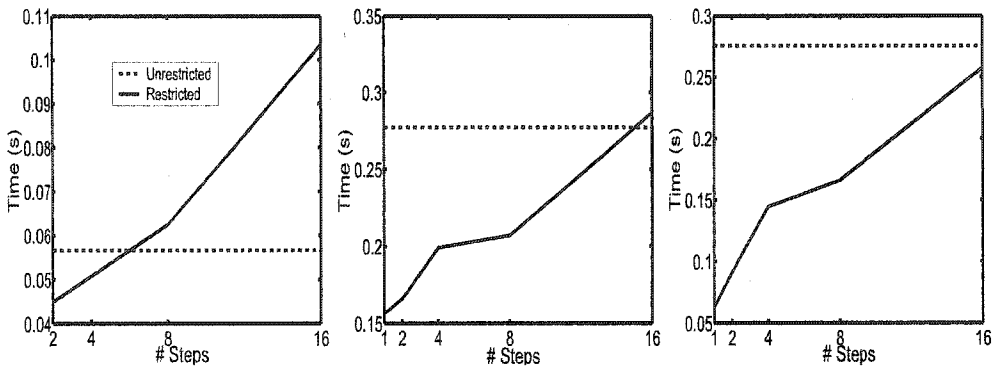

(a) Integrator (b) Consecutive Reaction (c) Parallel Reaction

Figure 3.7: Unrestricted and Restricted Input: Solution Times

the unrestricted case. Decreasing the input restriction also led to an increase in the overall number of mesh points.

Input saturation was found to occur on both the unrestricted cases for the consecutive and parallel reactions; however, restriction of the inputs for these two cases was found to remove input saturation. In the restricted input case, the range of values which the inputs were found to take on shrank for all three problems studied. This suggests that the RIOT formalization has a natural back off on the magnitude of the inputs.

The RIOT problem also provides a useful tool in benefits analysis for determining whether implementation of advanced control policies would result in large gains to a process. When combined with cost analysis, comparison of the unrestricted and restricted optima may provide useful information into whether substantial gains exist for more sophisticated controllers structures.

In the above case studies, only step functions were allowed in the input trajectories. The problem could have easily been extended to include ramp functions as well. The addition of ramp functions to the input trajectories can greatly reduced the number of IST necessary to approach the unrestricted optimum. In the integrator problem, a single ramp function would give a result comparable to the unrestricted optimum. In the consecutive and parallel reaction problems the use of three step and ramp functions would bring the result close to their unrestricted optimums. The number of parameters necessary for both step and ramp functions doubles and the solutions are not as simple to implement in practice. The

simplicity of the step functions is considered desirable in this work and will be used in the case studies for the PSV grade transitions of the next chapter.

4

Trajectory Optimization of the Syncrude Primary Separation Vessel

In this chapter, trajectory generation cases are examined for the PSV of the EXP2000 pilot plant at Syncrude Research. Prior to optimization studies, a model reformulation was required to ensure it was amenable to the investigations. Pre-processing was then done to scale the problem to ensure well-posedness. The section concludes by examining various case studies.

4.1 Modelling Under the Optimization Framework

Before optimization could take place the model equations presented in Chapter 2 were modified. The original set of differential/algebraic equations had a number of linear dependencies that were removed to eliminate singularities in the Jacobian. To determine which equations were linearly dependent, degree of freedom analysis was performed on the model. For this analysis, all external flow rates were held constant (degrees of freedom = 0). The number of variables and equations is stated as follows:

- bitumen volume fractions (**3 variables/layer**)
- solid volume fractions (**3 variables/layer**)
- fluid volume balance (**1 variable/layer**)
- bitumen settling velocities-froth/middlings interface (**3 variables**)
- solid settling velocities-froth/middlings interface (**3 variables**)
- fluid flow-froth/middlings interface (**1 variable**)
- bitumen settling velocities-middlings/tailings interface (**3 variables**)
- solid settling velocities-middlings/tailings interface (**3 variables**)
- fluid flow-middlings/tailings interface (**1 variable**)
- external flows, feed, froth, middlings and tailings withdrawal (**4 variables**)
- froth/middlings interfacial movement (**1 variable**)
- feed composition (**7 variables**)

There are a total of 47 variables describing the process. Looking at the number of equations:

- bitumen particle volume balances (**3 equations/layer**)
- solid particle volume balances (**3 equations/layer**)
- fluid volume balances (**1 equations/layer**)
- bitumen settling relationship-froth/middlings interface (**3 equations**)
- solid settling relationship-froth/middlings interface (**3 equations**)
- bitumen settling relationship-middlings/tailings interface (**3 equations**)
- solid settling relationship-middlings/tailings interface (**3 equations**)
- overall volume balances (**1 equations/layer**)

- Specified feed, middlings and tailings withdrawal (**3 equations**)
- Specified feed composition (**7 equations**)
- Wallis Shockwave Equation (**1 equation**)

There is a total of 47 equations, leaving zero degrees of freedom; however, as specified not all of these equations are linearly independent.

The linear dependence is introduced through the Wallis shockwave equation. The Wallis shockwave equation (4.1), which describes the motion of the interface between the froth and middlings layers, is restated here:

$$v_I = \frac{\sum_{j=1}^{3} \alpha_{b_j}^m v_{b_j}^m - \sum_{j=1}^{3} \alpha_{b_j}^f v_{b_j}^f}{\sum_{j=1}^{3} \alpha_{b_j}^m - \sum_{j=1}^{3} \alpha_{b_j}^f} \tag{4.1}$$

Simplifying equation (4.1) for the case where only one bitumen particle is used gives the following result.

$$v_I = \frac{\alpha_b^m v_b^m - \alpha_b^f v_b^f}{\alpha_b^m - \alpha_b^f} \tag{4.2}$$

Under steady state conditions, there is no interfacial movement giving $v_T \equiv 0$:

$$0 = \alpha_b^m v_b^m - \alpha_b^f v_b^f \tag{4.3}$$

Equation (4.3) is equivalent to that of the bitumen froth volume balance equation (2.5) under steady state conditions. Increasing the number of particles from one to three has no effect on the linear dependence of the Wallis shockwave equation.

The effects of the dynamic interface between the froth and middlings layer was examined. Figure 4.1 shows the data collected during the Syncrude Research transient studies using the EXP2000 pilot plant on the level of the froth/middlings interface. The step in feed ore occurs at a time of 75 minutes. For a step in feed ore, there does not appear to be a large effect on the position of the interface. Operator experience agrees that the interface level changes little in the EXP2000 and may be a result of the small resonance time in this vessel, with short periods of time for mass accumulation in each layer. For this reason, modelling the froth/middlings interface as static in this case is not expected to affect the results of the study, appreciably. Numerical comparisons of the PSV model for

simulation, and optimization is located in Appendix B. Removing the dynamic interface was not found to greatly effect the state trajectories. Discussion with operating personnel provided further confidence that this simplification was reasonable [24].

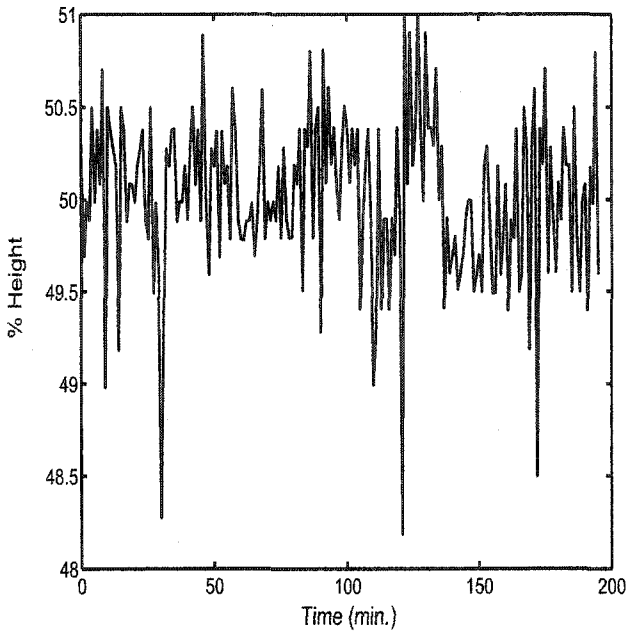

Figure 4.1: EXP2000 Transient Data: % Level Froth/Middlings Interface

Ill-conditioning of the Jacobian was also found to result from the presence of variables which had zero range. Through simulation it was found that the largest diameter solid particles reported solely to the tailings layer, with none of these particles reporting to the froth. Similarly none of the lowest density bitumen particles reported to the tailings. Both the aforementioned solid and bitumen particles have zero ranges in the froth and tailings, respectively. This resulted in ill-conditioning of the Jacobian. The model equations were then modified further to remove these variables, assuming that both were zero in their respective layers, by removing their corresponding particle balances and constitutive relationships. The studies performed in Appendix B showed that removing these equations had no appreciable effect on the state trajectories.

4.2 Optimization Pre-Processing

Removing linear dependencies in the set of differential/algebraic equations may result in a Jacobian which is no longer singular; however, the Jacobian can still be ill-conditioned, if the variables are poorly scaled. A poorly scaled Jacobian can result in poorly generated search directions, where some variables have a large associated gain in objective compared to others. This may result in infeasibility during optimization iterations, as well as increased solution times. Therefore the Jacobian is scaled such that the elements are as close to the same order of magnitude as possible.

For transient models, scaling may become a problem as some variables may take on wide ranges of values, while others remain close to a steady value. It may be beneficial to remove those variables that die off with time, as was done in the previous section for the large bitumen and solid particles. If this approximation is poor, exponential scaling factors may be used to remove this problem, so that the scaling factor increases with time, as the variable decreases. It is important to pick a exponential function that grows at a rate similar to the decay of the variable. Exponential scaling factors were not used in this case.

The relative velocities of the particles were found to be a few orders of magnitude different than other variable ranges. To account for this each relative velocity term was multiplied by the area of the vessel to help to alleviate this difference. Units were chosen to bring all the variables as close together as possible. For example, the relative settling velocities of the particles where computed using units of centimeters, as specified in the literature; however, when placed into the model the values were then converted to decimeters. After scaling the variables, the model was ready for optimization.

4.3 Case Studies

A number of case studies are now discussed. Two regular occurring steps in feed grade are examined followed by an investigation of steps between two extreme ore grades. The ore grades and recipes shown in Tables C.1:C.3 are used here. The first study investigates a step from a high to medium grade ore. The second study examines another commonly occurring step from a medium to low grade ore. The remaining case studies investigate

extreme ore transitions, including both steps from high to low and low to high grade ores.

The steady-state optima for each of the three ore recipes were found first.

4.3.1 Steady State

The steady-state optimal operating conditions were found by setting all derivative terms to zero and solving using NLP to maximize the recovery of bitumen feed to the vessel. The resulting problem takes the following form:

$$\begin{aligned} \max_{\mathbf{u}} \quad & \frac{\sum_j^{n_b} \alpha_j^f Q_f}{\sum_j^{n_b} \alpha_j^{fd} Q_{fd}} \\ s.t. \quad & \\ & \mathbf{f}(\mathbf{x}, \mathbf{u}) = 0 \\ & \mathbf{h}(\mathbf{x}, \mathbf{u}) \leq 0 \\ & \mathbf{x}^L \leq \mathbf{x} \leq \mathbf{x}^U \\ & \mathbf{u}^L \leq \mathbf{u} \leq \mathbf{u}^U \end{aligned} \tag{4.4}$$

where $\mathbf{f}$ contains all of the PSV modelling equations as developed for optimization with derivatives set to zero, and $\mathbf{h}$ contains the set of inequality constraints on the model. Here the inequalities dictate that the mass fraction of water in the froth layer be less than 35%, and that tailings density be less than 1.65g/cm^3. The vector $\mathbf{x}$ contains the states, which include the volume fractions of each layer, the relative and bulk flow velocities, *etc.* and the vector $\mathbf{u}$ represents the vector of inputs, *i.e.,* the middlings and tailings withdrawals and the flood flow rate. The problem was solved using sequential quadratic programming (SQP), with objective, projected gradient and constraint tolerances of 10^{-7}, 10^{-5}, and 1.69×10^{-8}, respectively.

For the objective tolerance, the norm of the difference between the projected and current objective function is used. For both the projected gradient and the constraint tolerances the infinity norm is used to ensure that the maximum element satisfies the tolerance.

Table 4.1 shows the optimal values of the recovery and inputs. The optimal results presented above are not guaranteed to be a global optima, since NLP is used to determine their values. At best the results are said to be local optimal. A number of initial guesses

Grade	Recovery	Q_m(L/s)	Q_t(L/s)	Q_{fl}(L/s)	x_w^f	ρ_t (g/cm^3)
High	94%	0.0	0.8449	0.4652	0.35	1.65
Medium	81%	0.3115	0.6641	0.5663	0.35	1.65
Low	57%	0.7460	0.4631	0.7658	0.35	1.65

Table 4.1: Optimal Steady State Values

were used, and all solutions were equivalent to those in Table 4.1. This increased the confidence in the solution, where no additional local optima were found.

As in practice, the high grade ore is found to produce the highest primary recovery of bitumen, decreasing for poorer ores. For high grade ores the middlings withdrawal is completely turned off, as the feed ore contains mostly large bitumen and solid particles which report solely to the froth and tailings, respectively. High grade ores require the least amount of flood water. For a medium grade ore, the presence of more fines and a higher concentration of less aerated bitumen particles requires the middlings withdrawal to turn on. Increases in the flood water are also necessary to help remove the additional fines from the middlings. The tailings flow rate begins to decrease as the percentage of large solid particles begins to drop, as less water is needed to satisfy the tailings density constraint. The trend continues for the lowest grade ore where larger middlings and flood flow rates are necessary, with the tailings withdrawal taking on its lowest value.

Table 4.1 shows that for each case the inequalities for the froth water fraction and tailings density are active, as expected. Pushing as much water up into the froth has the added effect of dragging along as much bitumen as possible, maximizing the recovery. This phenomena results in the activation of the froth quality constraint.

Keeping the tailings flow rate at its minimum allowable level corresponds to the smallest amount of bitumen reporting to the tailings, minimizing the loss out of the underflow. This phenomenon pushes to activate the tailings density constraint.

Simple sensitivity studies examine how the optimal recovery changes for deviations in the inequality limits. The inequality constraints are relaxed and the results are shown in tables 4.2 to 4.4. For all ores the objective function was found to be insensitive to variations in the froth water mass fraction. The optimal values of the middlings, tailings and flood water flow rates were also found to be insensitive. The changes in the inputs and recovery

were found to be several orders of magnitude larger than the convergence tolerances, and is not an artifact of the computation.

The reasoning for the insensitivity arises from the differences in the relative settling velocities of the bitumen particles and that of the bulk flow. The relative velocities for the bitumen are much larger than that of the bulk flow to the froth, so slight increases or decreases in the bulk flow have no meaningful effect on the recovery.

x_w^f	ρ_t (g/cm^3)	Recovery	Q_m(L/s)	Q_t(L/s)	Q_{fl}(L/s)
34%	1.65	94.03888%	0.0	0.844918	0.465201
36%	1.65	94.13627%	0.0	0.844553	0.467145
35%	1.7	95.87190%	0.0	0.765972	0.389778
35%	1.6	92.12833%	0.0	0.936289	0.552818

Table 4.2: Steady-State Inequality Sensitivities for a High Grade Ore

x_w^f	ρ_t (g/cm^3)	Recovery	Q_m(L/s)	Q_t(L/s)	Q_{fl}(L/s)
34%	1.65	81.51035%	0.313280	0.663371	0.565663
36%	1.65	81.65300%	0.309688	0.663371	0.567013
35%	1.7	84.021811%	0.337118	0.574744	0.506144
35%	1.6	79.049879%	0.256165	0.786532	0.629720

Table 4.3: Steady-State Inequality Sensitivities for a Medium Grade Ore

x_w^f	ρ_t (g/cm^3)	Recovery	Q_m(L/s)	Q_t(L/s)	Q_{fl}(L/s)
34%	1.65	56.94704%	0.746751	0.462962	0.765537
36%	1.65	57.07971%	0.745272	0.463338	0.766128
35%	1.7	59.04627%	0.624436	0.441857	0.625172
35%	1.6	54.63166%	0.900421	0.482583	0.937228

Table 4.4: Steady-State Inequality Sensitivities for a Low Grade Ore

The opposite is true for changes to the tailings density, where bulk flow dominates. The above sensitivity study shows that the recovery, as well as the middlings, tailings and flood flow rates show sensitivity to changes in tailings density. Since bulk flow is the dominant movement of bitumen into this layer, any change will result in substantially more bitumen being withdrawn from the tailings.

Now that the steady state optima have been evaluated, focus is placed on determining the optimal input trajectories for steps in feed grade. Common transitions will be considered

first.

4.3.2 Dynamic Optimization

Optimal trajectories for the grade transitions are discussed in the following sections. Four ore transitions are considered for dynamic optimization. They include two common and two extreme grade transitions. Optimal trajectories for these steps are determined while maximizing the integral of the recovery over time.

Preliminaries

Maximizing the recovery of bitumen over the transition time was found to give results that behaved in a highly irregular manner, and the optimizer was found to exploit the constant volume nature of the model. Figure 4.2 shows a typical set of optimal input trajectories. The input trajectories are highly irregular, and not a good representation of how the process

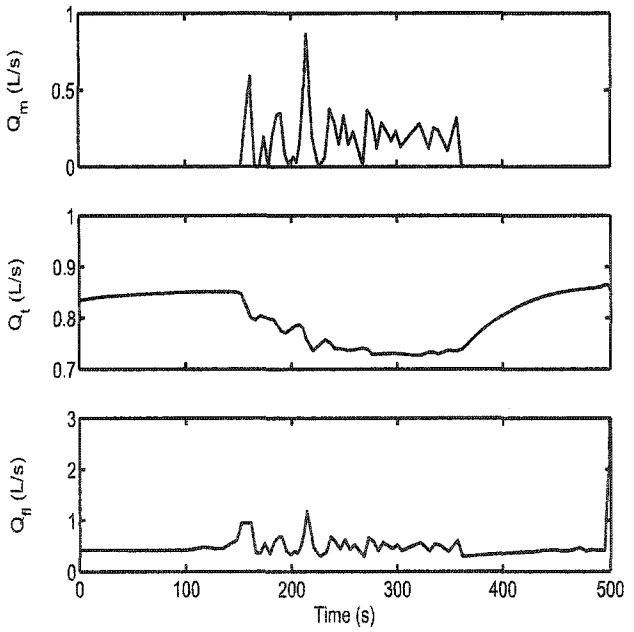

Figure 4.2: Optimal Input for PSV Model-Unrestricted

should be controlled. Also the model does not appear to reach a new steady state. For a better understanding of the underlying problem; Figure 4.3 shows the recovery and water mass fractions during the time interval. The recovery shows two distinct peaks where the

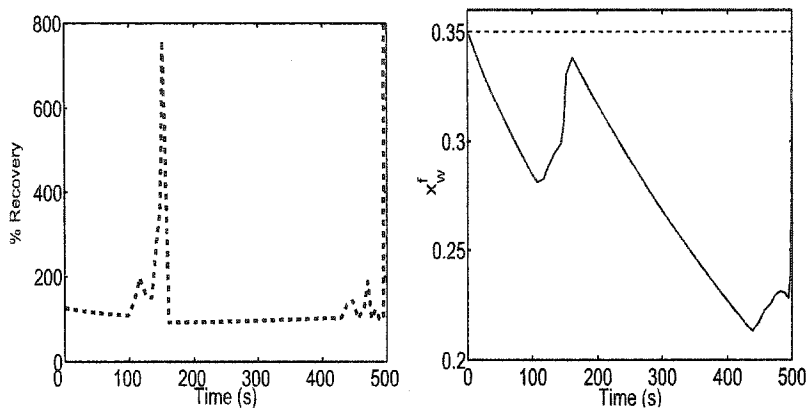

(a) Recovery (b) Froth Mass Fraction

Figure 4.3: Recovery and Water Mass Fraction Trajectories for Integral of Recovery Objective

recovery reaches approximately 800% during the first and 7000% during the latter. In general, recoveries larger than 100% were not expected; however, the constant volume balance around the vessel allows these increases to occur. Essentially it is possible to achieve recoveries greater than 100% by looking at the froth mass fractions. Bitumen is stored in the froth over time, which can be seen in Figure 4.3.2 as increases in the froth quality. Once enough bitumen was stored, the process was then hit with large amounts of flood to recover the stored bitumen. During this time more bitumen is leaving the vessel than entering and so a recovery greater than 100% results. The low sensitivity of the recovery to perturbations in the froth quality constraint from the previous section supports this conjecture. Storing the bitumen in the froth does not reduce recovery considerably, as during this time relative velocity terms dominate. Once enough bitumen was stored the bulk flow term was made to dominate.

The first peak represents a cycle in the optimal recovery that occurs around one time constant, where the water is increased to remove the stored bitumen. The second peak, which is much larger, is a result of the fixed time interval. Although at the end there is no constraint violation, extension of the time interval under final operating practices would result in violation of the froth quality constraint. Increasing the time horizon would only affect the number of small peaks, followed by the final large peak at the end of the interval.

In attempting to eliminate the oscillatory nature of the problem, flow bounds and steady state constraints at the interval bounds were used; however, no method provided sufficient dampening. To remove the oscillatory nature as well as to ensure that the process eventually reach an optimal steady state, penalty functions were used in the objective function to penalize deviations from the froth quality as well as from the final steady state.

The new objective function takes the following form:

$$\Phi\left[\mathbf{x}(t),\mathbf{z}(t),\mathbf{u}(t),t\right]=\int_0^{t_f}\frac{\sum_j^{n_b}\alpha_j^f Q_{fr}}{\sum_j^{n_b}\alpha_j^{fd}Q_{fd}}dt+\kappa(t)(\phi\left[\mathbf{x}(t),\mathbf{z}(t),\mathbf{u}(t),t\right]-\xi_o)^2 \tag{4.5}$$

where κ(t) is a tuning parameter which can be adjusted to penalize deviations from the desired values and ϕ is the set of relationships which are to be penalized. The variable ξ_o is the desired value for the function ϕ to equal.

Penalty functions were preferred over changing the inequalities to equalities, for ease of adapting the problem to the restricted form approach. The assumption that the optimum was located where the inequalities become equalities was expected to be valid as maximizing the total flow out of the froth and minimizing the total flow out of the tailings should have been optimal, as the steady state solutions suggested.

The optimal trajectory problem using the reduced model and modified objective function takes the following form:

$$\begin{aligned}
&\max_{\mathbf{u}(t)}\int_0^{t_f}\frac{\sum_j^{n_b}\alpha_j^f Q_f}{\sum_j^{n_b}\alpha_j^{fd}Q_{fd}}dt+\kappa(t)(\phi\left[\mathbf{x}(t),\mathbf{z}(t),\mathbf{u}(t),t\right]-\xi_o)^2\\
&s.t.\\
&\quad\mathbf{f}(\dot{\mathbf{x}}(t),\mathbf{x}(t),\mathbf{z}(t),\mathbf{u}(t),t)=0\\
&\quad\mathbf{g}(\mathbf{x}(t),\mathbf{z}(t),\mathbf{u}(t),t)=0\\
&\quad\mathbf{h}(\mathbf{x}(t),\mathbf{z}(t),\mathbf{u}(t),t)\leq 0\\
&\quad\mathbf{x}(0)=\mathbf{x}_o
\end{aligned} \tag{4.6}$$

where $\mathbf{x}_o$ is the vector of initial conditions for the differential equations, and has dimension n_x since the DAE is of index-1, and $\mathbf{f}$ and $\mathbf{g}$ are the set of differential and algebraic equations, respectively, from the PSV model. The vector ϕ contains the set of inequalities for both the tailings density and froth quality, as well as steady-state relationships.

Equation 4.6 is the infinite dimensional form of the unrestricted trajectory optimization for the PSV.

The penalty functions focused either on inequality, or steady-state concerns during different time intervals. Within approximately an interval of 2 time constants, focus was placed on operating close to the operating constraints. For the remaining time focus was put on driving the problem to steady state.

Extending equation 4.6 to restricted inputs gives the following infinite dimensional problem, where only steps will be considered.

$$
\begin{aligned}
&\max_{\mathbf{a}_o^k} \int_0^{t_f^k} \frac{\sum_j^{n_b} \alpha_j^f Q_{fr}}{\sum_j^{n_b} \alpha_j^{fd} Q_{fd}} dt + \kappa(t)(\boldsymbol{\phi}\left[\mathbf{x}^k(t), \mathbf{z}^k(t), \mathbf{u}^k(t), t^k\right] - \boldsymbol{\xi}_o)^2 \\
&s.t. \\
&\quad \mathbf{f}^k(\dot{\mathbf{x}}^k(t), \mathbf{x}^k(t), \mathbf{z}^k(t), \mathbf{u}^k(t), t^k) = \mathbf{0} \qquad (4.7) \\
&\quad \mathbf{g}^k(\mathbf{x}^k(t), \mathbf{z}^k(t), \mathbf{u}^k(t), t^k) = \mathbf{0} \\
&\quad \mathbf{h}(\mathbf{x}(t), \mathbf{z}(t), \mathbf{u}(t), t) \leq 0 \\
&\quad u_j^k = a_{o_j}^k + a_{1_j}^k t \quad t_k \in \mathbb{T}_j \\
&\quad u_j^k = u_j^{k-1} \quad t_k \notin \mathbb{T}_j \\
&\quad \mathbf{x}_F^{k-1} = \mathbf{x}_I^k \\
&\quad \mathbf{z}_F^{k-1} = \mathbf{z}_I^k \\
&\quad \mathbf{x}(0) = \mathbf{x}_o \\
&\quad j = 1..n_i, k = 1..n_{IST}
\end{aligned}
$$

Both unrestricted and restricted formulations, *i.e.* problems 4.6 and 4.7 are used to solve trajectory optimization problems for both common and extreme changes in feed ore.

High to Medium Ore

Using problem 4.6 the trajectories for a step from a high to medium grade ore were determined and are shown below in Figure 4.4. The mass fraction of water in the froth was found to have an irregular shape, but remained at the constrained value of 35% by mass, with the exception of numerical noise. The presence of the froth quality constraint resulted in the decreasing bitumen mass fraction being replaced by an increasing solids

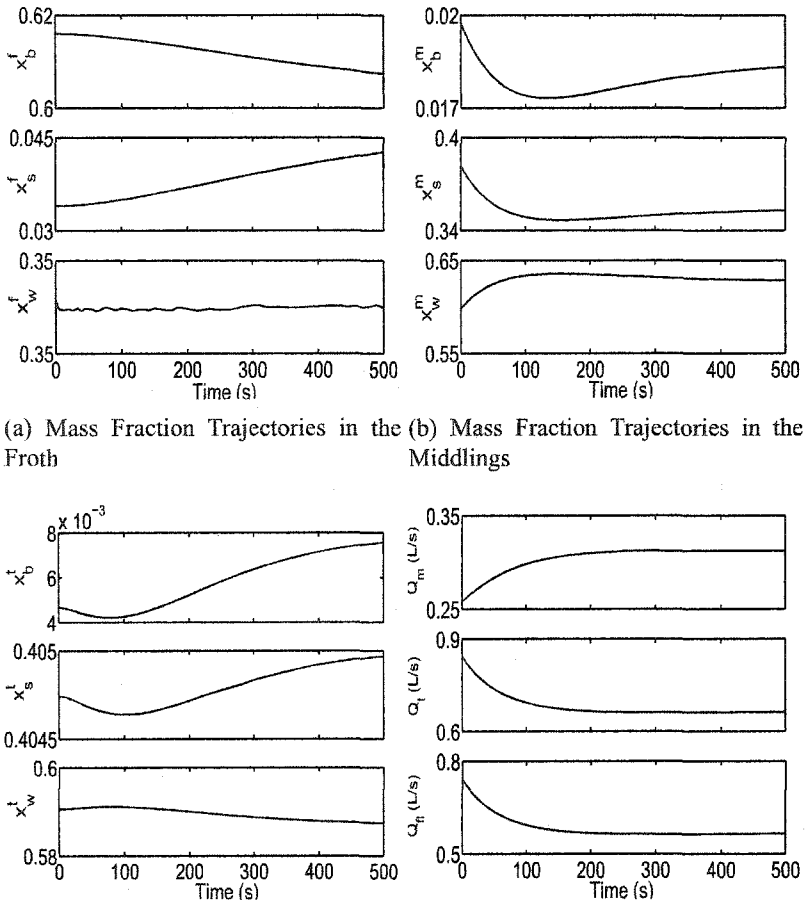

(a) Mass Fraction Trajectories in the Froth

(b) Mass Fraction Trajectories in the Middlings

(c) Mass Fraction Trajectories in the Tailings

(d) Input Trajectories

Figure 4.4: Optimal Trajectories: High to Medium Grade Ore Transition

content of exact magnitude. Only small disturbances in froth bitumen content were seen and were a result of the increased fines in the feed, as well as the decrease in large/less dense bitumen particles.

The input trajectories generated were also first order in nature and through the use of the penalty objective 4.5 the oscillatory nature of the solution was completely removed. Both the middlings and flood water flow rates exhibited an initial jump from their steady-state values to account for the instantaneous change in the feed ore. The underflow rate changed slowly over time as the amount of solids reporting to the tailings changed.

The optimal recovery for this grade change is shown in Figure 4.5, with an initial

recovery > 100%. The greater than 100% recovery was attributed to the same reason

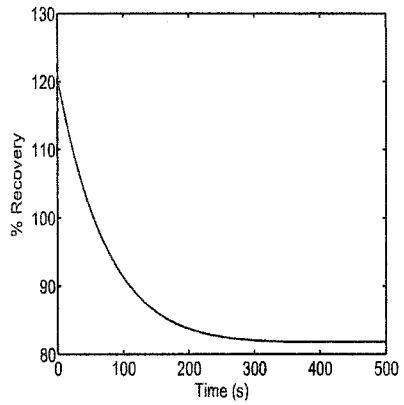

Figure 4.5: Optimal Recovery: High to Medium Grade Ore Transition

for oscillations that occured in the non-penalized problem. Initial conditions for a high quality ore were originally present within the vessel, and represented stored bitumen when compared to that operation under medium quality ore conditions. The instantaneous change in feed grade then produced a high recovery as this stored bitumen was recovered. Simply stated, the step down in the percentage of bitumen fed to the vessel resulted in increased recovery. Towards the end of the interval the recovery was found to approach that of the steady-state optimum found in section 4.3.1.

Sensitivity studies, like those performed in section 4.3.1, were then performed to evaluate the costs associated with the froth quality and tailings density constraints. Figure 4.6 shows the input and recovery trajectories for a step up and down of approximately 3% in the froth quality constraint. Both the input and recovery trajectories were found to be insensitive to changes in the froth quality, where only slight differences were seen. The insensitivity of the froth quality constraint was attributed to the bitumen flux across the froth/middlings interface being dominated by the large magnitude of the relative flow of the bitumen particles. Table 4.5 shows the magnitudes of the average relative particle velocities as well as the bulk flow across the froth interface. For the froth/middlings the relative velocities of the particles was one/two orders of magnitude larger than the bulk flow. Only large changes in the bulk flow would be expected to increase recovery substantially.

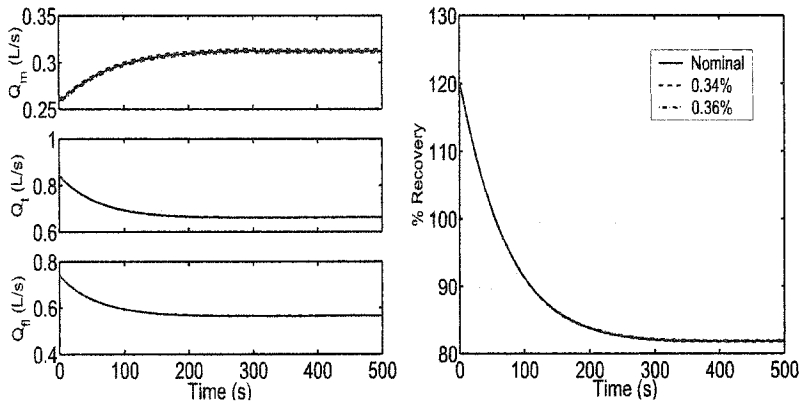

(a) Input Trajectories (b) Recovery

Figure 4.6: Froth Quality Sensitivity: High to Medium Grade Ore Transition

Froth/Middlings		Middlings Tailings	
Species	Settling Velocity	Species	Velocity
$v_{b_1}^f$	0.5743	$v_{b_1}^t$	0.5243
$v_{b_2}^f$	1.1038	$v_{b_1}^t$	0.2012
$v_{b_3}^f$	1.3895	$v_{b_1}^t$	n/a
v_w^f	0.0574	v_w^t	0.8398

Table 4.5: Average Species Settling Velocities

Figure 4.7 shows the sensitivity of the recovery and inputs to approximately 3% changes in the tailings density constraint. There was significant sensitivity in the recovery for a 3% decrease in the tailings density. This was expected, as flood water and underflow must be increased to pull more water into the tailings. The additional flux of water, shown in Table 4.5 was the same order of magnitude as the relative velocities of the particles. Increases in the bulk flow to the tailings causes significant changes on the amount of bitumen being dragged down. The opposite was true for perturbations to higher tailings densities.

The trajectories generated using problem 4.6 were smooth; however, tracking these trajectories manually would not be a simple task. The problem was then recast into the RIOT form of problem 4.7 and was solved using Direct Transcription. An additional five minutes before the step was given for preventative action by the operator (possible in practice).

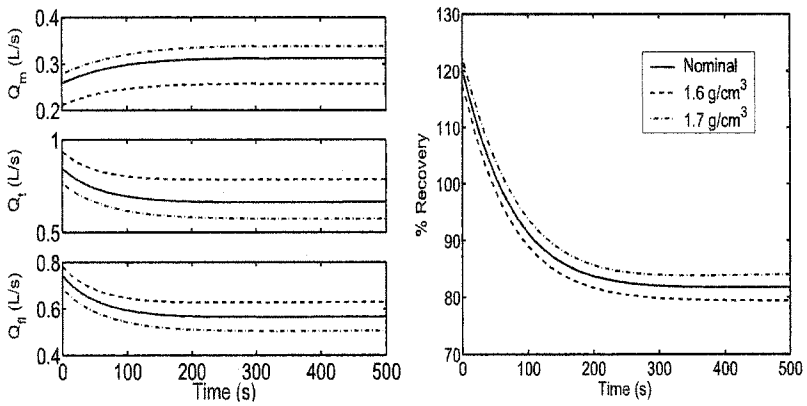

(a) Input Trajectories (b) Recovery

Figure 4.7: Tailings Density Sensitivity: High to Medium Grade Ore Transition

The following optimal input trajectories were found for input switching times of 150 and 100 seconds. The trajectories produced using the RIOT formulation produced state trajectories that had non-smooth properties. For many of the states a change in the inputs produced instantaneous change, causing the irregular curves.

Unlike in section 3.5, the input trajectories, which appeared to follow the unrestricted trajectories, differed in overall shape when compared to the unrestricted problem. The initial step in the middlings and flood water flow rates was removed and replaced with a more modest step. The differences in shape for this problem arose because of continuous operation at both the froth quality and tailings density constraints in the unrestricted form. The inability of the restricted input form to continuously react, resulted in a back off in input aggressiveness during operation. Figure 4.9 shows that only at certain instances in time were the operating constraints active. The small deviations from the tailings density and froth quality bounds, coupled with the sensitivity studies, suggested that the effects on the recovery were expected to be minimal.

The additional five minutes before the step in feed grade was introduced to provide the operator time to begin adjusting inputs prior to the step reaching the PSV. Only slight preventative actions in all the inputs were needed to achieve feasible operation, with no significant deviation from their respective optimal steady state values. Without the slight adjustments before the grade change, the RIOT formulation was found to be infeasible. The

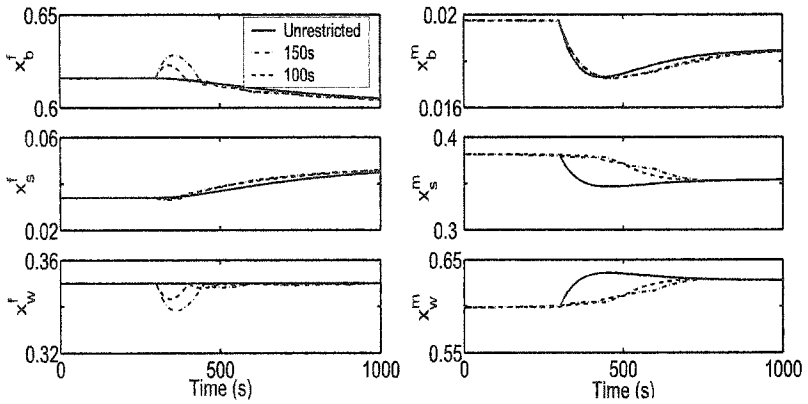

(a) Mass Fraction Trajectories in the Froth

(b) Mass Fraction Trajectories in the Middlings

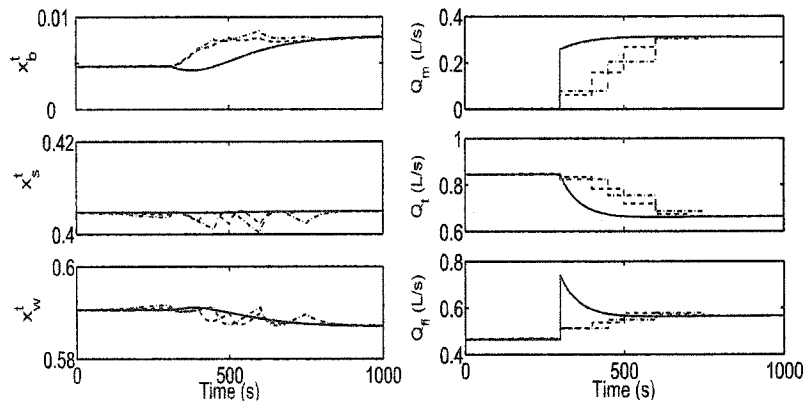

(c) Mass Fraction Trajectories in the Tailings

(d) Input Trajectories

Figure 4.8: Restricted Input Optimal Trajectories: High to Medium Grade Ore Transitition

addition of time for the preventative action is possible when operators have prior knowledge of what ore grades are coming into the pipeline.

Integrals of the recovery for the unrestricted and restricted forms are tabulated in Table 4.6. For both restricted and unrestricted forms the integrals of the recovery were relatively the same. The restricted versions were found to provide a higher solution; however, the difference was insignificant. The insensitivity of the primary bitumen recovery to input restriction was believed to be a result of the insensitivity of the froth quality constraint. Bulk flow of water to the froth was minimal and so the recovery was driven by density concerns in the middlings. The slight increase in the primary recovery

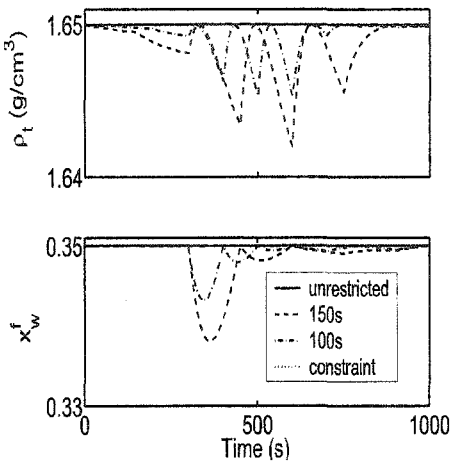

Figure 4.9: Unrestricted/Restricted Inequality Comparison

Case	Froth
Unrestricted	88.1%
100s	88.2%
150s	88.2%

Table 4.6: Restricted and Unrestricted Optimal Objectives: High to Medium Grade Ore Transition

for the restricted case was a result of increased middlings density. For the unrestricted problem the penalty functions were found to over-power this effect, as it results in only slight increases in recovery. The changes in middlings density are suspected of partly adding to the oscillation in the non-penalized problem.

Restricting the inputs in this case was found to be slightly beneficial, but the differences were insignificant.

Input restriction for this grade transition has shown that operator intervention alone will provide sufficient recovery. Adjustments are made only to maintain the desired froth quality and tailings density.

Medium to Low Ore

A step from a medium grade ore to a low grade ore was considered, using the formulation of problem 4.6. The optimal trajectories are presented in Figure 4.10. The trajectories generated are similar to those produced for the previous case. The water concentration in

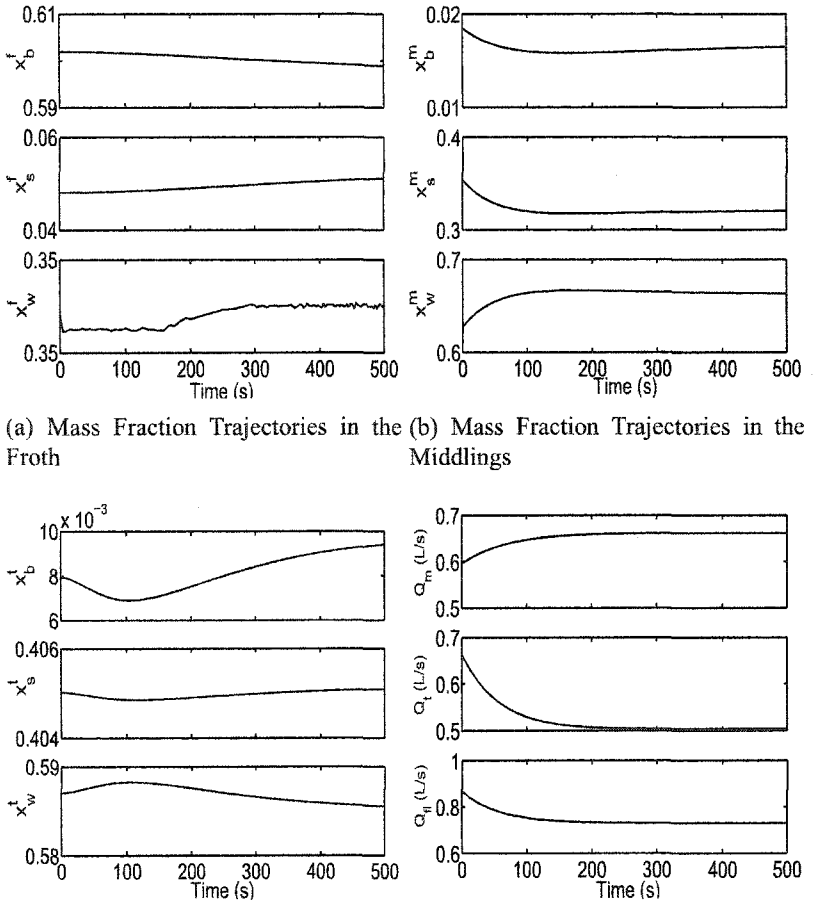

(a) Mass Fraction Trajectories in the Froth

(b) Mass Fraction Trajectories in the Middlings

(c) Mass Fraction Trajectories in the Tailings

(d) Input Trajectories

Figure 4.10: Optimal Trajectories: Medium to Low Grade Ore Transition

the froth was found to show first-order dynamics; however, the value was at the constrained value of 0.35, and was an artifact of the computation. The optimal input trajectories generated here initially required steps in the middlings and flood water flow rates, after which they follow monotonic trajectories. The tailings withdrawal did not require an initial step and monotonically decreased to its optimal steady state value for a low grade ore.

The optimal recovery for the step from medium to low grade ore is shown in Figure 4.11. Initially a recovery of greater then 100% occurs and is attributed to the process initial steady state starting at a higher grade ore. Like the input trajectories the recovery follows a similar monotonic trajectory, until reaching its optimal steady-state value for a low grade ore.

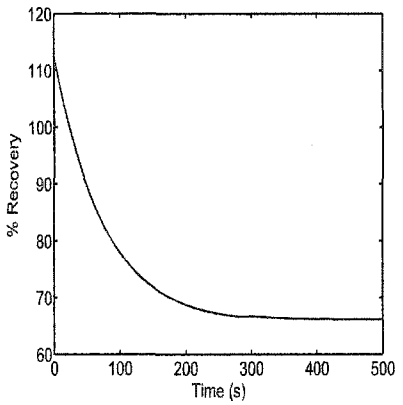

Figure 4.11: Optimal Recovery: Medium to Low Grade Ore Transition

Sensitivity of the inequality constraint values for the froth quality and tailings density were then examined using approximately a 3% perturbation in their nominal values. Figure 4.12 shows the results for the perturbations in the froth quality constraint. The

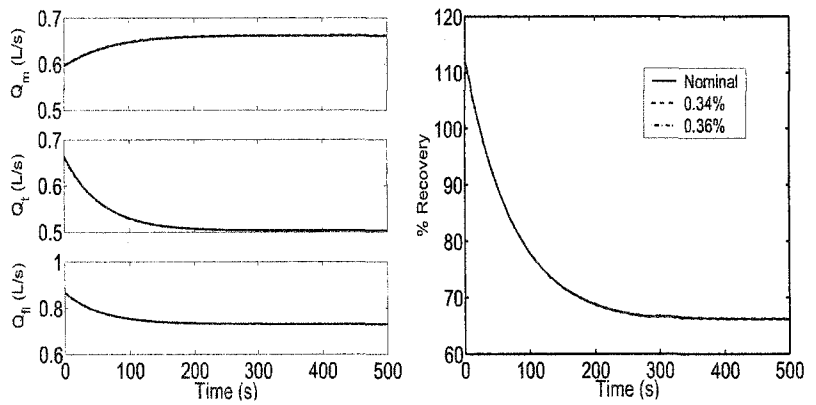

(a) Input Trajectories (b) Recovery

Figure 4.12: Froth Quality Sensitivity: Medium to Low Grade Ore Transition

results are similar to those found for the previous step from a high to medium grade ore. Again the insensitivity of the recovery and input trajectories to changes in the froth quality is attributed to large differences in the relative velocities of the particles compared to the bulk flow.

The effect of the tailings density on the recovery and input trajectories is shown in Figure 4.13. The tailings density, like in the previous study, shows greater sensitivity to

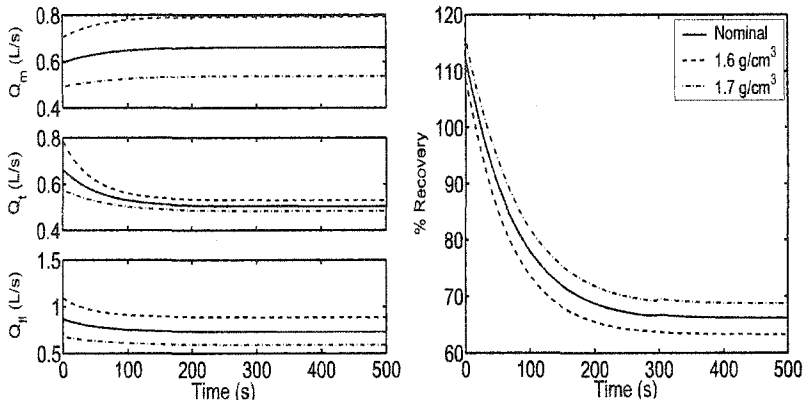

(a) Input Trajectories (b) Recovery

Figure 4.13: Tailings Density Sensitivity: Medium to Low Grade Ore Transition

both the input and recovery trajectories. The bulk flow into the tailings layer was found to be similar in magnitude to that of the relative velocities of the bitumen particles. The shape of the perturbed trajectories were found to be almost identical for both the inputs and recovery, with generally a shift up or down. For a tailings density of $1.6 g/cm^3$, tailings and flood water were both increased to accommodate the change. There was an unexpected reduction in the middlings withdrawal required for a lower density in the tailings, but can be attributed to the increase in the removal of material from the underflow.

The problem was then recast in RIOT form and the following trajectories for IST of 100s and 150s were generated. The restricted and unrestricted trajectories are compared in Figure 4.14. Only slight modifications to the inputs were necessary to satisfy the inequality constraints in the 300 seconds prior to the grade change. Input restriction removed the large initial steps present in the unrestricted case, at the grade transition time. The inputs showed reduced aggressiveness in the control, and followed gradually changing trajectories.

The restricted and unrestricted integral of the recovery during the grade transition are tabulated in Table 4.7. For the transition from a medium to low grade ore there was no difference between the recoveries for the unrestricted and restricted inputs. Again the large differences in magnitudes of the bitumen relative velocities and the bulk flow into the froth result in the insensitivity of the process to input restriction.

The lack of difference between the restricted and unrestricted forms suggests that the

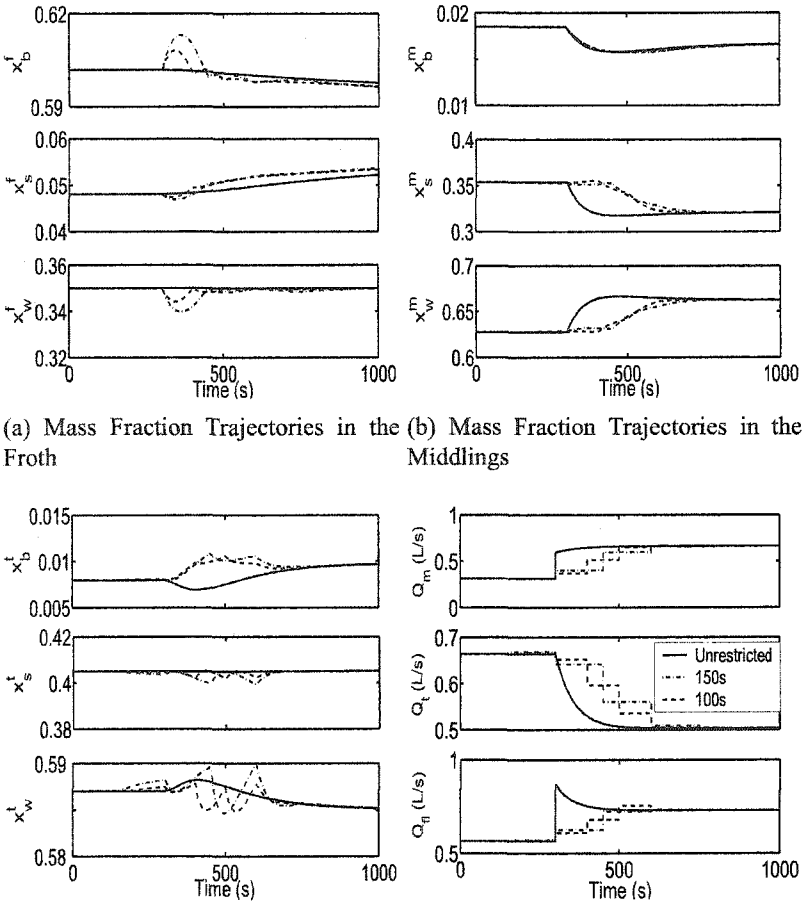

(a) Mass Fraction Trajectories in the Froth

(b) Mass Fraction Trajectories in the Middlings

(c) Mass Fraction Trajectories in the Tailings

(d) Input Trajectories

Figure 4.14: Restricted Input Optimal Trajectories: Medium to Low Grade Ore Transition

for this grade transition the adoption of a restricted input form is no better or worse then using a controller which can track the unrestricted trajectories. For this case only operator intervention is necessary to maintain the process within operating constraints.

4.3.3 Extreme Transitions

Two grade transitions found to be problematic in practice are considered. First a step from a high to low grade ore was considered, followed by a step from low to high grade ore. Sensitivity studies on the inequality constraints were considered, followed by the solution of the RIOT problem.

Case	Froth
Unrestricted	74.0%
100s	74.0%
150s	74.0%

Table 4.7: Restricted and Unrestricted Optimal Objectives: Medium to Low Grade Transition

High to Low Ore

The optimal trajectories for a high to low grade ore are shown in Figure 4.15. The input trajectories of Figure 4.3.3 are similar to those generated in the previous studies. Initial steps in both the middlings withdrawal and the flood water occur, after which each input approaches the optimal steady state values, monotonically. Froth quality is maintained at the constrained value of 0.35, and the tailings density also remained at its constrained bound throughout. The spike in froth quality is a result of the changing penalty functions at 300 seconds; however, the jump is insignificant. The optimal recovery during the interval is depicted in Figure 4.16. Greater than 100% recovery was found to occur initially, as was seen in the previous case studies, for this grade transition. As before, the high initial recovery is attributed to the initial operating conditions from a higher grade ore.

Sensitivity of the froth quality and tailings density constraints were performed with approximately a 3% increase and decrease in each of the constraints bounds. Examining the effects of froth quality, Figure 4.17 shows the recovery and input trajectories. As before, both the recovery and input trajectories are insensitive to changes in the froth quality constraint. There is essentially no visible difference for this grade transition, and again the bulk flow is found to be in the range of one to two orders of magnitude smaller than that of the bitumen particle relative velocities. The insensitive nature of the froth quality was believed to be a result of this difference.

The sensitivity of the recovery and input trajectories for changes in the tailings density is shown in Figure 4.18. The recovery and the input trajectories were found to be sensitive to changes in the tailings density constraint. The sensitivity of the middlings and flood water to changes in tailings density is much greater than the tailings withdrawal. The large change in the flood flow rate and middlings withdrawal rates suggests that increased load

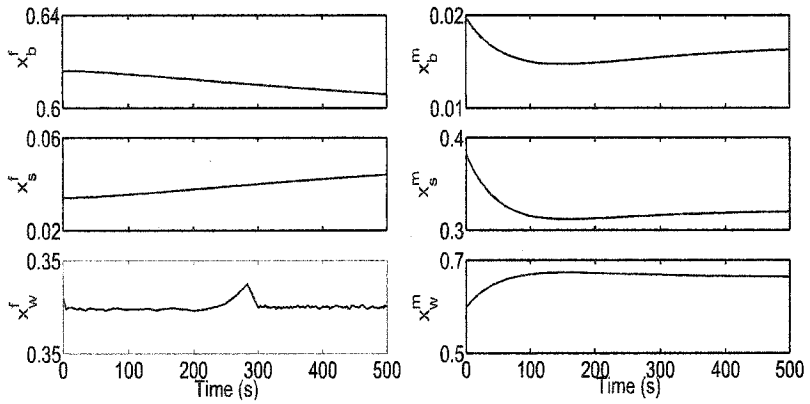

(a) Mass Fraction Trajectories in the Froth

(b) Mass Fraction Trajectories in the Middlings

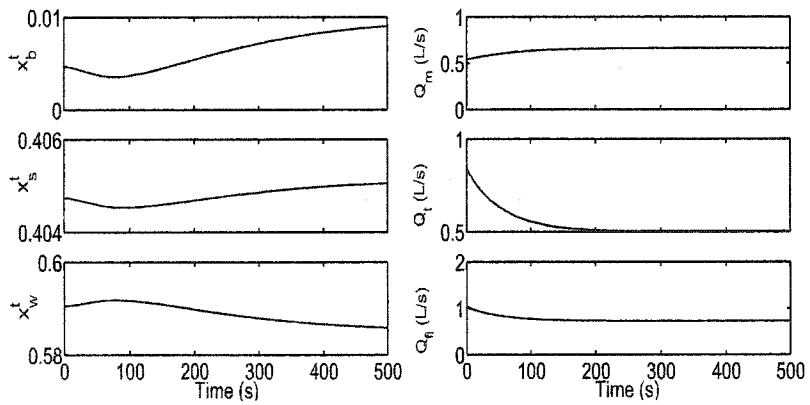

(c) Mass Fraction Trajectories in the Tailings

(d) Input Trajectories

Figure 4.15: Optimal Trajectories: High to Low Grade Ore Transition

will be placed on secondary recovery. The feed entering the vessel is high in fines and smaller bitumen particles, which have much lower relative velocity than coarse sands and large bitumen particles prominent in the original high grade ore.

Figure 4.3.3 shows that there is a relatively low sensitivity to the recovery for a period of 75-100 seconds after the grade transition. As the process approaches steady-state the effects of the change in tailings density are more profound.

The sensitivity of the recovery to perturbations in the tailings density was a result of the similarities between the magnitudes of the relative velocities of the bitumen particles and the bulk flow of fluid into the tailings. Increases in tailings density will require less

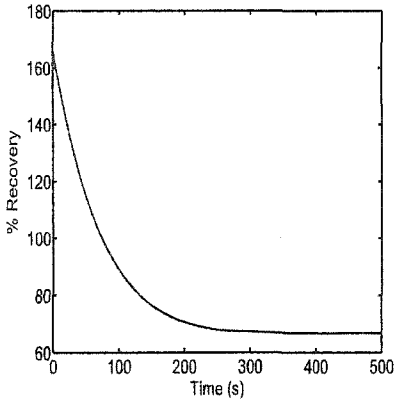

Figure 4.16: Optimal Recovery: High to Low Grade Ore Transition

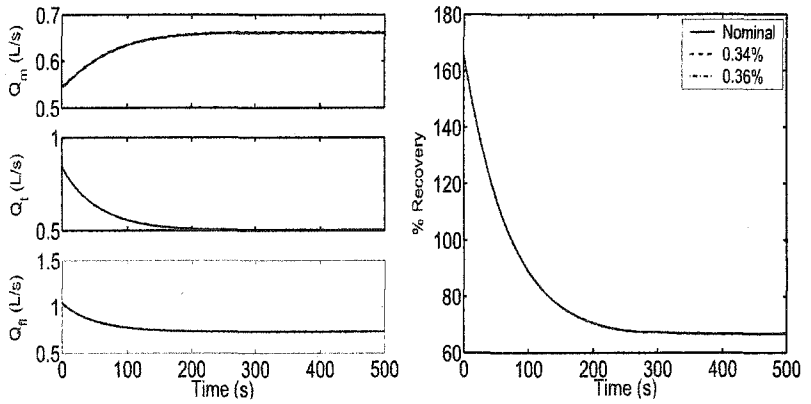

(a) Input Trajectories (b) Recovery

Figure 4.17: Froth Quality Sensitivity: High to Low Grade Ore Transition

water reporting to the tailings, decreasing the bulk flow, and thereby decreasing the flux of bitumen.

The problem is then recast into RIOT form and solved using Direct Transcription. The resulting state and input trajectories are shown in Figure 4.19. Only slight modifications to the inputs are necessary to satisfy the inequality constraints in the 300 seconds prior to the grade change. Input restriction removes the large initial steps present in the unrestricted case, at the grade transition time. The inputs show a back off in aggressiveness of the control, and follow gradually changing trajectories.

The restricted and unrestricted overall recoveries during the grade transition are tabulated

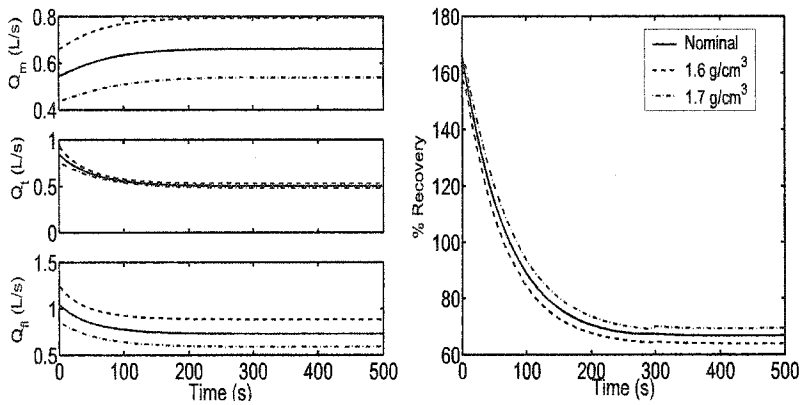

(a) Input Trajectories (b) Recovery

Figure 4.18: Tailings Density Sensitivity: High to Low Grade Ore Transition

in Table 4.8. For a low to high grade ore again the insensitivity of adapting the problem

Case	Froth
Unrestricted	81.2%
150s	81.6%
100s	81.6%

Table 4.8: Restricted and Unrestricted Optimal Objective: High to Low Grade Transition

to a restricted form again holds. Only minor differences in the integral of recovery are observed. The insensitivity of the froth quality, combined with the relative insensitivity of the tailings density constraint close to the transition, may lead to this result.

For a grade transition from a low to medium grade ore, the use of operator intervention alone is found to be adequate. The comparison between restricted and unrestricted results provides no push to adapt a more sophisticated control scheme.

Low to High Ore

The final case study will look into the transition from a low to high grade ore. The problem is first cast into the unrestricted form of problem 4.6 and solved using Direct Transcription. The optimal trajectories for the states and inputs are provided in Figure 4.20. The optimal input trajectories are similar in shape to all previous case studies, where initial steps are necessary in the flood water and middlings withdrawal. All flow rates then approach their

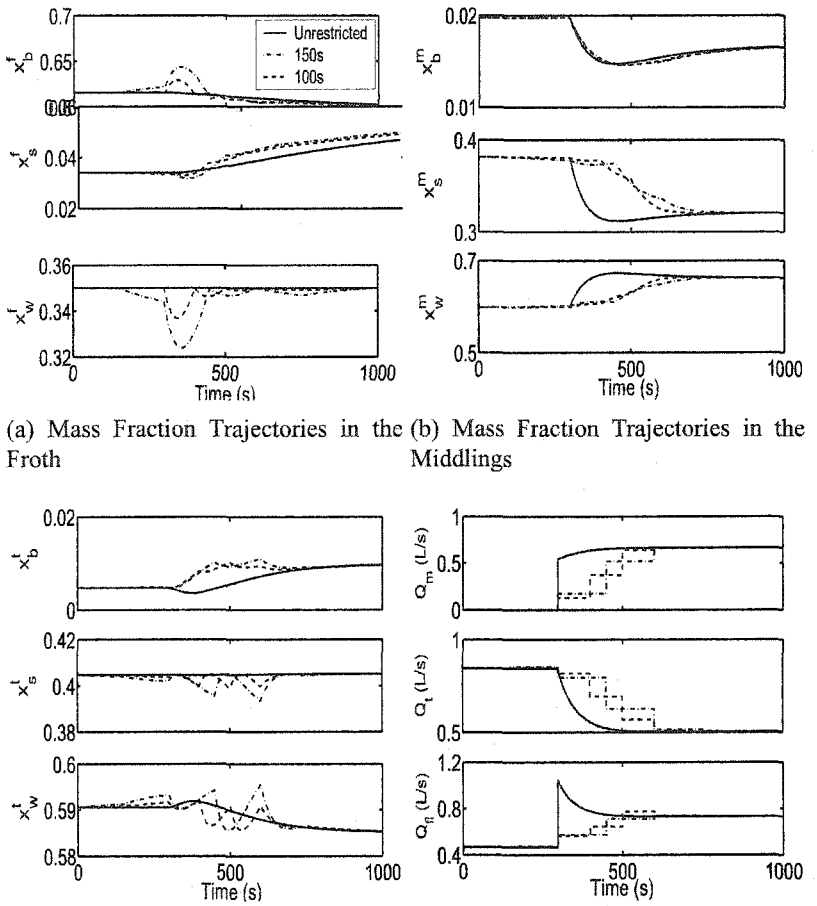

(a) Mass Fraction Trajectories in the Froth

(b) Mass Fraction Trajectories in the Middlings

(c) Mass Fraction Trajectories in the Tailings

(d) Input Trajectories

Figure 4.19: Restricted Input Optimal Trajectories: High to Low Grade Ore Transition

optimal steady-state values for the high grade ore. Discontinuities in Figure 4.20 are a result of middlings withdrawal being identically zero. The mass fraction of water in the froth is seen to remain around its constrained value of 0.35, with numerical noise. A slight spike in froth quality results near changes in the penalty functions; however, the change is an artifact of the computation.

The optimal recovery during the interval for a step from low to high grade ore is shown in Figure 4.21. Since the grade change starts from a low grade ore to a higher grade ore there are no recoveries greater than 100%. The initial recovery is lower than that for a low grade ore at steady state. The vessel is initially at steady-state conditions for a low grade

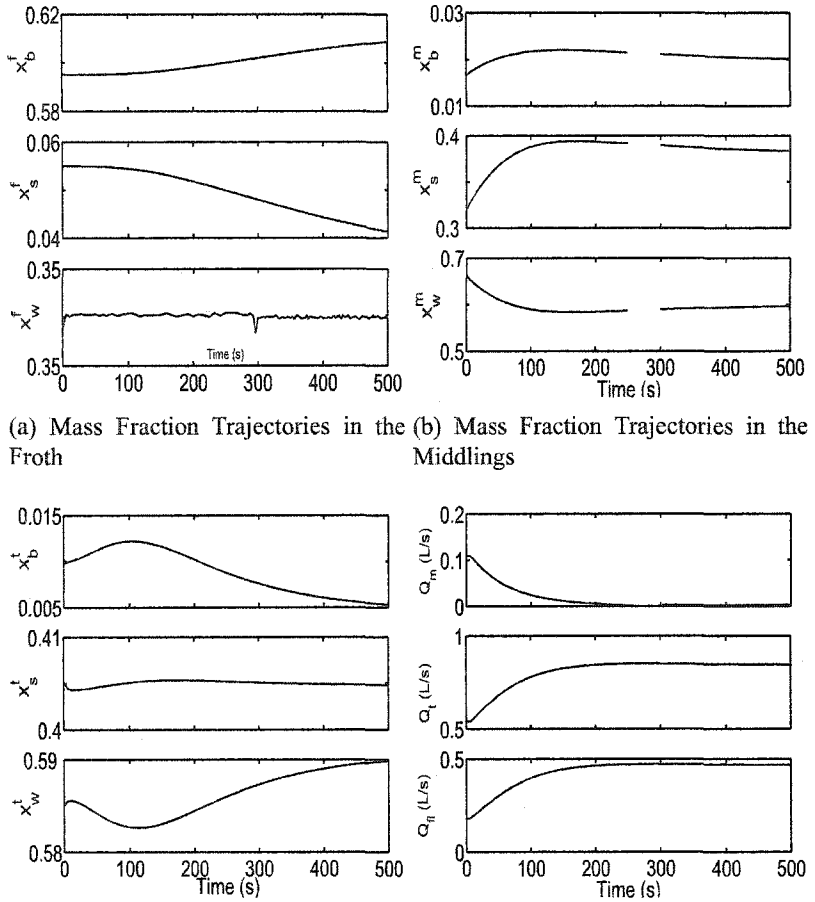

(a) Mass Fraction Trajectories in the Froth

(b) Mass Fraction Trajectories in the Middlings

(c) Mass Fraction Trajectories in the Tailings

(d) Input Trajectories

Figure 4.20: Optimal Trajectories: Low to High Grade Ore Tranisition

ore, when the instantaneous change in the ore grade occurs. The high quality feed pumps more bitumen in than is initially being recovered from the froth, resulting in the appearance of poor recovery. As the process reaches steady-state, the recovery is found to level out at the optimal value for the high grade ore.

Sensitivity studies were then done to evaluate the effects of changing both the froth quality and tailings density constraints on the vessel. Both the froth quality and tailings density were allowed to step up and down approximately 3% in their nominal values.

Figure 4.22 shows the responses of the recovery and input trajectories for changes in the froth quality levels. The froth quality constraint when varied was found, like in all previous

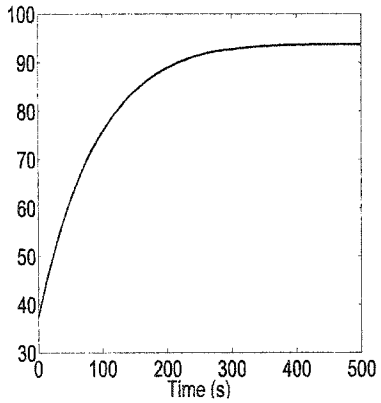

Figure 4.21: Optimal Recovery: Low to High Grade Ore Transition

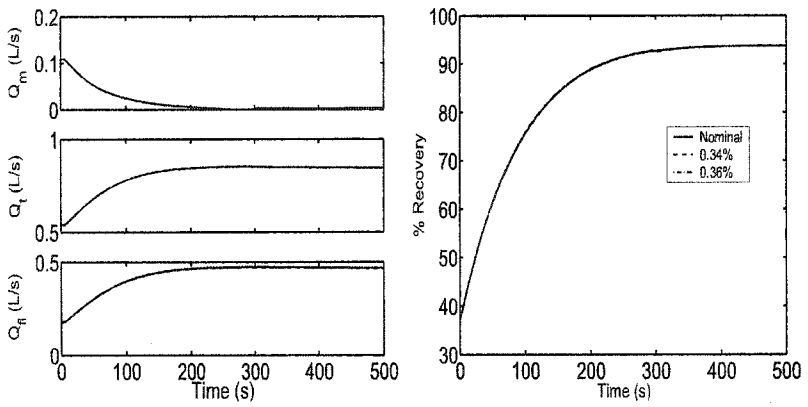

(a) Input Trajectories (b) Recovery

Figure 4.22: Froth Quality Sensitivity: Low to High Grade Ore Transition

case studies, to have an insignificant effect on the recovery and input trajectories. Again the insensitivity is attributed to the one to two orders of magnitude difference between the bitumen particle relative settling velocities and the bulk flow to the froth.

The optimal recovery and input trajectories, as in the previous studies were found to be sensitive to perturbations in the tailings density constraint. Figure 4.23 shows the effects of these perturbations. Unlike in the previous case study where there was high sensitivity in the flood and middlings flow rates, the input trajectories show decreased sensitivity. The middlings flow rate trajectory shows only slight deviations from the nominal trajectory, which is a result of the reduction of fines fed to the vessel. Additionally, the insensitivity

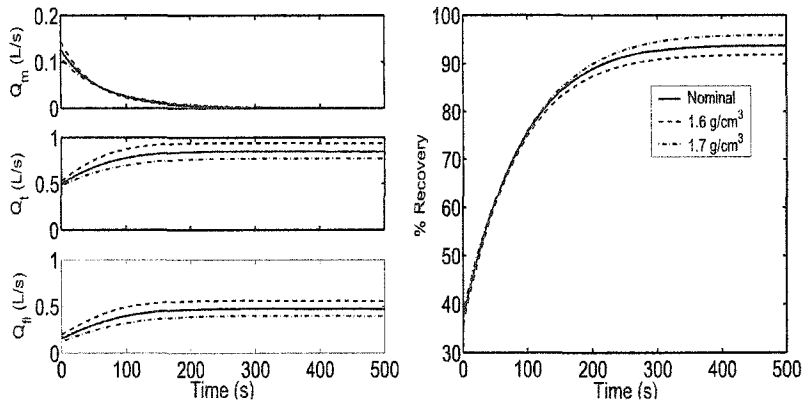

(a) Input Trajectories (b) Recovery

Figure 4.23: Tailings Density Sensitivity: Low to High Grade Ore Transition

of the steady-state middlings withdrawal rate for a high grade ore results in all middlings trajectories approaching zero.

The same reduction in sensitivity in the flood water flow rate is seen; however, it is not as dramatic as that seen in the middlings flow rate. The reduction in fines also leads to a decrease in the amount of flood water necessary to meet the tailings constraint. Water however, must still be added to account for the increase in coarse fines reporting to the tailings to maintain the tailings density constraint.

The recovery shows increased sensitivity only after approximately 1 time constant. The insensitivity after the grade change is suspected to occur after the time constant of the vessel. Only after sufficient time has passed will substantial changes in flux to the froth occur.

The optimal trajectory problem was then recast into the RIOT form, of problem 4.7, and was solved for IST of 100s and 150s. The resultant trajectories of the states and inputs are shown in Figure 4.24. The addition of step functions removes the smooth nature of the curves found in the unrestricted form. During the initial 300s of preventive action there is a slight shift in the flood water flow rate, to allow for a reduction in the mass fraction of water in the froth. The preventative action is necessary for a step from a low to high grade ore, as the shift to reduce the middlings withdrawal forces more water into the froth, while minimizing the flux into the tailings.

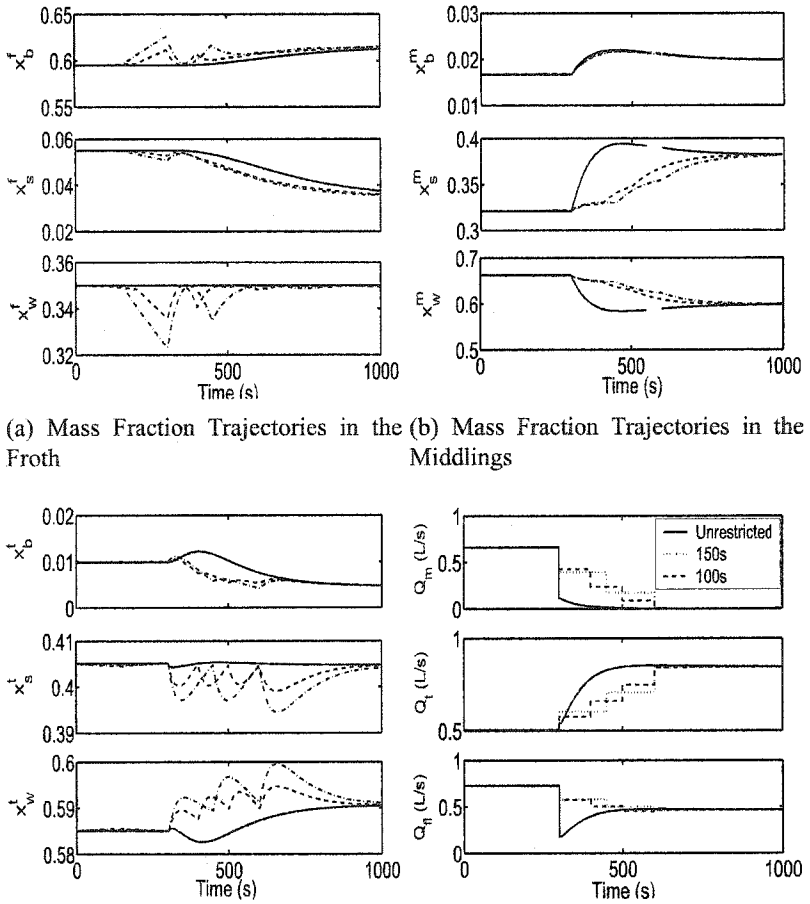

(a) Mass Fraction Trajectories in the Froth

(b) Mass Fraction Trajectories in the Middlings

(c) Mass Fraction Trajectories in the Tailings

(d) Input Trajectories

Figure 4.24: Restricted Input Optimal Trajectories: Low to High Grade Ore Transition

The objective for each of the unrestricted and restricted cases are listed in Table 4.9. The objective values are found to have a slight advantage to the unrestricted form; however, the difference is still negligible. Again for this grade change, the slight change in the objective is a fact of the process being insensitive to changes in the bulk flow. Manipulation of the inputs is found to have little effect on bitumen reporting to the froth. The use of input restriction for grade transitions from a low to high grade ore is found to be practical, with no need to adopt a sophisticated control structure to track the unrestricted optimal trajectories.

Case	Froth
Unrestricted	80.58%
100s	79.65%
150s	80.19%

Table 4.9: Restricted and Unrestricted Optimal Objectives: Low to High Grade Transition

4.4 Chapter Summary

A great deal of similarity was found between each of the case studies performed above. Firstly, all case studies were found to be oscillatory when the integral of the recovery was used as the objective function. Additional penalty constraints were necessary to force the inputs to follow realistic trajectories, as well as eventually settle towards an optimal steady-state.

The unrestricted optimal trajectories were found to be insensitive to changes in the froth quality constraint, as relative particle velocities for the bitumen particles were found to be on the order of one to two magnitudes in difference. The tailings density constraint was found to have a greater impact on the recovery and input trajectories; however, the sensitivity was found to occur approximately 1 time constant after the grade transition.

In all cases the restriction of inputs to step functions was performed and the results for all grade transitions suggested that there is no difference in recoveries between the restricted and unrestricted approaches. The lack of sensitivity towards the effects of bitumen flux to the froth with regards to the inputs confirms this result, as the bitumen reporting to the froth remains approximately constant for both restricted and unrestricted inputs. For some grade transitions the restricted form was found to show slight improvements in recovery, which was attributed to higher densities in the middlings. This higher density had the benefit of increasing the flux to the froth; however these effects were slight and so were removed by the penalty objective functions of the unrestricted case. The aforementioned density effects were also expected to add to the oscillation in the original non-penalized, unrestricted optimal trajectory cases.

For all grade transitions considered, input restriction was found to be insignificantly different from the unrestricted problem. Input restriction also had the benefit of reducing the aggressiveness of the control. In all cases the use of restricted inputs was found to be

acceptable and the addition of controllers, capable of tracking the unrestricted trajectories, was deemed not necessary. As well, large number of steps during a grade transition were found to produce minimal changes in recovery.

The proposed dynamic model for an oilsand gravity separation vessel could still be improved upon. The approximation of a particle size distribution for bitumen particles, which is broad in practice, was necessary to keep the problem to a reasonable size, such that timely solutions to the dynamic optimization problems were possible. The addition of more particles to the distribution may improve accuracy; however, each additional particle adds more equations, and increases the computational load.

The effects of using a steady state hindered settling relationship to describe a dynamic system will affect the range of applicability of the solution; however, further study must be done to evaluate this. Additionally, not considering the solution chemistry, and mixing issues removes certain degrees of freedom from the problem which may provide further differences in the objective of the process. Middlings density/viscosity was not considered in this model, where the increases in middlings viscosity above a certain limit can be detrimental to the process. The introduction of a middlings viscosity constraint may provide changes in the recovery; however, due to a lack of a good mathematical relationship, viscosity was not considered in this investigation.

5 Recommendations and Conclusions

5.1 Conclusions

In this work, existing dynamic models for gravity separation of bitumen from an oilsand slurry were taken from literature; and optimal input trajectories were determined using existing dynamic optimization theory. Additionally, the method of restricted inputs was proposed, where optimal trajectories were limited to step and ramp functions. This approach was applied to numerous grade transition case studies for the primary separation vessel (PSV). The conclusions are broken up into two sections: 1) input restriction and 2) PSV trajectory optimization.

5.1.1 Restricted Inputs

The method of restricted inputs was found to reduce the solution time of trajectory optimization problems, when a small number of step and ramp functions were used. The shortening in solution times was attributed to the reduction in the degrees of freedom associated with the problem. However, as the number of step and ramp functions are increased, the solution time was found to become greater than that of the original unrestricted problem. The increase in solution time is a combination of both increased

degrees of freedom, as well as the addition of more equality constraints. In all the case studies considered, the restricted input approach was found to generate input trajectories that were less aggressive. Large steps that occur in the unrestricted case studies were removed, and the overall range of values for the inputs decreased.

In general, input restriction was found to have losses in performance when compared to the unrestricted solutions. The sensitivity of the performance loss, with respect to input restriction, was found to vary depending on the problem and the number of steps and ramps used. The difference between the unrestricted and restricted objectives was found to be a useful control benefits evaluation tool. The large difference between unrestricted and restricted objectives provides incentives towards adopting more sophisticated controllers, which can track the unrestricted input trajectories.

5.1.2 Primary Separation Vessel Trajectory Optimization

The model for the primary separation vessel of an oilsands process was taken from literature. Additional changes were necessary to remove linear dependence from the modelling equations, for dynamic optimization.

Trajectory optimization of the Syncrude PSV provided similar results for all grade transitions considered. Initial trajectory optimizations of the PSV dynamic model were found to be oscillatory in nature and penalty terms in the objective function were necessary to dampen the input trajectories.

Two types of penalty functions were necessary: 1) those which dampen out the oscillation due to storage of bitumen in the froth and increased middlings density, and 2) those which bring the overall process to steady-state.

The first type of penalty function assumed that the process operated at the froth quality and tailings density constraints, which were the dominating phenomena during steady-state. The second set of penalty functions were designed to bring the process to the optimal steady-state operating conditions of the transitional ore. Initially, large penalization was placed on the removing the oscillation. After a period of approximately two time constants, emphasis was then placed on achieving steady-state. In all cases the switch between the two different penalty regimes was nearly smooth.

The resultant optimal state and input trajectories generated using the penalty objective function were found to be smooth, moving towards a new steady state. State and input trajectories were found to be insensitive to the froth quality constraint; whereas greater sensitivity was seen for the tailings density constraint. The insensitivity exhibited by the froth quality constraint was a result of the large difference between the relative bitumen particle velocities and bulk flow terms across the froth/middlings interface. The insensitivity is one of the contributors to the aforementioned oscillations in the input trajectories. The recovery was found to be sensitive to changes in the tailings density. This is a result of the similar magnitudes between the relative particle settling velocities and the bulk flow terms. Generally, the sensitivity in tailings density was insignificant, right after a grade change.

Comparison of the unrestricted and restricted optimal trajectory problems for all of the grade transitions were found to produce the same result. The recovery was insensitive to the restriction of the inputs. In some cases input restriction was found to cause slight, however insignificant increases in the objective. These slight increases were attributed to increased middlings density during the transition. These effects were removed by the penalty objective function in the unrestricted cases, and are suspected of adding to the oscillatory nature of the problem. The insignificant differences between the restricted and unrestricted solutions, shows that there is little incentive in adopting some sort of closed loop control strategy.

5.2 Recommendations

Further evaluation of the model, as well as improving parameters estimates, is necessary to improve the confidence in the physical and empirical parameters. Many of the output trajectories showed no significant transients within the range of experimental error. The development of more transient experiments, with some form of persistent excitation, would help to better fit the model to the actual process. As well, the experimental data was taken with recycle from secondary flotation recycle, not included in the PSV model. Further experimental studies without recycle from secondary separation may provide better correlation between the model and data.

A look into different model formulations may be beneficial. While the removal of the interface for the EXP2000 was a fairly safe assumption, this may not be true for a full size oilsands gravity separation vessel. Further studies may be required to evaluate the validity of the assumption of a static interface between the froth and middlings layers.

The development of viscosity relationships for mixtures of bitumen, water and sand would allow for additional constraints to protect against vessel gelling or other upset conditions. Furthermore, the use of the actual middlings viscosity, as opposed to that of water, in determining the settling velocities of the particles is expected to give a more accurate result.

Additional studies into determining an appropriate set of particles, which would produce an accurate representation of the bitumen particle size distribution, would be beneficial. The effects of chemistry and mixing on the particle size distribution within the hydrodynamic pipeline, and the characterization of this relationship between the particle size distribution and ore grade will increase overall understanding of the process. A well characterized feed ore will help the operator to understand exactly what type of ore is approaching, and what corrective action will be necessary.

Actual implementation of these optimal trajectories requires that the PSV operators have advanced knowledge of the ore coming from the mine. The need for online data for fines and grade of the ore within the pipeline, combined with a reliable empirical relationship for the particle size distribution, are the main inputs necessary before actual determination and implementation of these optimal trajectories can be accomplished.

In the studies conducted, five minutes were given for preventative action; however, additional studies may be performed to determine the smallest amount of time required. Operation guidelines may then be developed, through the use of studies like those transition studies in Chapter 4.

Expansion of the model to include secondary separation, as well as the centrifuges and inclined plate settlers, could provide a understanding of how the PSV and secondary recovery should be operated to minimize the load placed on the downstream separation of water and solids. The insensitivity of the froth quality found in the studies performed, suggests that including the centrifuges and inclined plate settlers into the solution process

will find different operating conditions for the PSV. Currently the constitutive relationships are not well know for these units. Either well-identified phenomenological or empirical models employing black box system identification approaches is required before any overall cost optimization could be done.

Work is still required before well informed control interventions can be used to control an oilsand gravity separation vessel. This thesis provides the framework for determining optimal input trajectories for different ore grade transitions. The open-loop control practices associated with the these vessels made it desirable to limit these optimal input trajectories to easily implementable sets of step and ramp functions. This work further suggests that sufficient control of this vessel can be done manually, while still maximizing the amount of bitumen recovered from the PSV. The eventual result of these studies, combined with the recommendations above, is a set of operating guidelines for operations personnel.

Bibliography

[1] Ascher, U.M., L.R. Petzold, *Computer Methods for Ordinary Differential Equation and Differential-Algebraic Equations*, SIAM, Philadelphia PA, 1998.

[2] Ascher, U., L. Ping, Sequential Regularization Methods for Nonlinear Higher-Index DAEs *SIAM J. Sci. Comp.*, **18**, 1997, pp. 160-181.

[3] Asprey, S.P., Macchietto, S., *Design Robust Optimal Dynamic Experiments* J. Proc. Cont. (12) 2002, 545-556.

[4] Asprey S.P., S. Macchietto, Statistical Tools for Optimal Dynamic Model Building *Comp. Chem. Eng.* **24**, 2000, 1261-1267.

[5] Babolian, E., M.M. Hosseini, Reducing Index, and Pseudospectral Methods for Differential-Algebraic Equations *App. Math. Comp.*, **140**, 2003, pp.77-90.

[6] Baltes, M., R. Schneider, C. Strum, M. Reuss, Optimal Experimental Design for Parameter Estimation in Unstructured Growth Models *Biotechnol. Prog.* **10**, 1994, 480-488.

[7] Banga, J.R., Versyck, Van Impe, J.F., *Computation of Optimal Identification Experiments for Nonlinear Dynamic Process Models: a Stochastic Global Optimization Approach*, Ind. Eng. Chem. Res. (41) 2002, 2425-2430.

[8] Bauer, I., Bock, H.G., Körkel, S., Schlöder, J.P., *Numerical Methods for Optimum Experimental Design in DAE Systems*, J. Comp. App. Math., (120) 2000, 1-25.

[9] Bellman, R.E., *Dynamic Programming*, Princeton University Press, (1958).

[10] Betts, J.T., *Practical Methods for Optimal Control Using Nonlinear Programming*, SIAM (2001).

[11] Betts, J.T., W.P. Huffman, Mesh refinement in direct transcription methods for optimal control *Optim. Control Appl. Methods*, **19**, (1998), 1–21.

[12] Biegler, L.T., Solution of Dynamic Optimization Problems by successive quadratic programming and orthogonal collocation. *Comp. Chem. Eng.*, **8**(3/4), (1984), 243–248.

[13] Brenan, K.E., S.R. Campbell, L.R. Petzold, *Numerical Solution of Initial-Value Problems in Differential-Algebraic Equations*, North-Holland, New York, 1989.

[14] Brokett, R.W., *Finite Dimensional Linear Systems* Wiley, New York, 1969.

[15] Campbell, S.L., Intelligent DAE Solvers and User Friendly Design, Simulation, and Analysis Packages *Proc. IEEE Intern. Conf. Systems, Man, Cybernetics*, 2003.

[16] Campbell, S.L., E. Moore, Y. Zhong, Utilization of Automatic Differentiation in Control Algorithms *IEEE Trans. Auto. Cont.* **395**, 1994, 1047-1052.

[17] Chapra, S.C, R.P. Canale, *Numerical Methods for Engineers*, McGraw-Hill, 3rd Ed., (1998).

[18] Chen B.H., S.P. Asprey, On the Design of Optimally Informative Dynamic Experiments for Model Discrimination in Multiresponse Nonlinear Situations *Ind. Eng. Chem. Res.* **42**, 2003, 1379-1390.

[19] Concha, F., E.R. Almendra, Settling Velocities of Particulate Systems, 2. Settling Velocities of Suspensions of Sphereical Particles. *Int. J. Miner. Process.*, **6**, 1979, 31-41.

[20] Cuthrell, J.E., L.T. Biegler, Simultaneous Optimization and Solution Methods for Batch Reactor Control Profiles *Comp. Chem. Eng.*, **13**(1/2), (1989), 49–62.

[21] Cuthrell, J.E., L.T. Biegler, On the Optimization of Differential-Algebraic Process Systems *AIChE*, **33**(8), (1987), 1257–1270.

[22] Dabros, M., P. Stuart, J.F. Forbes, M. Perrier, M. Fairbank, Improving the Broke Recirculation Strategy in a Newsprint Mill, *Pulp & Paper Canada*, **105**(4), (2004), 45–48.

[23] Dadebo, S. A., K. B. McAuley, Dynamic Optimization of Constrained Chemical Engineering Using Dynamic Programming *Comput. Chem. Eng.*, **19**(5), (1995), 513–525.

[24] Discussions with Syncrude Operations Personnel Syncrude Research Centre, June 2004.

[25] EXP 2000: Separation Circuit *Research Dept. Prog. Rep.* **31**(10), 2002

[26] Fedorchuk-Hrynda S., E. McDonald, J. Freimark, B.J. Loza Sycrude - The Basic Facts Syncrude Portal, 2003.

[27] Feehery, W.F., P.I. Barton, Dynamic Simulation and Optimization with Inequality Path Constraints *Comp. and Chem. Eng.*, **20**(Supp.), (1996), S707–S712.

[28] Forbes, M., A Simple Dynamic Model of the Syncrude PSV. *Syncrude Research Dept. Progress Report*, **27**(8), 144–172.

[29] Gear, C.W., The Simultaneous Numerical Solution of Differential-Algebraic Equations *IEEE Trans. Circuit Theory*, CT-81, 1971, pp.89-95.

[30] Goh, C.J., L.K. Teo, Control Parametrization: A Unified Approach to Optimal Control Problems with General Constraints *Automatica* , **24**, (1988),3–18.

[31] Guay, M., S. Kansal, J.F. Forbes, Trajectory Optimization for Flat Dynamical Systems *Ind. Eng. Chem. Res.*, **40**, (2001), 2089–2102.

[32] Kwong T.K., F.A. Seyer, J.H. Masliyah Theoretical and Experimental Studies of a Gravity Separation Vessel. *Ind. Eng. Chem. Proc. Des. Dev.*, **20**, (1982), 154–160.

[33] Kasperski, K.L. *A Review of Oil Sands Aqueous Extraction Research* Natural Resources Canada, CANMET-WRC.

[34] Logsdon, J.S., L.T. Biegler, Accurate Solution of differential algebraic equations. *Ind. Chem. Eng. Res.*, **28**, (1989), 1628–1639.

[35] Logsdon, J.S., L.T. Biegler, Decomposition Strategies for Large Scale Dynamic Optimization Problems. *Chem. Eng. Sci.*, **47**, (1992), 851–864.

[36] Luus, R., Application of iterative dynamic programming to state constrained optimal control problems *Hung. J. Ind. Eng.*, (1991), 245–254.

[37] Luus, R., *Iterative Dynamic Programming*, Chapman and Hall/CRC Monographs and Surveys in Pure and Applied Mathematics, (2000).

[38] Mangesh K.D., R.D. Ravindra, Optimal Control of Fed-Batch Fermentation Involving Multiple Feeds Using Differential Evolution *Process Biochemistry* 2003.

[39] Masliyah, J., Cluett, W., Oxenford, J., Tipman, R. *Dynamic Simulation of a Gravity Separation Vessel,* Control, Mineral/Metallurgical Processing, 1984.

[40] Mattson, S., G. Söderlind, Index Reduction in Differential-Algebraic Equations Using Dummy Derivatives *SIAM J. Sci. Comp.*, **14**, 1993, pp.677-692.

[41] Raghunathan, A.U., L.T. Biegler, An MPEC Formulation for Dynamic Optimization of Distillation Operations, *Comp. and Chem. Eng.*, **28**, (2004), 1–27.

[42] Raghunathan, A.U., L.T. Biegler, Mathematical Programs with Equilibrium Constraints (MPECs) in Process Engineering *Comp. & Chem. Eng.*, **27**, (2003), 1381–1392.

[43] Ray, W.H., *Advanced Process Control* McGraw Hill, New York, 1981.

[44] Sparse Optimal Control Software, Users Manual, Boeing, Release 6.2.

[45] Swanson, V.F., The Development of a Formula for the Direct Determination of Free Settling Velocity of Any Size Particle *Trans AIME*, **238**, 1967, 160-166.

[46] Swanson, V.F., Modification to Swansons's Free Settling Equation *Trans AIME*, **258**, 1975, 102-103.

[47] Taylor, J.H., Dawit Kebede, Modelling and Simulation of Hybrid Systems in Matlab. *Proc. IFAC World Congress*, San Fransico, CA, July 1996.

[48] Taylor, J., *Tools for Modeling and Simulation of Hybrid Systems - A Tutorial Guide* Dept. Electrical and Comp. Eng. University of New Brunswick, Sept. 1999.

[49] Villadsen, J., *Solution of Differential Equation Models by Polynomial Approximation*, Prentice-Hall, Englewood Cliffs, N.J., 1978.

[50] Wallis, G.B., *One-Dimensional Two-Phase Flow* McGraw-Hill, Toronto, 1969.

[51] Wang, Y., H. Seki, S. Ohyama, K. Akamatsu, M. Ogawa, M. Ohshima, Optimal Grade Transition Control for Polymerization Reactors *Comp. Chem. Eng.*, **24**, (2000), 1555–1561.

[52] Wiercigroch, M., *Modelling of Dynamical Systems with Motion Dependent Discontinuities,* Chaos, Solitons and Fractals, (11) 2000, 2429-2442.

[53] Xinyou, Yin., J. Goudriaan, E.A. Lantinga, J. Vos, H.J. Spiertz, A Flexible Sigmoid Function of Determinate Growth *Annals of Botany*, **91**, 2003, 361-371.

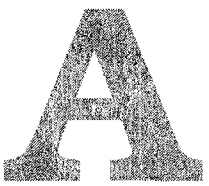

PSV Physical Parameters and Parameter Estimation

The following appendix defines the physical parameters associated with the PSV model defined in Chapters 2 and 4. The physical parameters here are fit to those for the EXP2000 pilot plant located at Syncrude Research centre. This appendix also outlines a method for parameter identification for dynamic models, and uses this method to determine certain physical, as well as empirical parameters.

A.1 Physical Parameters

Those physical parameters which are not included in the parameter estimation problem are tabulated in Tables A.1 and A.2

All remaining parameters were determined using the parameter estimation problem in the next section.

Parameter	Magnitude	Units	Comments
A	0.085	n/a	Normalized Area
V_f	0.1998	n/a	Normalized Volume of Froth
V_m	0.6445	n/a	Normalized Volume of Middlings
V_t	0.1557	n/a	Normalized Volume of Tailings
V_{vessel}	1	n/a	Normalized Volume of PSV
g	980.6	cm/s^2	Gravitation Constant
ρ_s	2.650	g/cm^3	Density of Solid
ρ_w	0.9718	g/cm^3	Density of Water
v	0.00325	$g/cm \cdot s$	Viscosity of Water

Table A.1: Physical Parameters

Parameter	Magnitude	Comments
γ_1	0.6	Hindering Factor 1 [28]
γ_2	1.6	Hindering Factor 2 [28]
θ_{sphere}	0.942	Spherical Settling Factor
$\theta_{platelet}$	2.43	Platelet Settling Factor
β_{sphere}	3.03	Spherical Settling Factor
$\beta_{platelet}$	5.7	Platelet Settling Factor

Table A.2: Settling Factors

A.2 Parameter Estimation

First the parameter identification of dynamic systems is introduced, using Direct Transcription to solve the dynamic optimization problem, with the objective of minimizing the residuals. The method is then applied to EXP2000 transient experimental data, and the results are discussed.

A.2.1 Parameter Estimation of Dynamic Systems

The method of optimal experimental design and parameter identification has received attention in recent literature. A sequential process of optimal experimental design and parameter identification is used to achieve the desired parameters to some statistical degree of significance. For the current work, the data for analysis has been collected and so experimental design will be neglected in this case. The reader is referred to the following work ([8], [7], [3]) for optimal experimental design.

The method of parameter optimization for dynamical systems can be taken from any of

the above references; however, the method presented by Betts [44] is discussed. Chapter 3 reviews dynamic optimization and Direct Transcription.

The optimal parameter optimization problem can be stated as follows:

$$\begin{aligned}
&\min_{\mathbf{p}} \frac{1}{2}\mathbf{r}^T\mathbf{r} \\
&s.t. \\
&\quad \mathbf{f}(\dot{\mathbf{x}}(t), \mathbf{x}(t), \mathbf{z}(t), \mathbf{u}(t), \mathbf{p}, t) = \mathbf{0} \\
&\quad \mathbf{g}(\mathbf{x}(t), \mathbf{z}(t), \mathbf{u}(t), \mathbf{p}, t) = \mathbf{0} \\
&\quad \mathbf{h}(\mathbf{x}(t), \mathbf{z}(t), \mathbf{u}(t), \mathbf{p}, t) \leq \mathbf{0} \\
&\quad \mathbf{x}(t)^L \leq \mathbf{x}(t) \leq \mathbf{x}(t)^U \\
&\quad \mathbf{z}(t)^L \leq \mathbf{z}(t) \leq \mathbf{z}(t)^U \\
&\quad \mathbf{u}(t)^L \leq \mathbf{u}(t) \leq \mathbf{u}(t)^U \\
&\quad \mathbf{p}^L \leq \mathbf{p} \leq \mathbf{p}^U
\end{aligned} \tag{A.1}$$

Where $\mathbf{r}$ represents the residuals, which can be stated as:

$$r_k = w_{ij}\left[x_i(\theta_{ij}) - \hat{x}_{ij}\right] \tag{A.2}$$

$$r_k = w_{ij}\left[z_i(\theta_{ij}) - \hat{z}_{ij}\right] \tag{A.3}$$

$$r_k = w_{ij}\left[u_i(\theta_{ij}) - \hat{u}_{ij}\right] \tag{A.4}$$

where i represents the calculated state, or input variable of interest, at time θ_{ij}, where $\hat{x}$, $\hat{z}$, and $\hat{u}$ represent the measured value. The constants w are added weights.

The above problem is then discretized and Direct Transcription is used to give an underlying optimization problem (Ch. 3.3.2). Additional considerations must be taken into account to calculate the states and inputs at times θ_j, which are not necessarily the same as the mesh points from discretization. To account for differences in the values of the states and inputs, interpolating polynomials are used. SOCS uses a Hermite interpolating polynomials for the dynamic variables.

$$x_i(\theta_i j) = (1-3\delta^2+2\delta^3)x_{i,k}+(3\delta^2-2\delta^3)x_{i,k+1}+(h_j\delta-2h_j\delta^2+h_j\delta^3)f_{i,k}+(-h_j\delta^2+h_j\delta^3)f_{i,k+1} \tag{A.5}$$

Where i represents the index of the desired state, j the data evaluation time and k the relevant discretization point given by $t_k < \theta_j < t_{k+1}$, where $h_k = t_{k+1} - t_k$ is the length of the discretization interval and $\delta = (\theta_i j - t_k)/h_k$, which describes the location of the data point.

For non-dynamic variables $\mathbf{u}$ and $\mathbf{z}$, the method of interpolation used depends on the numerical method used to approximate the derivative and integral terms. For higher order methods, the increased number of function evaluations during a discretization interval can be used for interpolation. SOCS uses a quadratic interpolant when the Hermite-Simpson method is used, and linear interpolation when using the trapezoidal method.

The above method can then be solved using the correct algebraic optimizer. Discretization and numerical approximation errors are still evaluated and mesh refinements and order manipulation is done as required.

A.2.2 PSV Parameter Identification

There are a number of time independent parameters, both physical and empirical, which must be fit to the process. The parameter optimization problem follows that presented above, where phases [44] are introduced to reproduce the experimental design of the

transient data. The problem can be stated as follows:

$$
\begin{aligned}
&\min_{\mathbf{p}_k} \frac{1}{2}\mathbf{r}_k^T\mathbf{r}_k \\
&s.t. \\
&\quad \mathbf{f}_k(\dot{\mathbf{x}}_k(t), \mathbf{x}_k(t), \mathbf{z}_k(t), \mathbf{u}_k(t), \mathbf{p}_k, t_k) = \mathbf{0} \\
&\quad \mathbf{g}_k(\mathbf{x}_k(t), \mathbf{z}_k(t), \mathbf{u}_k(t), \mathbf{p}_k, t_k) = \mathbf{0} \\
&\quad \mathbf{h}_k(\mathbf{x}_k(t), \mathbf{z}_k(t), \mathbf{u}_k(t), \mathbf{p}_k, t_k) \leq \mathbf{0} \\
&\quad \boldsymbol{\varphi}_1^I(\mathbf{x}_1^I, \mathbf{z}_1^I, \mathbf{u}_1^I, \mathbf{p}_1^I, t_1^I) = \mathbf{0} \\
&\quad \boldsymbol{\phi}_{j-1}^F(\mathbf{x}_{j-1}^F, \mathbf{z}_{j-1}^F, \mathbf{u}_{j-1}^F, \mathbf{p}_{j-1}^F, t_{j-1}^F) = \boldsymbol{\phi}_j^I(\mathbf{x}_j^I, \mathbf{z}_j^I, \mathbf{u}_j^I, \mathbf{p}_j^I, t_j^I) \\
&\quad \mathbf{x}_k(t)^L \leq \mathbf{x}_k(t) \leq \mathbf{x}_k(t)^U \\
&\quad \mathbf{z}_k(t)^L \leq \mathbf{z}_k(t) \leq \mathbf{z}_k(t)^U \\
&\quad \mathbf{u}_k(t)^L \leq \mathbf{u}_k(t) \leq \mathbf{u}_k(t)^U \\
&\quad \mathbf{p}_k^L \leq \mathbf{p}_k \leq \mathbf{p}_k^U \\
&\quad \text{k=1,..,3,} \quad \text{j=2,3}
\end{aligned}
\tag{A.6}
$$

where 3 intervals (k) are used to capture the experimental design of a step up and down in the feed ore. In the first interval a regular ore is used, followed by a step to a lower grade ore in the second interval and then a step back to the regular ore in the last interval. Here φ is used to constrain derivatives to zero during the initial interval, and ϕ is used to ensure state continuity at the phase bounds.

Additional algebraic relationships were also added to convert the volume fractions to mass fractions. The concentrations from the EXP 2000 transient tests were then approximated using the model. The parameters and their optimal values are shown below in Table A.3. Figure A.1 shows the composition trajectories of the model using the above parameters.

The Figure A.1 show that the model does not fit the experimental data with great confidence. Many of the concentrations of the species show no movement after the step down in feed ore. Two main problems are associated with using this data for parameter identification purposes; 1) there is insufficient excitation of the disturbance for evaluation of the parameters; and 2) the experimental design used here included a recycle loop from

Parameter	Magnitude	units	Comments
λ_b	0.327355		Bitumen Middlings Withdrawal Factor [28]
λ_s	1.25704		Solid Middlings Withdrawal Factor [28]
σ_b^f	0.492595		Bitumen Froth/Middlings Settling Factor
σ_b^t	0.300630		Bitumen Middlings/Tailings Settling Factor
σ_s^f	0.0		Solids Froth/Middlings Settling Factor
σ_s^t	0.0, 0.0, 1.0		Solids Middlings/Tailings Settling Factor
ρ_b	0.8, 0.75, 0.7	g/cm^3	Density of Aerated Bitumen
d_b	0.028, 0.058, 0.07	mm	Diameter of Bitumen Bubbles
d_s	7.8, 13.1124, 125.0	μm	Diameter of Solid Particles
Qm	0.3685	dm^3/s	Middlings Withdrawal Rate
Qt	0.42275	dm^3/s	Tailings Withdrawal Rate
V_{mix}	415.035	dm^3	Effective Tumbler and Mixing Tank Volume

Table A.3: Estimated Parameters

the secondary flotation unit. The use of a single step does not provide enough insight into the actual process, especially for parameter identification purposes. The magnitude of the step in feed ore was found to be insufficient as many of the outputs which were expected to vary were found to remain constant. The measurement errors associated with recovery and composition are large in nature, approximately 5% of the measured value. A sufficient step in feed ore should be used to overcome this problem. Those variables that did show transient behaviour also did so in an unexpected fashion. The sluggishness of the data also suggests that the recycle also effectively increases the time constant of the process, and the use of only primary recovery is expected to give better results.

In the future for parameter identification for this model it is recommended that sufficient excitation of substantial magnitude be used for disturbance trajectories. For the experimental design, either the model must be updated to include secondary flotation, or secondary flotation be turned off. Improved sampling and analysis techniques should be considered to reduce measurement errors as much as possible.

Some results can still be drawn from the above analysis, the effective volume of the mixer and tumbler found here provides a useful result and will be used. Also there is a definite trend for fines to be described using an entrainment model alone, which has become commonly accepted [33]. The above results show that it may be necessary to include entrainment factors for the fines trapped in bitumen to more accurately describes solids

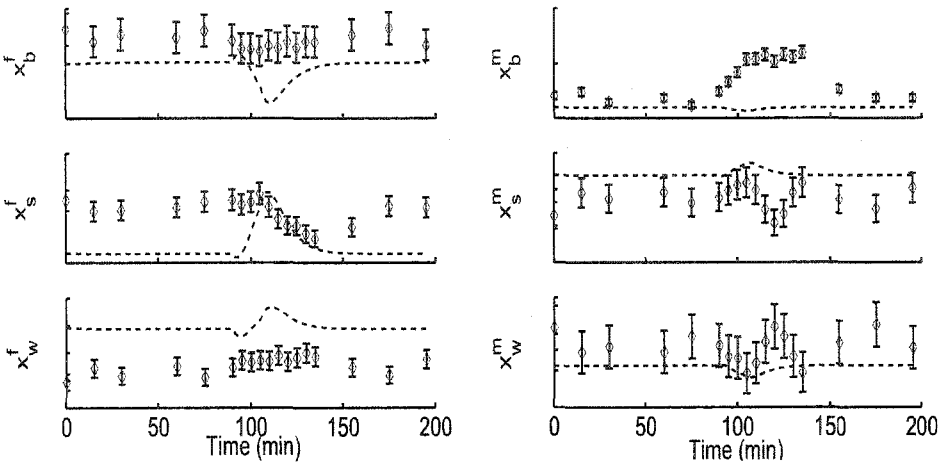

(a) Froth Layer Compositions (b) Middlings Layer Compositions

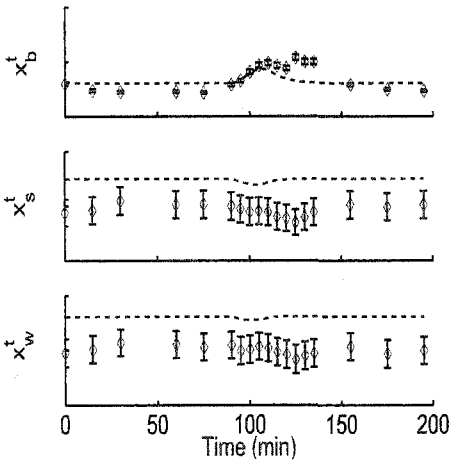

(c) Tailings Layer Compositions

Figure A.1: Parameter Identification Trajectory Comparison

in the froth. The parameters identified above will be used as they provide a reasonable reflection of normal operating compositions.

B

PSV Optimization and Simulation Model Comparison

As stated in Chapter 4 the presence of linear dependence and variables with zero range was found to cause the Jacobian to be singular, or ill-conditioned. This appendix examines the effect of the assumptions made to formulate the PSV modelling equations in a form usable for optimization. The assumptions are first restated.

The material balances for water were removed in all layers, where the appearance of these variables in the bulk flow equations 2.20 and 2.21 are replaced with the expression:

$$\alpha_w^i = 1 - \sum_{j=1}^{n_p} \alpha_j^i$$

where i is either the froth, middlings or tailings layers.

The use of the Wallis shockwave equation was found to introduce linear dependency in the modelling equations.

$$v_I = \frac{\sum_{j=1}^{3} \alpha_{b_j}^m v_{b_j}^m - \sum_{j=1}^{3} \alpha_{b_j}^f v_{b_j}^f}{\sum_{j=1}^{3} \alpha_{b_j}^m - \sum_{j=1}^{3} \alpha_{b_j}^f} \tag{B.1}$$

At steady-state, the equation is equivalent to the sum of the bitumen material balances in the froth layer. This equation, and the equations describing the dynamic interface between

the froth/middlings layer were removed. The removal of the dynamic nature of the froth middlings interface removed many of the discontinuities discussed in the chapter 2.

Lastly, certain variables were generally found to have zero range in the original model. The largest less dense bitumen particles were not found to report to the tailings layer; similarly the largest and heaviest solid particles were not found to report to the froth. For this reason, the variables were zero throughout the entire solution, resulting in ill-conditioning of the Jacobian. Equations and terms in the layer material balances, as well as the relevant constitutive relationships, were removed, as discussed in Chapter 4.

Numerical integrations of the two different models were conducted to determine the effects of the optimization assumptions. Two studies were conducted, including both extreme conditions from a low to high grade ore and from a high to low grade ore. The extreme grade transitions were chosen as these two exhibit the largest difference between solutions.

Inputs were held constant at their respective steady-state values for the disturbance ore. From here on the model developed in Chapter 2 and the model developed for optimization will be referred to as the original and reduced models, respectively.

Figure B.1 shows the state trajectories for both the original and reduced PSV models, for a step from a high to low grade ore. The only visible differences between the two models occurs in the froth layer mass fractions; however, the difference is quite small. There is no deviation between initial and final steady-state values for all layers.

The differences in the froth mass fractions during the transition between steady-states is possibly the result of the change in the froth volume, which affects the time constant of this layer. Another possible explanation is the two-way flow of materials across the froth layer, not modelled in the reduced model.

The removal of both the water material balances, and variables with zero range were not found to have any effect on the solution. In these cases, the equations provided no new information in the model.

The transition from a low to high grade ore is considered next, where the input values are held at the steady-state optimum for a high grade ore. Figure B.2 shows the state trajectories. The lack of middlings compositions is a result of $Q_m = 0$.

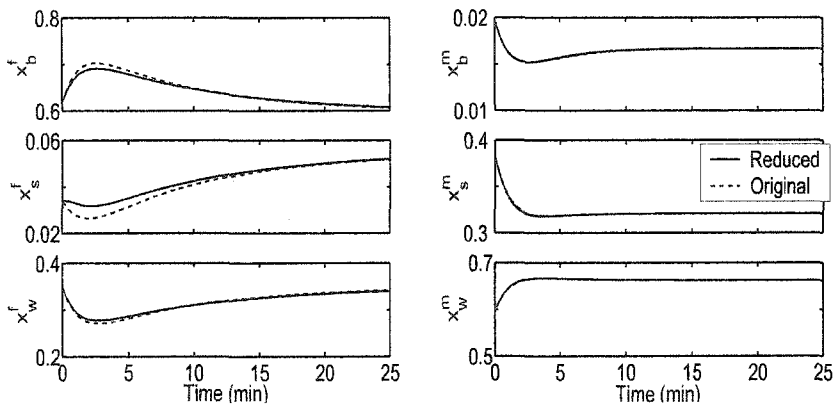

(a) Froth Layer Compositions (b) Middlings Layer Compositions

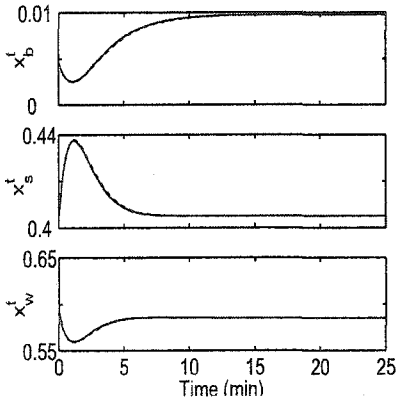

(c) Tailings Layer Compositions

Figure B.1: Comparison of Optimization and Reduced PSV Models: High to Low Grade Transition

In this case the froth and tailings compositions show no significant difference. The results of this section support the conjecture that it is not the change in the time constants in each layer, due to volume change, that causes the deviation in the previous case, but the two-way mixing between froth/middlings layer in the original model.

The reduced model shows only slight differences when compared to the original model of Chapter 2. From a simulation standpoint, the removal of the dynamic froth/middlings interface, the water material balances and the variables with zero range do not appear to affect the state variables of the model and solution to the optimization case studies in Chapter 4.

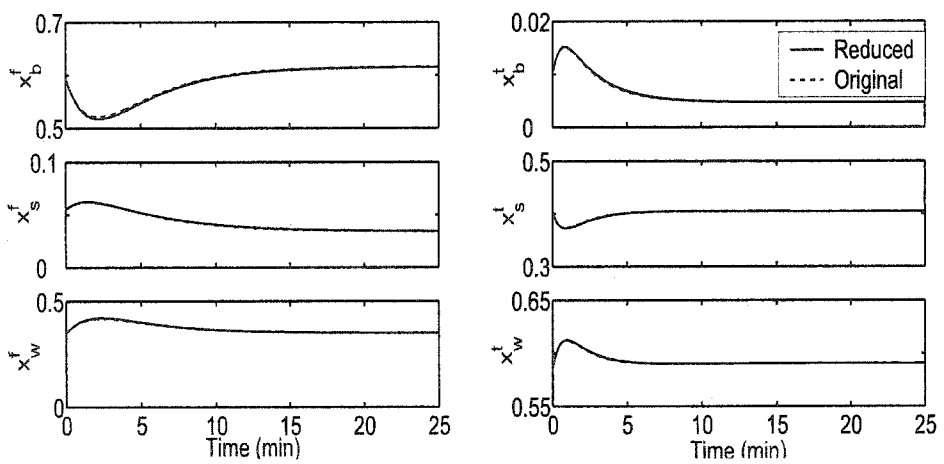

(a) Froth Layer Compositions (b) Tailings Layer Compositions

Figure B.2: Comparison of Optimization and Reduced PSV Models: Low to High Grade Transition

C

Ore Recipes and Particle Size Distributions

This appendix lists the mass fractions of bitumen, water and solids for the ore grades used in the case studies. The particle size distributions were then determined using the method outline in Forbes [28].

Species	Mass Fraction
Total Bitumen	15%
Small	0
Medium	0.06
Large	0.09
Total Sands	0.81 (0.15 fines)
Clay/Fines/Silts	0.081
Coarse Fines	0.0405
Coarse Sands	0.6885
Water	0.04

Table C.1: High Grade Ore

Species	Mass Fraction
Total Bitumen	12%
Small	0.021
Medium	0.048
Large	0.051
Total Sands	0.84 (0.25 fines)
Clay/Fines/Silts	0.168
Coarse Fines	0.042
Coarse Sands	0.63
Water	0.04

Table C.2: Medium Grade Ore

Species	Mass Fraction
Total Bitumen	9%
Small	0.03825
Medium	0.036
Large	0.01575
Total Sands	0.87 (0.35 fines)
Clay/Fines/Silts	0.261
Coarse Fines	0.0435
Coarse Sands	0.5655
Water	0.04

Table C.3: Low Grade Ore